DETERMINATION OF THE VALUES OF CRITICAL DUCTILE FRACTURE CRITERIA AND PREDICTION OF FRACTURE INITIATION IN SHEAR PUNCHING PROCESSES

September 2018

Department of Mechanical Engineering

Graduate School of Science and Engineering

Saga University, Japan

PHYO WAI MYINT

DETERMINATION OF THE VALUES OF CRITICAL DUCTILE FRACTURE CRITERIA AND PREDICTION OF FRACTURE INITIATION IN SHEAR PUNCHING PROCESSES

By

PHYO WAI MYINT

Master Degree in Mechanical Engineering
Bauman Moscow State Technical University, BMSTU
Russia.
Bachelor of Engineering (Mechanical)
Mandalay Technological University, MTU
Myanmar.

A dissertation submitted in partial fulfillment of the requirements for the degree of

Doctor of Philosophy

in the Department of Mechanical Engineering
Graduate School of Science and Engineering
Saga University
JAPAN

Supervisor
PROFESSOR SEIYA HAGIHARA

September 2018
JAPAN.

ABSTRACT

Punching processes are widely used for the production of automobile parts, mechanical components, and other parts. To produce highly accurate parts, it is important to estimate the ratio of the sheared surface to the cut surface. Many researchers applied the finite-element method (FEM) to analyze the ratio of the sheared surface to the fracture surface on cut surfaces by using fracture criterion which is considered to be material constant. However, it is difficult to determine the fracture criteria on the cut surface by tensile tests or bending tests because the punching process involves many complicated steps. In this research, FEM was applied to the punching processes to determine the values of critical fracture criteria (C) by using the ductile fracture criteria proposed by Cockcroft-Latham, Oyane, and Ayada. The ductile fracture criteria were compared with the boundary between the sheared surface and the fracture surfaces using experiments performed with a simple punching system. The values of ductile fracture criteria for the fracture initiation of the formed cut surface were predicted under the various clearances between the punch and the die with various punch diameters. The influence of stress triaxiality and the effect of punch diameter on the sheared surface length were also studied.

The results proved that the critical fracture criterion (C) value is not material unique constant. The accurate clearance-dependent critical fracture criteria of SPCC which can be used in the prediction of fracture initiation in the punching and fine blanking processes with the maximum punch diameter of 25 mm can be obtained from this research.

The new idea of using clearance-dependent ductile fracture criteria to reduce costs and time for experiments to obtain critical fracture criterion was also introduced in the analysis of the influence of process parameters on the sheared surface length in fine blanking processes. The numerically verified optimized process parameters for the production of fine sheared surface of SPCC steel in fine blanking processes were described.

Certificate of Approval

Department of Mechanical Engineering
Graduate School of Science and Engineering
Saga University
1 Honjomachi, Saga 840-8502, Japan.

This is to certify that the dissertation submitted by

PHYO WAI MYINT

with the title of "Determination of the Values of Critical Ductile Fracture Criteria and Prediction of Fracture Initiation in Shear Punching Processes" has been approved by the dissertation committee for the dissertation requirement for the **Doctor of Philosophy** degree in the Department of Mechanical Engineering at September, 2018 graduation.

Dissertation committee: Chairman

Dr. Seiya HAGIHARA
Professor, Department of Mechanical Engineering
Saga University, Japan.

Member
Dr. Nobusuke HATTORI
Professor, Department of Mechanical Engineering
Saga University, Japan.

Member
Dr. Bo ZHANG
Professor, Department of Mechanical Engineering
Saga University, Japan.

Member
Dr. Shigeki MORITA
Associate Professor, Department of Mechanical Engineering
Saga University, Japan.

ACKNOWLEDGEMENTS

First of all, I would like to thank to my respectful supervisor professor Seiya HAGIHARA, for his unflagging supports, belief and encouragement. I have been fortunate to study under his supervision. It is not possible to submit this dissertation without his valuable guidance, suggestions and motivations. As my supervisor, he taught me to try to become a good researcher and also the ethics of a scientist.

I also would like to express my special thanks to dissertation committee members, professor Nobusuke HATTORI, professor Bo ZHANG and associate professor Shigeki MORITA for their suggestions and advices. I am grateful to associate professors Shinya TAKETOMI and Yuichi TADANO for their kind suggestions and comments during my study in Saga University.

I also would like to express my thanks to Japanese Government and MEXT for their supports to study in Japan for three years. I would like to thank to the students from the laboratory of computational solid mechanics for their helps and supports. My deep gratitude also goes to professor Dr. Mi Sandar Mon, Head of Department of Mechanical Engineering, Yangon Technological University for allowing me to study in Japan.

My heartfelt thanks also go to my father U Myo Myint and my mother Daw Ohn Yin who had had their heart on supporting me for their whole life. I am also thankful to my wife Daw Myint Myint Nyein Soe and my daughter Ma Phyo Mon Mon Myint for their love and encouragement during my stays in Japan.

Contents

List of Figures

List of Tables

Nomenclature

Symbol	Name
$\sigma_1,\ \sigma_2,\ \sigma_3$	three principal stresses
σ_m	hydrostatic stress
J_1	first stress invariant
J_2	second stress invariant
J_3	third stress invariant
$\bar{\sigma}$	equivalent von Mises stress
η	stress triaxiality
ϕ	maximum shear stress ratio, yield function in Gurson model
ξ	normalized third stress invariant
θ	lode angle
σ_0	flow stress
f	void volume fraction
s	deviatoric part of the stress tensor
q_1, q_2	interaction effects between the voids
f^*	effective void volume fraction
f_c	critical void volume fraction
f_u	ultimate void volume fraction
f_f	void volume fraction at fracture
$\dot{f}_{growth}$	growth rate of existing voids
$\dot{f}_{nucleation}$	nucleation rate of new voids

Symbol	Name
$\dot{\varepsilon}_v$	volumetric strain rate
f_N	void volume fraction for nucleation
S_n	standard deviation
$\dot{\varepsilon}_M^p$	Equivalent plastic strain rate
ε_n	Mean nucleating strain
D_0	initial amount of damage
ε_{th}	threshold strain for initiation of damage
ε_{cr}	strain at failure
D_{cr}	critical damage value
α	the damage exponent
p	effective equivalent plastic strain
ε_p	plastic strain
σ_{max}	maximum principal stress
σ_H	hydrostatic stress
σ_{eq}	equivalent von Mises stress
ε_{eq}	equivalent plastic strain
ε_R	the strain at fracture
α, C	material constants

Chapter (1) Introduction

1.1 Introduction

Punching processes are widely used for producing automobile parts, metal components, and other parts. Manufacturers aim to produce parts at low cost, in less time, and with high quality. For producing high-quality products, it is important to obtain a finely sheared surface in the punching process. The cutting surface or edge in the punching process consists of different zones such as roll-over, shear, fracture, and burr formation zones. The ratio of different zones is influenced by various parameters, such as the punch-die clearance, punch and die corner radii, material properties, tool wear and misalignment.

It is important to estimate the ratio of the sheared surface to the cut surface before making a punch and a die to produce accurate parts. The optimal tools and punching conditions must be selected in the conventional punching and fine blanking processes. The punching process involves many complicated steps and it is difficult to determine the fracture criteria which show the shear limit point (ratio of sheared surface length to thickness) on the punched profile by tensile tests or bending tests.

The Finite Element Method (FEM) has been applied to calculate the ductile fracture criteria which can be used to predict the fracture initiation in the conventional punching and fine blanking processes. Many researchers used different ductile fracture criteria to study the conditions of punched profile, to optimize the process parameters and tool geometries to obtain finely sheared surface in the conventional punching and fully sheared surface in the fine blanking processes. Researchers predicted the shear limit point and studied the influence of the process parameters by setting the fracture criteria to be material constant for one material.

In this research, phenomenological ductile fracture criteria were used to predict fracture initiation of SPCC and S45C in the punching processes and the critical ductile fracture criteria, (C) values were determined. The influences of process parameters and tool geometry on the

cut surface in fine blanking processes were studied by using the clearance-dependent ductile fracture criteria.

1.2 Literature review

Researchers have used different criteria with different affected parameters to predict the initiation of fracture surface formation in the metal-forming process. McClintock et al. derived a ductile fracture criterion by analyzing the growth of a cylindrical void [1], and Cockcroft and Latham derived a fracture criterion based on the maximum principal tensile stress [2]. The effect of spherical void growth was studied by Rice and Tracey in elastic–perfectly plastic material [3]. Oyane derived criteria for ductile fracture prediction of pore-free materials and porous materials from the equations of plasticity theory by including a hydrostatic stress component [4]. Gurson employed the void volume fraction, which incorporates void nucleation and growth [5]. Tvergaard improved the model of Gurson by taking into account the effects of nucleation and coalescence of voids [6]. The stress distribution through the thickness of sheet metal was studied by Stoughton and Yoon to identify the mode of failure [7]. Khan and Liu established a phenomenological fracture criterion using the magnitude of the stress vector and the first invariant of the stress tensor [8]. In that work, the results obtained from the criterion had a better agreement with experimental results than the results obtained from the maximum shear stress fracture criterion proposed by Stoughton and Yoon. Lou and Huh extended shear-controlled ductile fracture to a three-dimensional stress space to include the effects of stress triaxiality and the load parameter [9].

Different types of punching processes can be performed, such as by using a normal punching machine consisting of a die and punch or using a fine blanking machine consisting of a die, blank holder, punch, and counter-punch. The punching process involves complicated steps such as contact of the punch, elastic and plastic deformation, shearing, and crack

formation. The influence of superposed hydrostatic pressure on ductile fracture initiation was studied by Goijaerts et al. and proposed a new model that is valid for both tensile tests and blanking [10]. The split arbitrary Lagrange–Euler method combined with remeshing for large, localized deformation of an elastic–plastic finite-element analysis model of the blanking process was studied by Brokken et al. [11]. Their findings demonstrated the handling capability of the finite element approach based on the arbitrary Lagrange–Euler method combined with remeshing for the large, localized deformation.

Hambli and Reszka studied different phenomenological criteria to determine the critical fracture criteria and this study shows that the criteria proposed by Cockcroft and Latham, Oyane and Ayada are good ones [12]. The effect of punch-die clearance on the different zones of the cut surface for fine blanking can be found in [13], and the results indicate that the increase of the clearance decreases the depth of shear zone and increases the depth of fracture zone. The blanking operation of very thin sheet metals by using the Cockcroft–Latham fracture criterion can be found in [14]. Komori studied the crack initiation and propagation during shearing and tensile tests by using both phenomenological and mechanism-based fracture criteria [15]. Tanaka et al. evaluated the fracture criteria proposed by Oyane and Cockcroft and Latham for different types of punching and the conditions of cut surface obtained by both criteria were described [16].

The effects of surface roughness on the sheared surface length and fracture height in the micro-punching process were investigated by Xu et al. The results indicate that the better sheared surface quality and length, the lower fracture height can be obtained by the ion beam finished micro-punch and smooth surface of micro-die finished by ion beam irradiation [17]. Miniaturization in sheet metal working process was studied by Kals and Eckstein. In that work, the effects of grain size and orientation on the sheared surface length, burr formation and drawn-in edge in the punching process were described [18]. The size effect model of micro-

blanking was established by Xu et al. to investigate the influences of mold clearance and grain size on the deformation and fracture behavior in micro-blanking process. It was found that the blanking edge and distributions of different zones are affected by grain size and the ratio of blanking clearance to grain size [19].

Subramonian et al. studied the effect of punch-die clearance on the tool life and edge quality of parts for the blanking process [20]. In that work, the range of punch-die clearances which gives the minimum punch stress was identified and the relationship between the shear zone length and punch corner radius with the effect of compressive stresses in the deformation zone was described. Yu and Zhao used the ductile fracture initiation and propagation criterion to investigate the blanking of thick sheet metal [21]. In that work, the effect of stress triaxiality on ductile fracture and the influence of blanking clearance on fracture were studied. Mohr and Marcadet used the phenomenological Hosford–Coulomb model to predict ductile fracture initiation at low stress triaxialities [22]. Meng et al. used phenomenological ductile fracture criteria to study the deformation behavior in progressive microforming [23]. Through the results, it was found that Ayada criterion can predict fracture, rollover and shearing zone in the shearing stage and Cockcroft and Latham criterion can predict the depth of fracture zone which has a good agreement with experimental result in blanking.

Based on the above review of previous research, the value of critical fracture criterion (C) was held constant for one material and that value was used to predict fracture initiation and to study the influences of process parameters on the cut surface. The effect of punch diameter on the sheared surface length was not considered and only one blank thickness was considered.

1.3 Objectives of the research

The aim of this research is to determine the values of critical ductile fracture criteria which can be used in the actual conventional punching and fine blanking processes to predict the fracture initiation point (shear limit point).

This research also intends to investigate whether the critical ductile fracture criterion, (C) value is a material constant or depends on the clearance between the punch and die.

The investigation of effect of punch diameter on the sheared surface length, consideration of two blank thicknesses, prediction of stress triaxiality effect were involved in this research. This research also intends to analyze the influences of process parameters in the fine blanking process and to optimize parameters from which fully sheared surface of SPCC can be obtained.

1.4 Outlines of the research

There are seven chapters in this thesis. The current chapter, chapter (1) describes the introduction, literature review and objectives of this research. The metal forming processes, the complicated steps in the punching process can be found in the chapter (2). What is more, the chapter (2) consists of force and stress distribution during punching process, illustration of typical load stroke curve and the schematic figure which shows the different zones on the punched profile. Chapter (3) describes the materials used in this research, the experimental devices and experimental results. The relationship between the ratio of sheared surface length to thickness and the clearance for both materials obtained from the punching experiments can be found in this chapter. Chapter (4) concerns with theoretical explanation of ductile fracture. The three types of ductile fracture criteria and the fracture criteria used in the prediction of ductile fracture initiation in the conventional punching and fine blanking processes are mentioned in this chapter. The Finite Element Analysis (FEA) of punching process was

mentioned in the chapter (5). The procedures of FEA, determination of the values of critical ductile fracture criteria, the influence of punch diameter on the cut surface can be seen in this chapter. The relationship between the values of critical ductile fracture criteria (C) and the clearance (% thickness) between the punch and the die which can be used in the actual punching process and fine blanking process was described in this chapter. FEA of fine blanking process can be seen in the chapter (6). The influences of process parameters on the cut surface, the optimized tool geometry and process parameters to obtain fully sheared surface in the fine blanking process are discussed in this chapter. The summary of research, limitations and the future plan are summarized in the chapter (7).

Chapter (2) Metal Forming and Punching Processes

2.1 Introduction

Sheet-metal forming processes are used for both serial and mass-production. It can be divided into two groups: cutting processes- shearing, blanking, punching, notching, piercing, and so on; and plastic deformation processes- bending, stretch forming, deep drawing and various other forming processes [24]. Metal forming represents highly significant group of processes for producing industrial and military components and consumer goods [25]. Among them, punching processes are widely used in the production of automobile parts and mechanical components.

2.2 Punching processes

Punching processes are widely used in the production of metal components in automobile industries by using punch and die. In the punching processes, the speed of the punch, the geometry of punch and die, the punch force, the type of lubricant used in the process and the clearance between the punch and the die which is always shown percent thickness of the blank [% t] are the key factors. Punching process consists of different phases, contact of punch, elastic and plastic deformation, shearing and crack formation and the last one is breakthrough [26]. The phases of punching process are shown in the following Fig. 2.1.

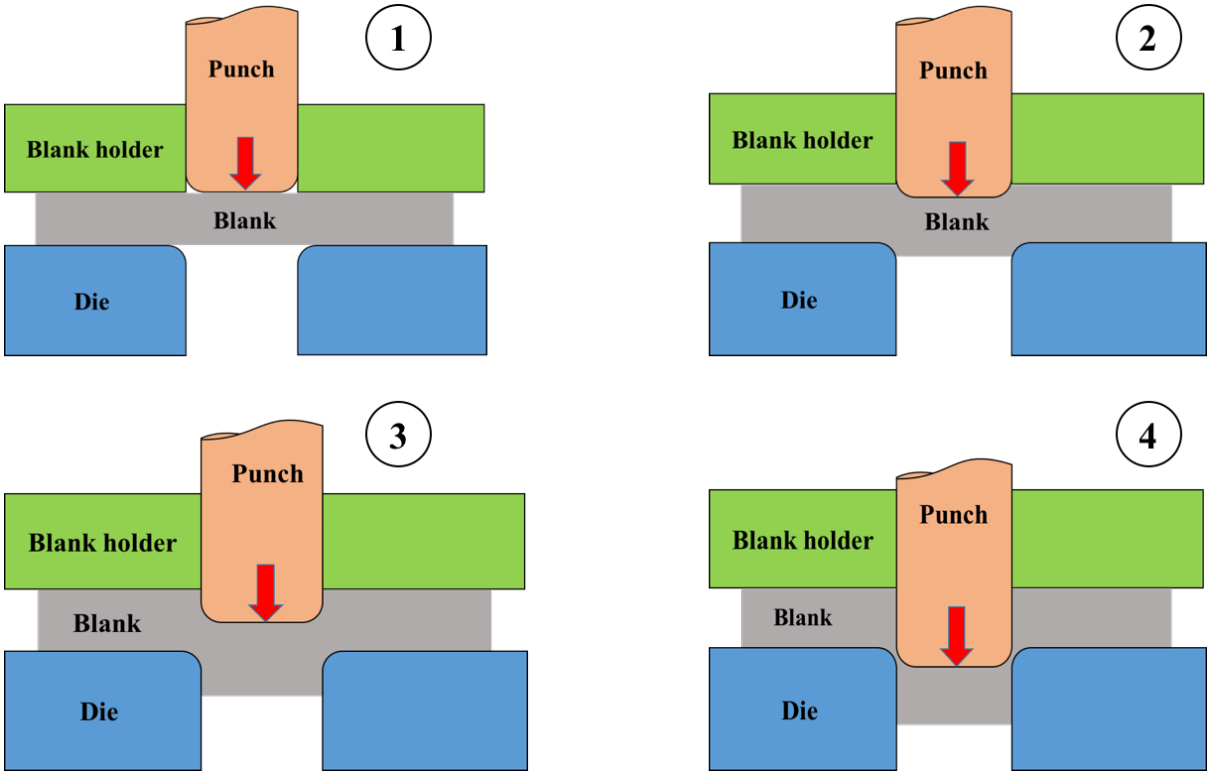

Fig. 2.1 The four steps in the punching process, step (1)-Contact of punch with the blank, step (2)-Elastic and plastic deformation, step (3)-Shearing and formation of crack, step (4)-Rupture or final breakthrough.

The punch contacts the blank and the compressive stress is exerted on the blank by the punch in the step (1). The elastic and plastic deformations of the blank are formed in the step (2) because of the punch movement. The stress is increased and the shearing process can be occurred in the step (3). The crack formation was started in this step and fracture is occurred when the two cracks from punch and die sides meet. The final breakthrough or rupture can be found in the step (4).

2.2.1 Distribution of forces and stress during punching process

The forces acting along the cutting edge during the punching process are not linear. The forces acting vertically and horizontally in the clearance zone are shown in the Fig. 2.2 with

the symbols of F_V and F_X. The compressive forces distribution is not uniform and the distance between the vertical and horizontal forces cause bending moment. This moment is compensated by a counter bending moment that is created by bending stress and horizontal normal stresses between the work piece and tool. The resulting frictional forces also can be seen in the figure. These frictional forces increase the total blanking force [26].

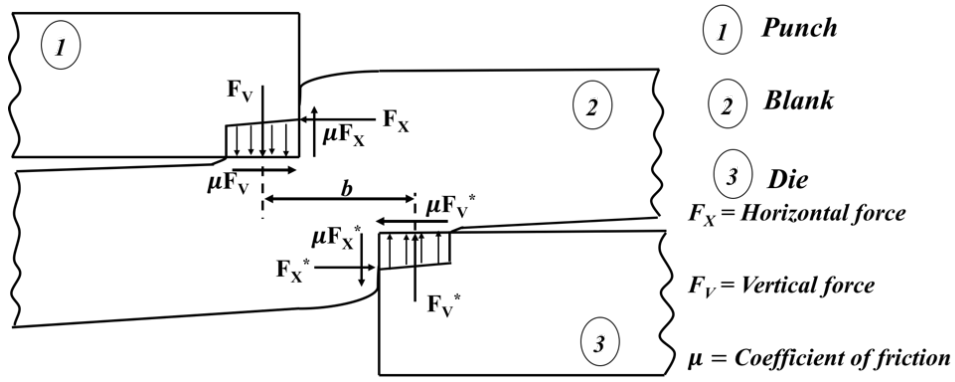

Fig. 2.2 Force distribution in the blank during punching process [26].

2.2.2 Typical load-stroke curve of punching process

The punching force varies along the cutting edge during the punching process. The punching operation consists of four phases of punching force variation. The relationship between the punching force and punch displacement or theoretical load-stroke curve of punching process is shown in the Fig. 2.3.

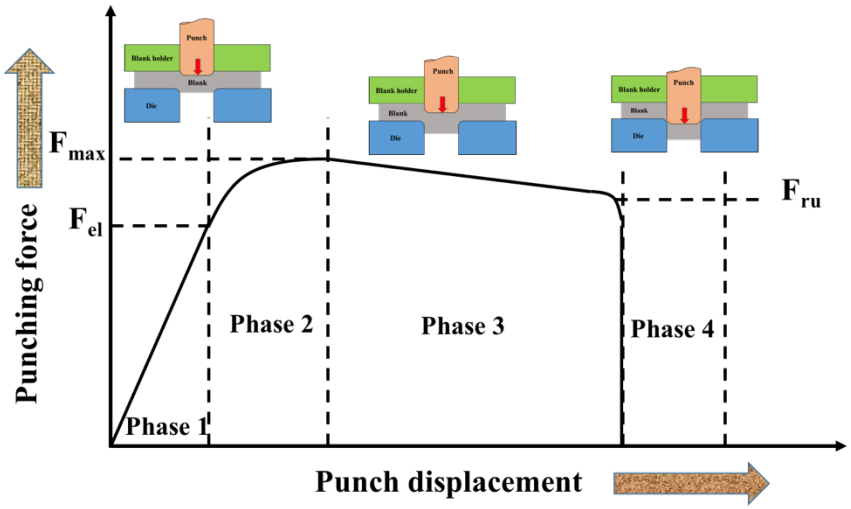

Fig. 2.3 Typical load-stroke curve of punching process.

The material deforms elastically between the punch and the die in phase one. The starting point of plastic deformation and straining hardening caused by material flow is formed in phase two. The effect of strain hardening leads to the increase of the punching force until it reaches the maximum value $F_{max.}$ The shearing process was formed in the third phase and the punching force decreases to the value of fracture initiation force $F_{ru,}$ because of the decrease in the cross section of the blank. The fracture initiation starts at the phase four after the deformation limit is exceeded. The cutting force decreases and the final rupture is occurred in this phase.

The slightly difference may be occurred between the load-stroke curve obtained from punching experiments and the typical load-stroke curve of punching process since the friction forces, geometrical accuracy, the changes of material property and deflection of tool are not considered in the typical load-stroke curve [27].

2.3 Characteristics of cut surface

2.3.1. Formation of different zones on the cut surface

The cut surfaces produced by punching consist of different zones: rollover, shear zone, fracture zone and burr formation. The secondary shear surface may be occurred depending on the material properties and the clearance between the punch and the die. The elastic and plastic deformation at the beginning of punching causes the rollover or draw in and burr formation. The formation of the different zones is influenced by a number of parameters such as material properties, thickness, the clearance between the punch and the die, tool wear, punch velocity and misalignment [27].

2.3.2 Theoretical cut surface obtained by punching process

The theoretical cut surface obtained by punching process is shown in the Fig. 2.4.

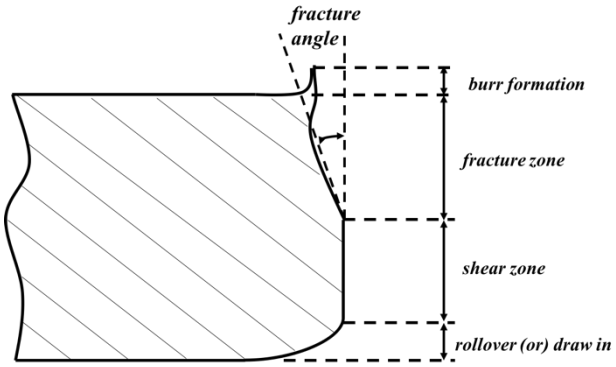

Fig. 2.4 Theoretical cut surface produced by punching.

The main factor for determining the shape and the quality of the cut surface is the clearance between the punch and the die which is written in the percent of the blank thickness (% t). If the clearance is increased, the length of shear zone is decreased and the length of fracture zone is increased. The parameters such as punch-die corner radii, thickness and material properties of blank affect the shear limit point or fracture initiation point on the

punched edge. In the punching process, a large shear surface and small fracture surface and burr are preferable.

Manufacturers aim to produce parts at low cost, in less time, and with high quality. For producing high quality products, it is important to obtain a finely-sheared surface in the punching process. Hence, the researchers have used different criteria with different affected parameters to predict the initiation of fracture surface formation in the punching process. The best and most economical product can be obtained under minimum scrap and minimum number of operations. Strength, hardness, toughness, elasticity, plasticity, brittleness, ductility, and malleability are mechanical properties used as measurements of how metals behave under a load [24].

Chapter (3) Materials and Experiments

3.1 Materials

Materials play an important role in engineering. Transportation, housing, clothing, communication, recreation, and food production- virtually every segment of our everyday lives is influenced to one degree or another by materials [28]. One of the most important on the materials used in industries and forming process is formability (ductility), which is a measure of degree of deformation before fracturing. The larger sheared surface, small fracture surface and less burr formation are preferable in the punching process which is one of metal forming processes. In this thesis, the materials of SPCC and S45C are used to predict the shear limit point or fracture initiation point in the punching process and to determine the values of critical ductile fracture criteria. The material SPCC is used in the manufacturing of automobile parts, constructions, in the production of electrical appliances and for many other usages. The material S45C is used extensively by all industry sectors for applications requiring more strength and wear resistance. It was used in the manufacturing of keys, connection rods, hydraulic clamps, studs, shafts and others.

3.2 Uniaxial tensile test and material properties

The uniaxial tensile test is commonly used to evaluate the strength and ductility of materials. The yield stress, tensile strength, Young modulus and Poisson`s ratio obtained from the uniaxial tensile test are described as material properties. The relation between the load and displacement curve was obtained from the tensile test and this curve was converted to stress and strain curve. However, the flow stress and plastic strain curve is needed in the Finite Element Analysis. In order to predict the metal behaviors under the multi-axial loading conditions, it is needed to plot tensile testing results in terms of true stress and true strain. The geometrical dimensions of the tensile test specimen are shown in the Fig. 3.1. The relationships

between the flow stress and plastic strain for SPCC and S45C are shown in the Fig. 3.2 and Fig. 3.3. The material properties used in the FEA for the punching processes are mentioned in the Table 3.1.

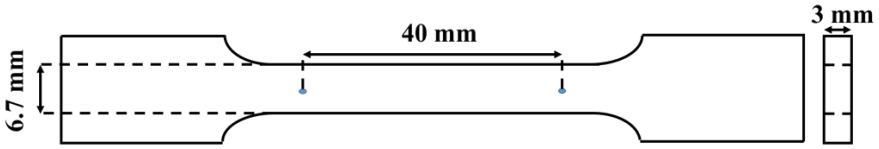

Fig. 3.1 Geometrical dimensions of the uniaxial tensile test specimen.

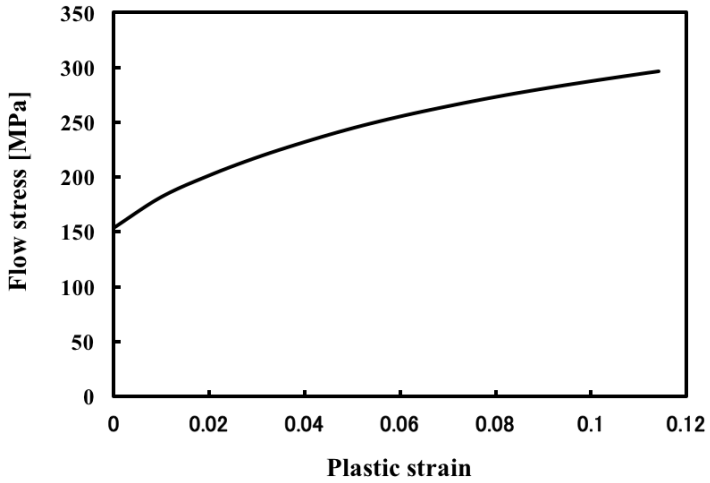

Fig. 3.2 The graph of the flow stress versus plastic strain (SPCC).

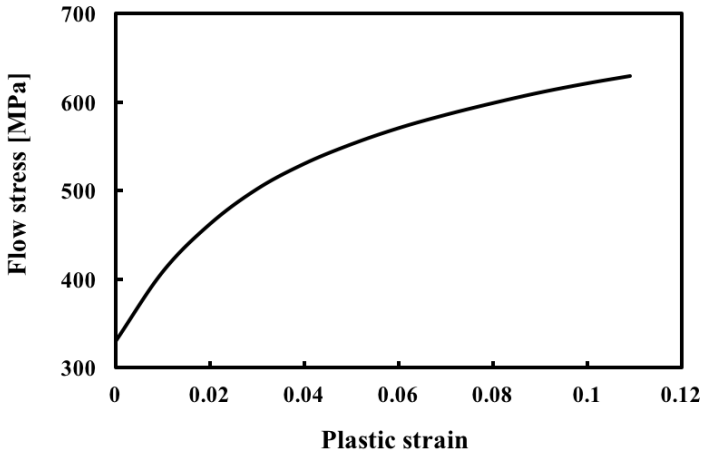

Fig. 3.3 The graph of the flow stress versus plastic strain (S45C).

Table 3.1 Material properties of SPCC and S45C

		SPCC	S45C
Young's modulus	[GPa]	200	216
Poisson's ratio		0.3	0.3
Yield stress	[MPa]	154	330

3.3 Experimental devices for punching

The punching device (MIYAGI Coperation, Hi-set A-3-150) was used to observe the cut surface during the punching experiments. The punching experiments were performed by using a general-purpose die (punch die set) and a universal tension and compression testing machine (AutoGraph AG-250kN, SHIMADZU). The punching device, universal tension and compression testing machine and the schematic of the punch and die are shown in the Fig. 3.4, 3.5 and 3.6.

Fig. 3.4 The punching device which is used in the punching experiments.

Fig. 3.5 The universal tension and compression testing machine which is used in the punching experiments.

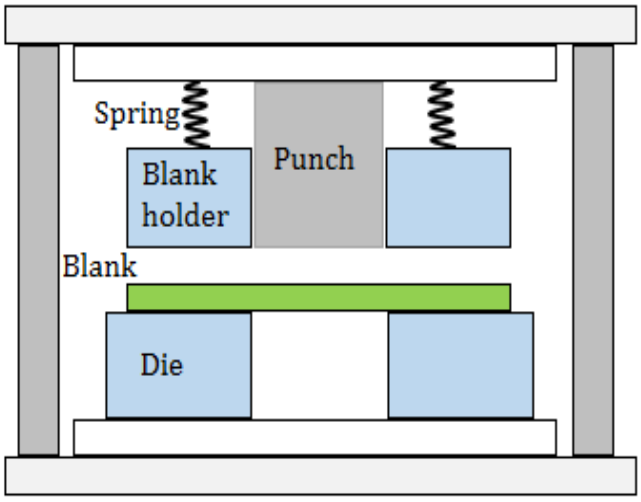

Fig. 3.6 Schematic of blank material in general purpose die (punch die set) which is installed in the universal tension and compression testing machine for the punching experiments with the various punch-die clearances.

3.3.1 Geometrical dimensions of punch and die, blank and the clearances

In the aforementioned researches, the researchers predict fracture initiation of a material by using only one blank thickness. However, blank thicknesses of 1.6 mm and 3.2 mm are used in this work and the nature of cut surface obtained by punching process was studied by using the different punch diameters and clearances.

The punch speed was the same as the crosshead speed of the testing machine, which was set to 25 mm/s in the experiments. The values of punch diameters, die diameters and clearance/plate-thickness ratio for two materials SPCC and S45C which used in the punching experiments are shown in the Table 3.2.

Table 3.2 The values of punch diameter, die diameter and clearance/plate-thickness ratio of SPCC and S45C used in the experiments.

Punch Diameter (mm)	Die Diameter (mm)	Clearance (%t)
10	10.2, 10.6, 10.8	3.125, 6.25, 9.375,12.5, 18.75, 25.0
15	15.2	3.125, 6.25
20	20.2	3.125, 6.25
25	25.2, 25.6, 25.8	3.125, 6.25, 9.375, 12.5, 18.75, 25.0

3.3.2 Illustration of different zones on the cut surface

The shear limit point or boundary between the sheared surface and the fracture surface was measured on circular punched samples by using a microscope (VH-Z100). The work piece, schematic figure of cut surface and the nature of cut surface obtained by the punching are shown in the Fig. 3.7. The two surfaces, sheared surface and fracture surface can be found on the blank profile.

The lengths of the maximum sheared surface and the minimum sheared surface were measured and then averaged the lengths for each case. The thickness of the blank before and after punching is slightly different. However, that difference was also taken into account. The blank thickness after each punching process was measured and then the average value was calculated for each clearance. The experiments were performed five times for each clearance value and the results were averaged to obtain accurate results.

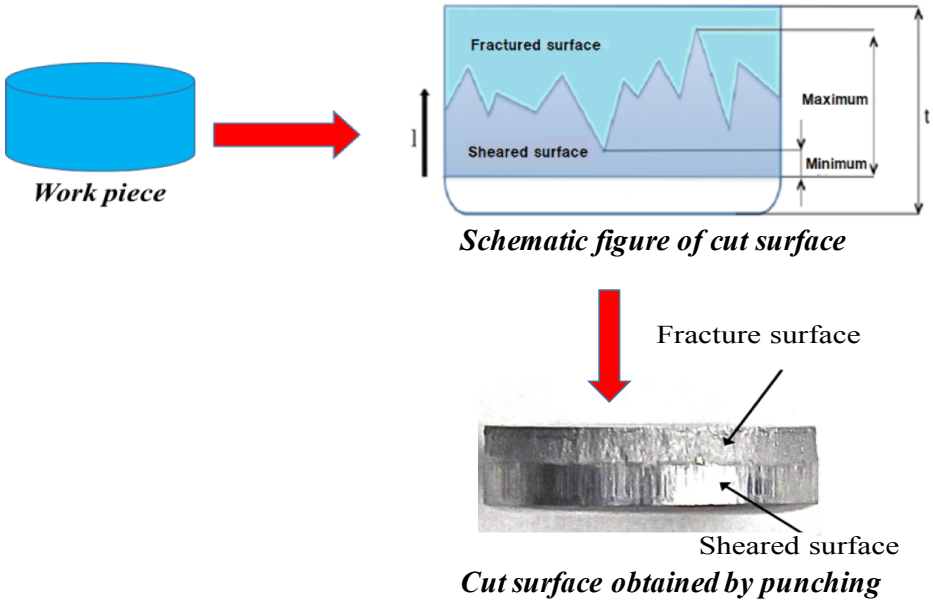

Fig. 3.7 Work piece, schematic figure of cut surface and the nature of cut surface obtained by punching experiment.

3.4 Experimental results of SPCC

3.4.1 The blank thickness after punching

The thickness of the blank after each punching process under each clearance was measured and then the average value was calculated. The results and average values for blank thicknesses of 1.6 mm and 3.2 mm are shown in the Table 3.3 and 3.4.

Table 3.3 Blank thicknesses after punching experiments of SPCC (t 1.6)

Punch diameter [mm]	10			15	20	25		
Clearance [mm]	0.1 [6.25 %t]	0.3 [18.75%t]	0.4 [25 %t]	0.1	0.1	0.1	0.3	0.4
Blank thickness after punching [mm]	1.571	1.564	1.559	1.569	1.562	1.577	1.574	1.567
	1.570	1.564	1.563	1.567	1.565	1.570	1.564	1.578
	1.570	1.565	1.562	1.567	1.567	1.574	1.568	1.563
	1.572	1.565	1.558	1.567	1.563	1.573	1.568	1.560
	1.581	1.565	1.565	1.570	1.568	1.575	1.574	1.569
Average	**1.573**	**1.565**	**1.561**	**1.568**	**1.565**	**1.574**	**1.570**	**1.567**

Table 3.4 Blank thicknesses after punching experiments of SPCC (t 3.2mm)

Punch diameter [mm]	10			15	20	25		
Clearance [mm]	0.1 [3.125%t]	0.3 [9.375%t]	0.4 [12.75 %t]	0.1	0.1	0.1	0.3	0.4
Blank thickness after punching [mm]	3.127	3.106	3.105	3.105	3.113	3.107	3.097	3.10
	3.132	3.110	3.106	3.113	3.099	3.104	3.095	3.095
	3.128	3.113	3.103	3.108	3.110	3.103	3.099	3.096
	3.128	3.107	3.104	3.106	3.111	3.110	3.102	3.097
	3.135	3.110	3.104	3.107	3.105	3.106	3.102	3.096
Average	**3.130**	**3.109**	**3.104**	**3.108**	**3.108**	**3.106**	**3.099**	**3.097**

3.4.2 The lengths of sheared and fracture surfaces

The maximum and minimum sheared surface lengths obtained from the first time (one time) punching experiment for the blank thicknesses of 1.6 and 3.2 mm and different clearances with the punch diameter of 10 mm are shown in the following Figures.

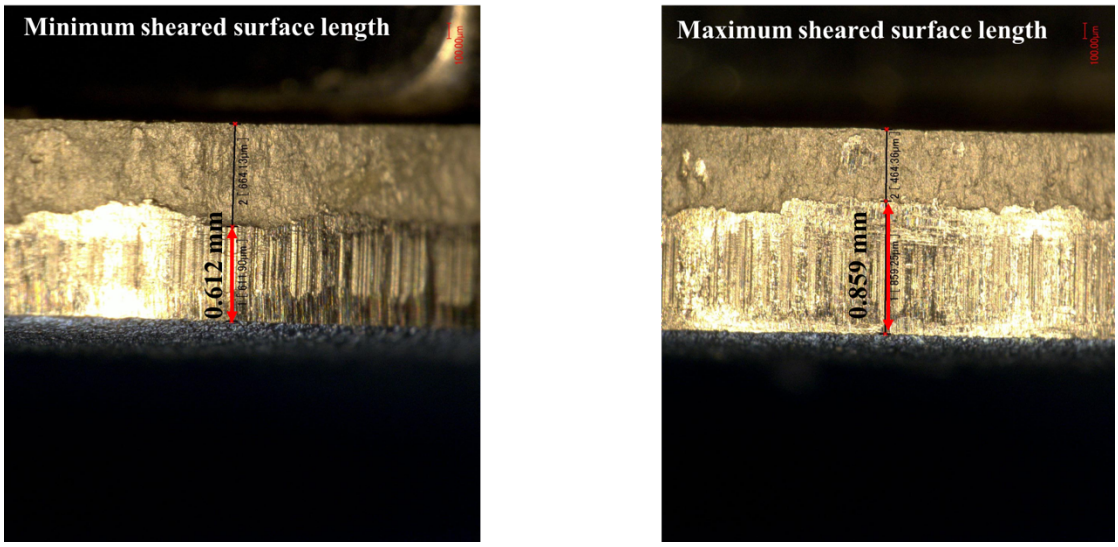

Fig. 3.8 Minimum and maximum sheared surface lengths obtained from the punching experiment with the punch diameter of 10 mm, blank thickness of 1.6 mm and clearance of 0.1 mm (6.25%t).

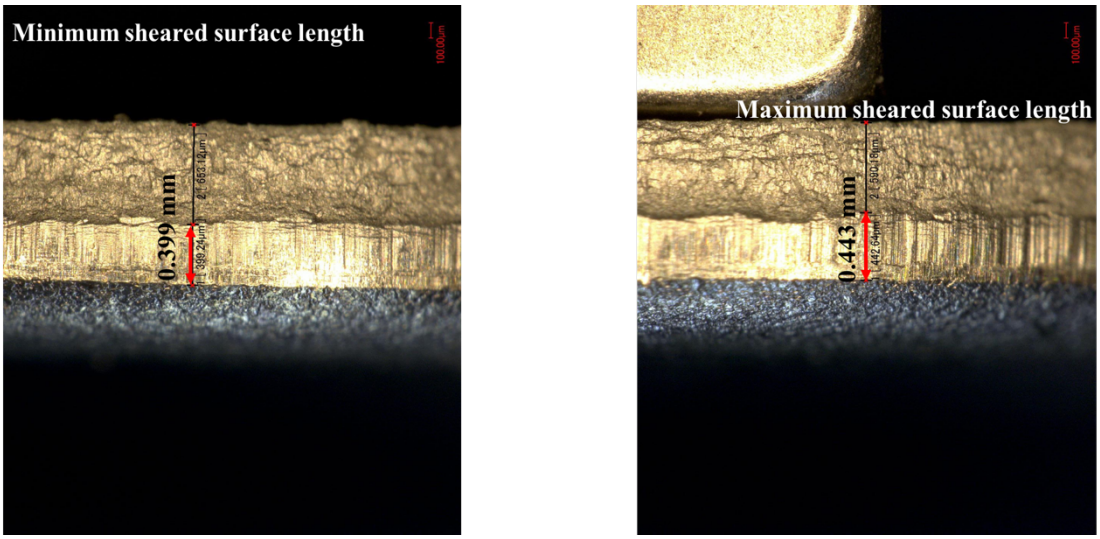

Fig. 3.9 Minimum and maximum sheared surface lengths obtained from the punching experiment with the punch diameter of 10 mm, blank thickness of 1.6 mm and clearance of 0.3 mm (18.75%t).

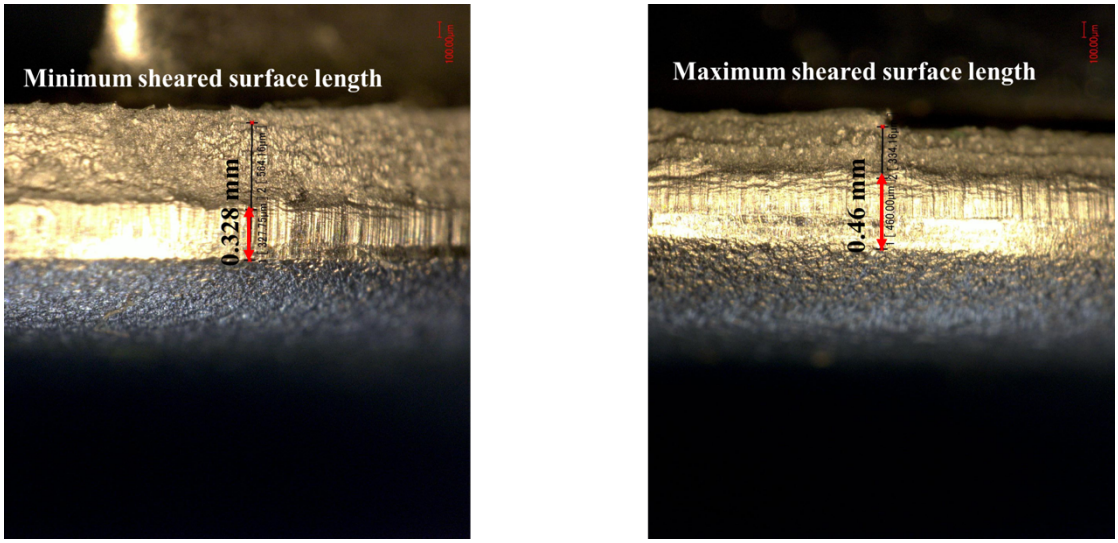

Fig. 3.10 Minimum and maximum sheared surface lengths obtained from the punching experiment with the punch diameter of 10 mm, blank thickness of 1.6 mm and clearance of 0.4 mm (25%t).

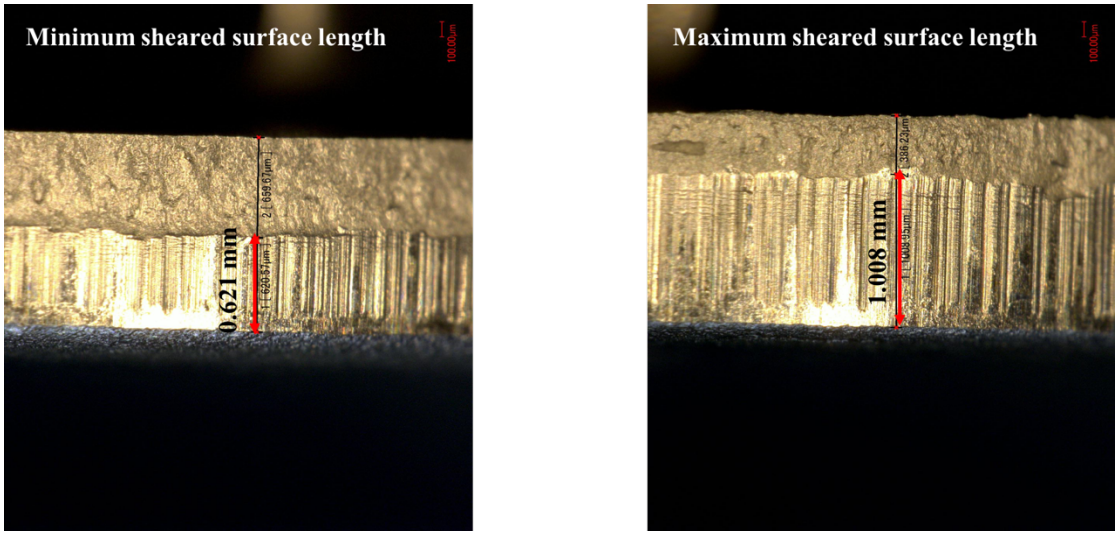

Fig. 3.11 Minimum and maximum sheared surface lengths obtained from the punching experiment with the punch diameter of 15 mm, blank thickness of 1.6 mm and clearance of 0.1 mm (6.25%t).

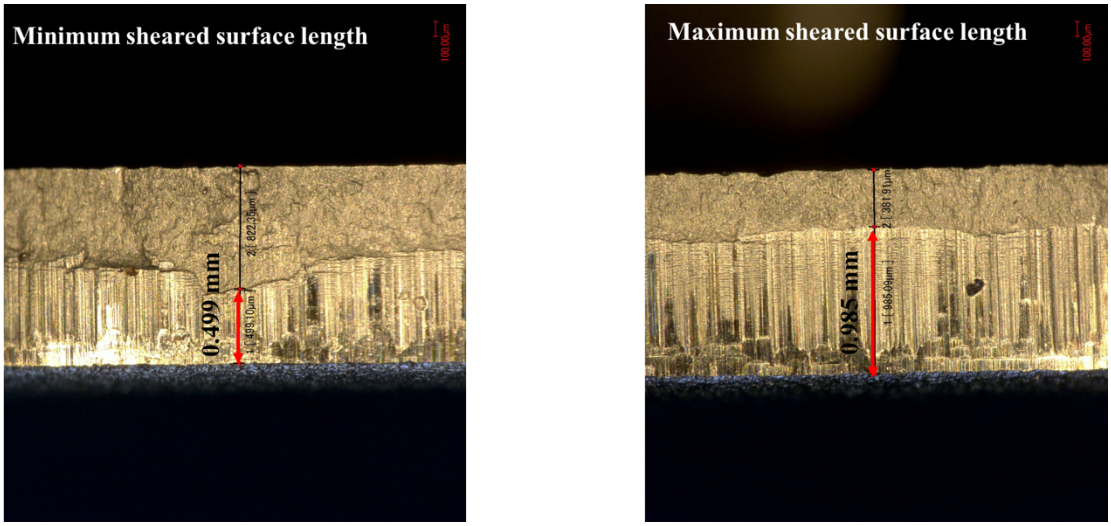

Fig. 3.12 Minimum and maximum sheared surface lengths obtained from the punching experiment with the punch diameter of 20 mm, blank thickness of 1.6 mm and clearance of 0.1 mm (6.25%t).

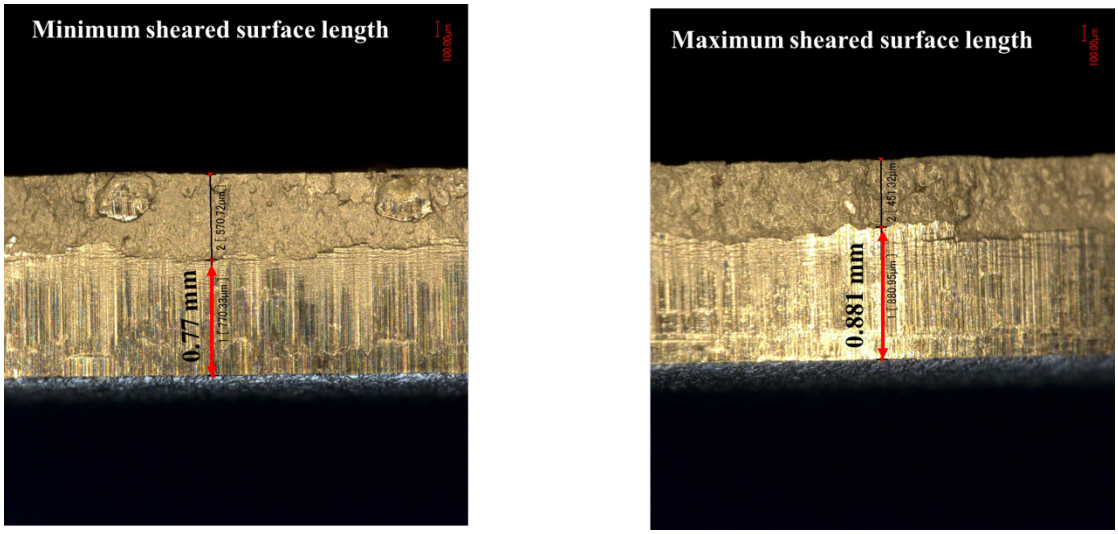

Fig. 3.13 Minimum and maximum sheared surface lengths obtained from the punching experiment with the punch diameter of 25 mm, blank thickness of 1.6 mm and clearance of 0.1 mm (6.25%t).

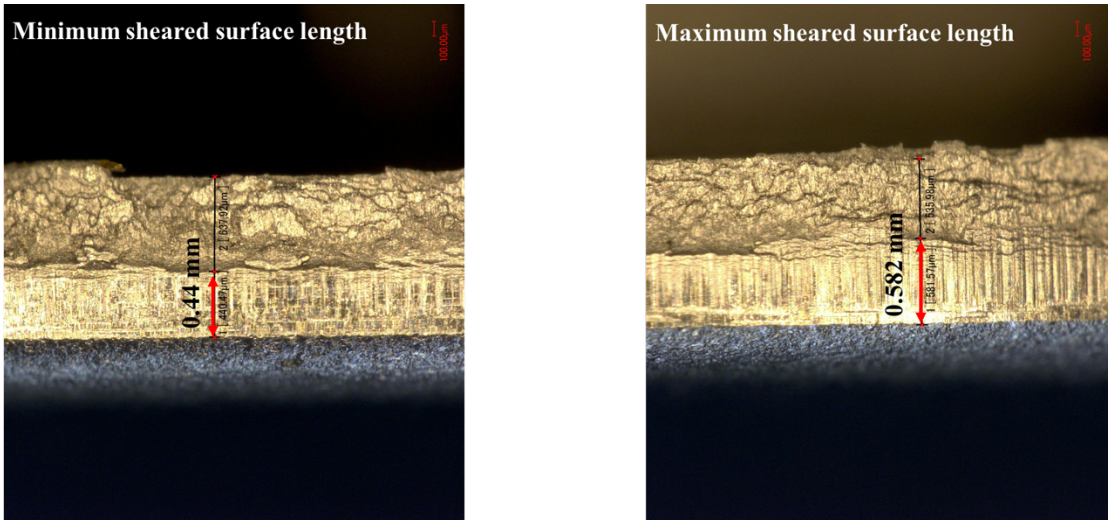

Fig. 3.14 Minimum and maximum sheared surface lengths obtained from the punching experiment with the punch diameter of 25 mm, blank thickness of 1.6 mm and clearance of 0.3 mm (18.75%t).

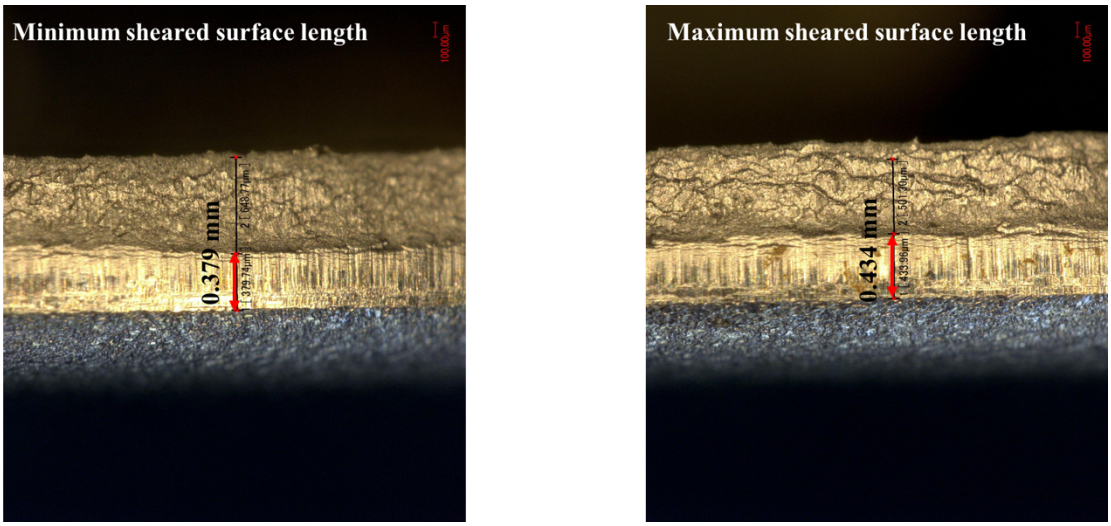

Fig. 3.15 Minimum and maximum sheared surface lengths obtained from the punching experiment with the punch diameter of 25 mm, blank thickness of 1.6 mm and clearance of 0.4 mm (25%t).

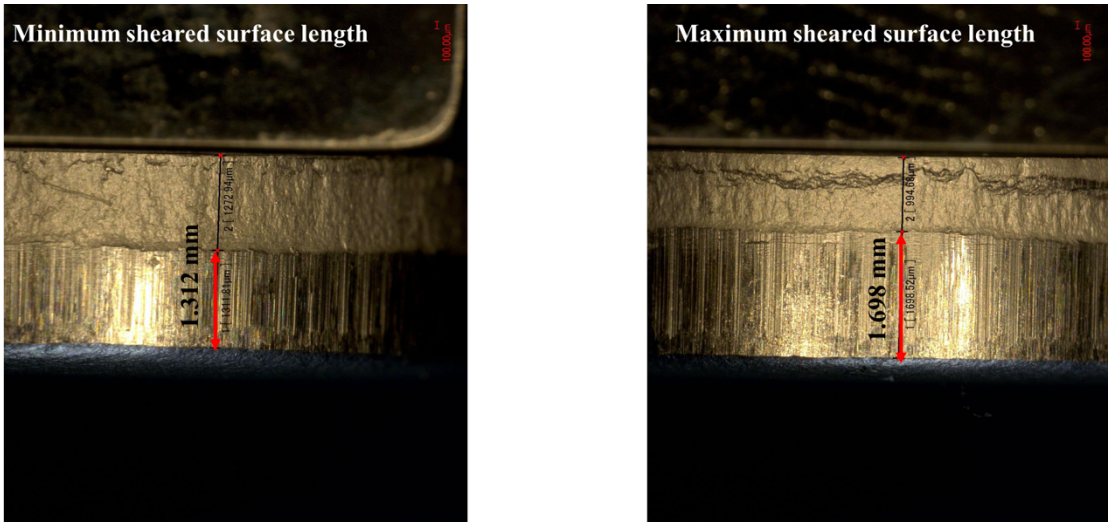

Fig. 3.16 Minimum and maximum sheared surface lengths obtained from the punching experiment with the punch diameter of 10 mm, blank thickness of 3.2 mm and clearance of 0.1 mm (3.125 %t).

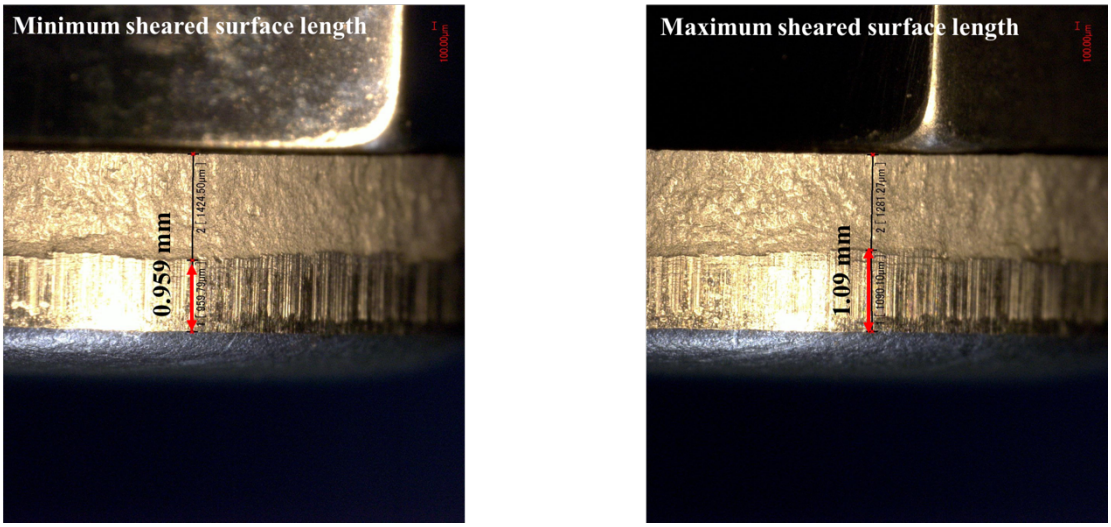

Fig. 3.17 Minimum and maximum sheared surface lengths obtained from the punching experiment with the punch diameter of 10 mm, blank thickness of 3.2 mm and clearance of 0.3 mm (9.375 %t).

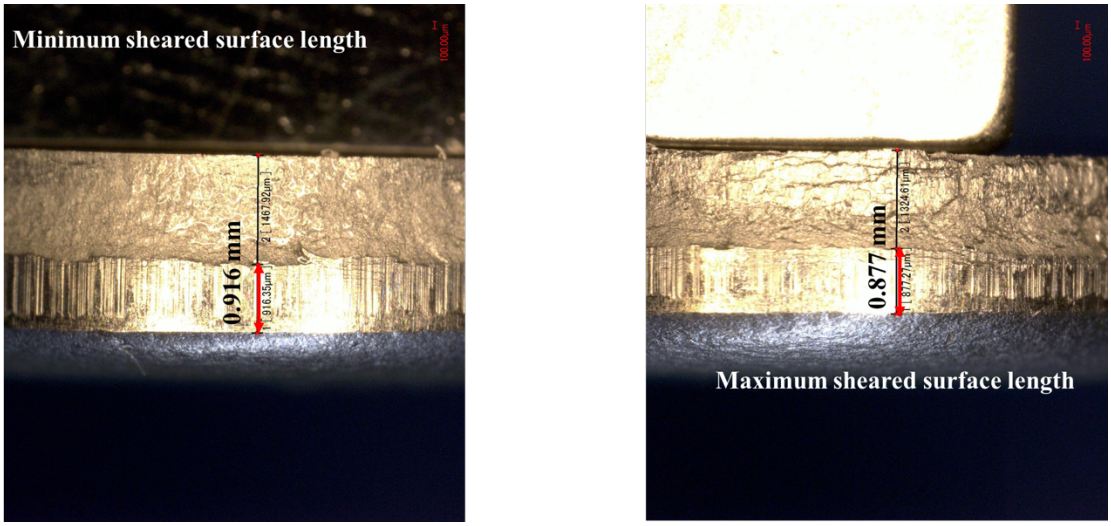

Fig. 3.18 Minimum and maximum sheared surface lengths obtained from the punching experiment with the punch diameter of 10 mm, blank thickness of 3.2 mm and clearance of 0.4 mm (12.5 %t).

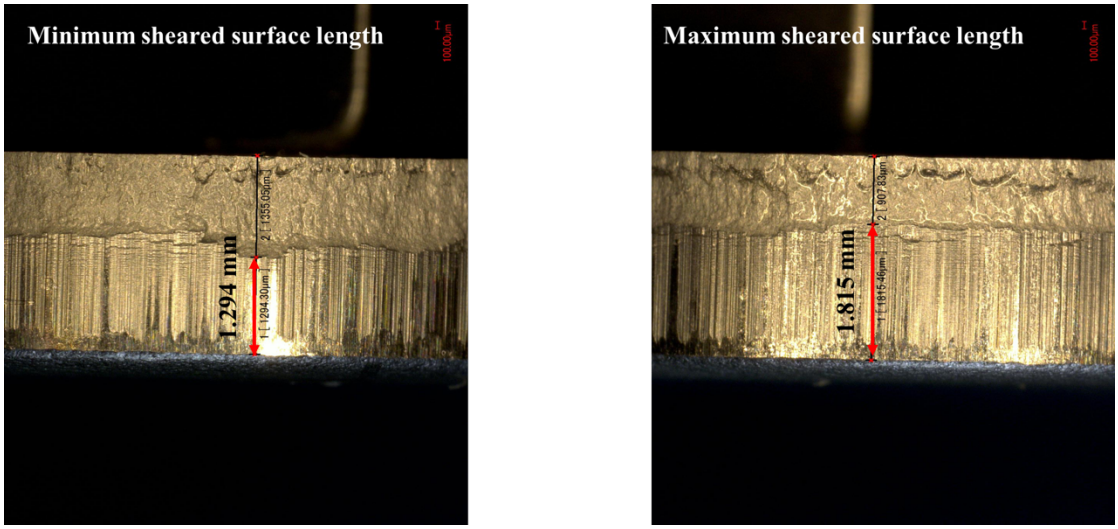

Fig. 3.19 Minimum and maximum sheared surface lengths obtained from the punching experiment with the punch diameter of 15 mm, blank thickness of 3.2 mm and clearance of 0.1 mm (3.125 %t).

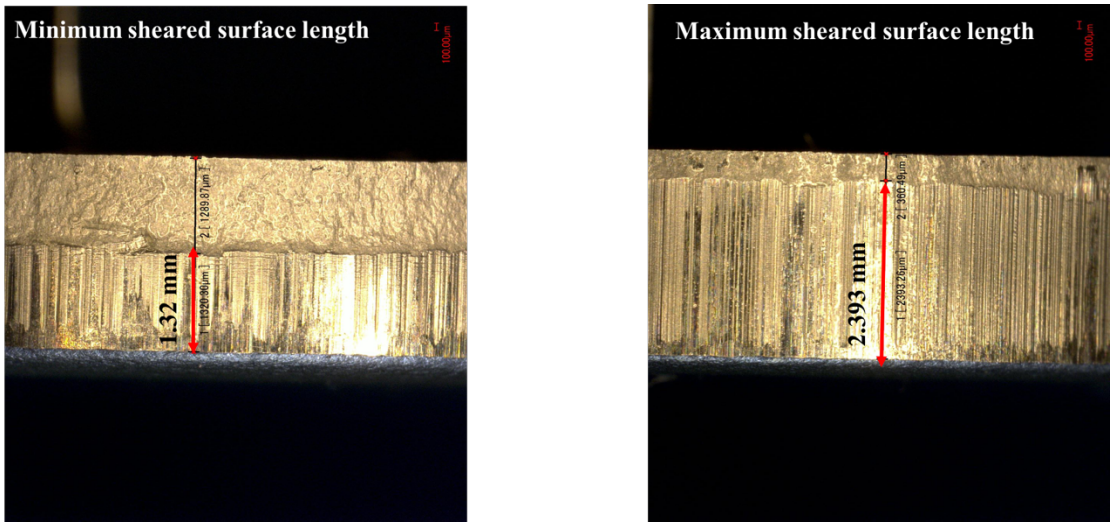

Fig. 3.20 Minimum and maximum sheared surface lengths obtained from the punching experiment with the punch diameter of 20 mm, blank thickness of 3.2 mm and clearance of 0.1 mm (3.125 %t).

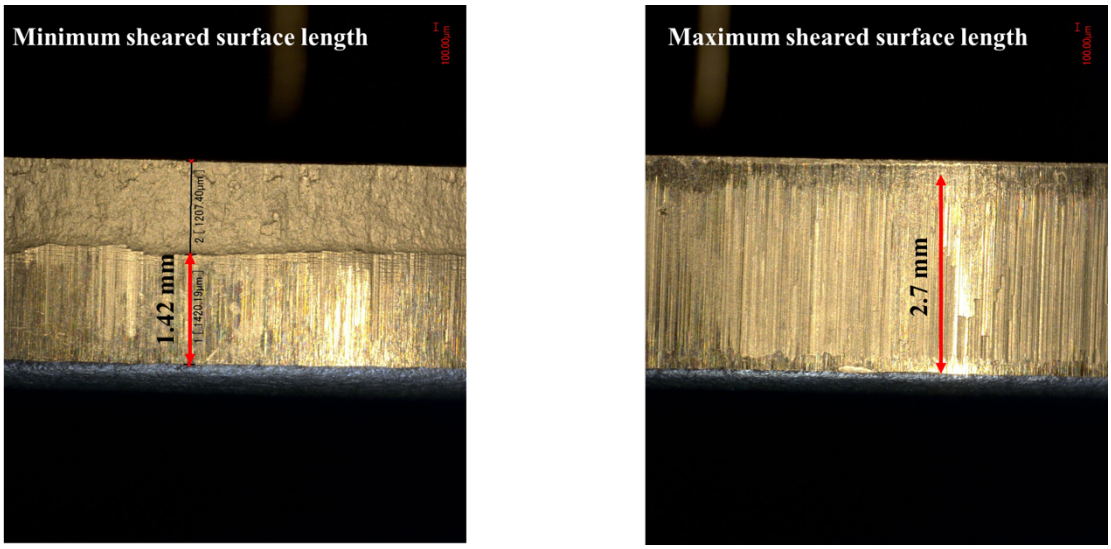

Fig. 3.21 Minimum and maximum sheared surface lengths obtained from the punching experiment with the punch diameter of 25 mm, blank thickness of 3.2 mm and clearance of 0.1 mm (3.125 %t).

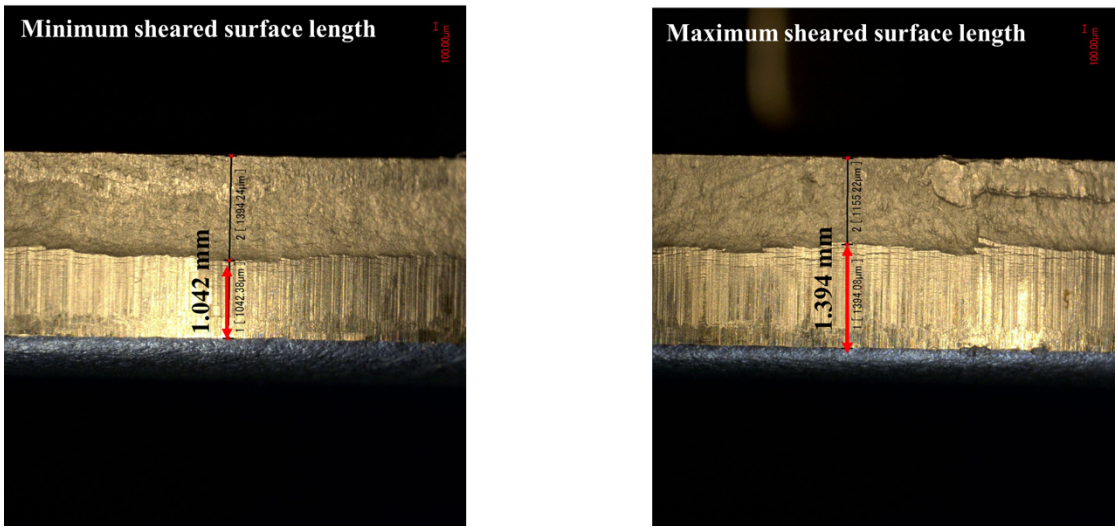

Fig. 3.22 Minimum and maximum sheared surface lengths obtained from the punching experiment with the punch diameter of 25 mm, blank thickness of 3.2 mm and clearance of 0.3 mm (9.375 %t).

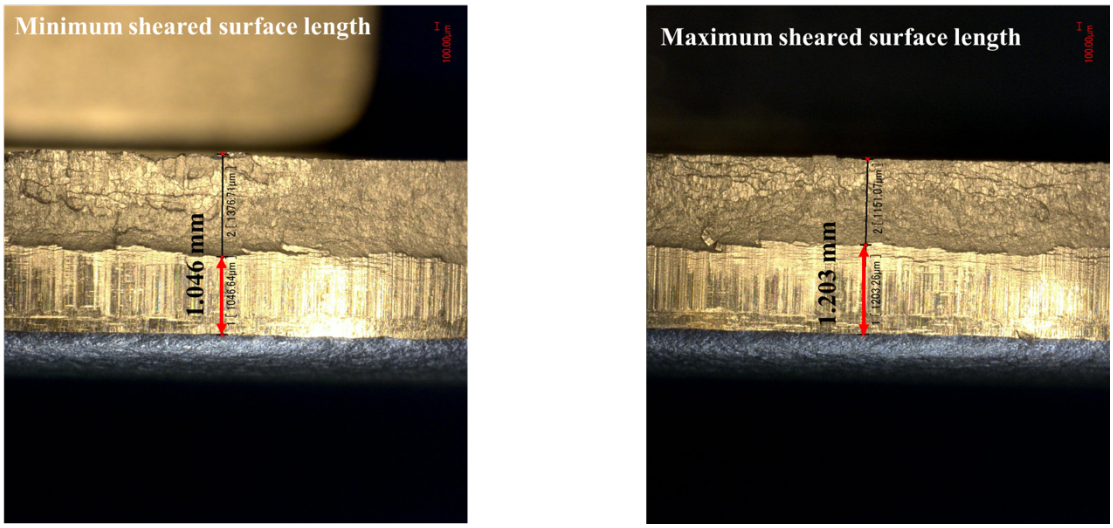

Fig. 3.23 Minimum and maximum sheared surface lengths obtained from the punching experiment with the punch diameter of 25 mm, blank thickness of 3.2 mm and clearance of 0.4 mm (12.5 %t).

The punch diameters and clearances used in the experiments, number of punching experiments, the minimum, maximum and the average sheared surface lengths obtained from the punching experiments for all conditions of the blank thickness of 1.6 mm are summarized in the Table 3.5 and conditions of blank thickness of 3.2 mm are summarized in the Table 3.6.

Table 3.5 Sheared surface lengths obtained from punching experiments (SPCC, t= 1.6 mm)

Sheared surface lengths for blank thickness of 1.6 mm, (SPCC)				
Punch diameter and clearance	No. of experiments	Minimum (mm)	Maximum (mm)	Average (mm)
ϕ10 CL0.1	1	0.612	0.859	0.736
	2	0.636	0.879	0.757
	3	0.659	0.794	0.727
	4	0.577	0.889	0.733
	5	0.588	0.801	0.694
	Average	0.615	0.845	0.729
ϕ10 CL0.3	1	0.399	0.443	0.421
	2	0.349	0.46	0.405
	3	0.379	0.477	0.429
	4	0.356	0.436	0.396
	5	0.354	0.436	0.395
	Average	0.368	0.45	0.406
ϕ10 CL0.4	1	0.328	0.46	0.394
	2	0.315	0.462	0.388
	3	0.312	0.412	0.362
	4	0.371	0.516	0.444
	5	0.328	0.419	0.373
	Average	0.331	0.454	0.392
ϕ15 CL0.1	1	0.621	1.008	0.815
	2	0.809	1.024	0.917
	3	0.64	1.001	0.82
	4	0.614	0.969	0.792
	5	0.579	1.002	0.791
	Average	0.653	1.001	0.827
ϕ20 CL0.1	1	0.499	0.985	0.742
	2	0.653	0.987	0.82
	3	0.644	1.013	0.829
	4	0.662	1.002	0.832
	5	0.727	0.972	0.849
	Average	0.637	0.992	0.815
ϕ25 CL0.1	1	0.77	0.881	0.826
	2	0.814	0.948	0.881
	3	0.625	0.929	0.777
	4	0.759	1.022	0.891
	5	0.72	1.029	0.874
	Average	0.738	0.962	0.849
ϕ25 CL0.3	1	0.44	0.582	0.511
	2	0.451	0.577	0.514
	3	0.509	0.525	0.518
	4	0.46	0.536	0.498
	5	0.449	0.54	0.495
	Average	0.462	0.552	0.507
ϕ25 CL0.4	1	0.379	0.434	0.407
	2	0.384	0.467	0.425
	3	0.373	0.712	0.393
	4	0.378	0.434	0.406
	5	0.349	0.351	0.35
	Average	0.373	0.419	0.396

Table 3.6 Sheared surface lengths obtained from punching experiments (SPCC, t= 3.2 mm)

Sheared surface lengths for blank thickness of 3.2 mm, (SPCC)				
Punch diameter and clearance	No. of experiments	Minimum (mm)	Maximum (mm)	Average (mm)
ϕ10 CL0.1	1	1.312	1.698	1.505
	2	1.346	1.733	1.539
	3	1.229	1.759	1.494
	4	1.264	1.789	1.527
	5	1.299	1.75	1.535
	Average	1.29	1.75	1.52
ϕ10 CL0.3	1	0.959	1.09	1.025
	2	0.964	1.103	1.034
	3	0.955	1.181	1.068
	4	0.882	1.055	0.969
	5	0.959	1.220	1.09
	Average	0.944	1.13	1.037
ϕ10 CL0.4	1	0.916	0.877	0.897
	2	0.869	1.129	0.999
	3	0.717	0.903	0.809
	4	0.942	0.895	0.919
	5	0.864	1.09	0.977
	Average	0.862	0.979	0.92
ϕ15 CL0.1	1	1.294	1.815	1.555
	2	1.246	2.648	1.947
	3	1.364	2.159	1.761
	4	1.325	1.976	1.65
	5	1.273	2.643	1.958
	Average	1.3	2.248	1.774
ϕ20 CL0.1	1	1.32	2.393	1.857
	2	1.351	2.098	1.724
	3	1.368	2.315	1.842
	4	1.351	2.445	1.898
	5	1.394	2.661	2.028
	Average	1.357	2.382	1.869
ϕ25 CL0.1	1	1.42	2.7	2.06
	2	1.342	2.726	2.034
	3	1.355	2.683	2.019
	4	1.342	2.696	2.019
	5	1.394	2.709	2.051
	Average	1.394	2.709	2.051
ϕ25 CL0.3	1	1.042	1.394	1.218
	2	1.138	1.338	1.238
	3	0.604	1.381	0.992
	4	1.116	1.138	1.127
	5	1.034	1.255	1.144
	Average	0.987	1.301	1.144
ϕ25 CL0.4	1	1.046	1.203	1.125
	2	0.916	1.142	1.029
	3	1.029	1.199	1.114
	4	0.899	1.242	1.071
	5	1.003	1.129	1.066
	Average	0.979	1.183	1.081

3.4.3 The ratio of sheared surface length to thickness

Table 3.7 The ratios of sheared surface length to thickness (SPCC, t= 1.6 mm)

The ratios of sheared surface length to thickness (*l*/*t*) (t=1.6 mm)				
Punch diameter and clearance	No. of experiments	Minimum	Maximum	Average
ϕ10 CL0.1	1	0.389	0.546	0.468
	2	0.404	0.559	0.481
	3	0.419	0.505	0.462
	4	0.367	0.566	0.466
	5	0.374	0.509	0.441
	Average	0.391	0.537	0.464
ϕ10 CL0.3	1	0.255	0.283	0.269
	2	0.223	0.294	0.259
	3	0.243	0.305	0.274
	4	0.227	0.279	0.253
	5	0.226	0.279	0.252
	Average	0.235	0.288	0.261
ϕ10 CL0.4	1	0.209	0.295	0.252
	2	0.202	0.296	0.249
	3	0.2	0.264	0.232
	4	0.238	0.331	0.284
	5	0.209	0.268	0.239
	Average	0.212	0.291	0.251
ϕ15 CL0.1	1	0.396	0.643	0.519
	2	0.516	0.653	0.585
	3	0.408	0.635	0.523
	4	0.392	0.619	0.505
	5	0.369	0.639	0.504
	Average	0.416	0.639	0.527
ϕ20 CL0.1	1	0.319	0.629	0.474
	2	0.417	0.631	0.524
	3	0.412	0.647	0.529
	4	0.423	0.641	0.532
	5	0.464	0.621	0.543
	Average	0.407	0.634	0.52
ϕ25 CL0.1	1	0.489	0.559	0.525
	2	0.517	0.602	0.559
	3	0.397	0.59	0.494
	4	0.483	0.649	0.566
	5	0.458	0.653	0.556
	Average	0.469	0.611	0.539
ϕ25 CL0.3	1	0.281	0.37	0.325
	2	0.287	0.367	0.328
	3	0.325	0.334	0.329
	4	0.293	0.341	0.317
	5	0.286	0.344	0.315
	Average	0.294	0.352	0.323
ϕ25 CL0.4	1	0.242	0.277	0.259
	2	0.245	0.298	0.271
	3	0.238	0.263	0.251
	4	0.241	0.276	0.259
	5	0.223	0.224	0.224
	Average	0.238	0.268	0.253

Table 3.8 The ratios of sheared surface length to thickness (SPCC, 3.2 mm)

The ratios of sheared surface length to thickness (l/t) (t= 3.2 mm)				
Punch diameter and clearance	No. of experiments	Minimum	Maximum	Average
ϕ10 CL0.1	1	0.419	0.543	0.481
	2	0.43	0.554	0.492
	3	0.393	0.562	0.477
	4	0.404	0.572	0.488
	5	0.415	0.566	0.491
	Average	0.412	0.559	0.486
ϕ10 CL0.3	1	0.309	0.351	0.329
	2	0.31	0.355	0.332
	3	0.307	0.379	0.344
	4	0.284	0.339	0.312
	5	0.309	0.393	0.351
	Average	0.304	0.363	0.334
ϕ10 CL0.4	1	0.295	0.283	0.289
	2	0.279	0.364	0.322
	3	0.231	0.291	0.261
	4	0.304	0.288	0.296
	5	0.278	0.351	0.315
	Average	0.278	0.315	0.296
ϕ15 CL0.1	1	0.416	0.584	0.5
	2	0.401	0.852	0.626
	3	0.439	0.695	0.567
	4	0.426	0.636	0.531
	5	0.409	0.851	0.63
	Average	0.418	0.723	0.571
ϕ20 CL0.1	1	0.425	0.77	0.597
	2	0.435	0.675	0.555
	3	0.44	0.745	0.593
	4	0.435	0.787	0.611
	5	0.449	0.856	0.652
	Average	0.437	0.767	0.602
ϕ25 CL0.1	1	0.457	0.869	0.663
	2	0.432	0.878	0.655
	3	0.436	0.864	0.649
	4	0.432	0.868	0.649
	5	0.449	0.87	0.66
	Average	0.441	0.87	0.656
ϕ25 CL0.3	1	0.336	0.449	0.393
	2	0.367	0.432	0.399
	3	0.195	0.446	0.32
	4	0.36	0.367	0.364
	5	0.334	0.405	0.369
	Average	0.318	0.419	0.369
ϕ25 CL0.4	1	0.338	0.388	0.363
	2	0.296	0.369	0.332
	3	0.332	0.387	0.359
	4	0.29	0.401	0.346
	5	0.324	0.365	0.344
	Average	0.316	0.382	0.349

The ratios of sheared surface length to thickness were calculated by using the sheared surface lengths form the Table 3.5 and 3.6. The ratios of sheared surface length to thickness for all cases are summarized in the Table 3.7 and 3.8.

The experimental results for the ratio of sheared surface length to thickness (*l/t*) (as a function of the clearance (percent thickness [%t]) for the different punch diameters are shown in the Fig. 3.24. The values of the ratios of sheared surface length to thickness are average values from the maximum and minimum values of ratio of sheared surface length to thickness. The figure shows that the increase in the clearance (%t) causes a decrease the length of the sheared plane on the cut surface. The experimental results show that the clearance is control parameter for the length of sheared surface. For the smallest clearance of 3.125 %t, the largest sheared surface can be obtained with the largest punch diameter of 25 mm. The difference between the lengths of sheared surfaces obtained with the punch diameters of 10 mm and 25 mm is the largest for the smallest clearance and decreases with increasing the clearances. The ratios of sheared surface length to thickness (*l/t*) obtained from the experiments were used in the FEA to determine the threshold value of ductile fracture criterion.

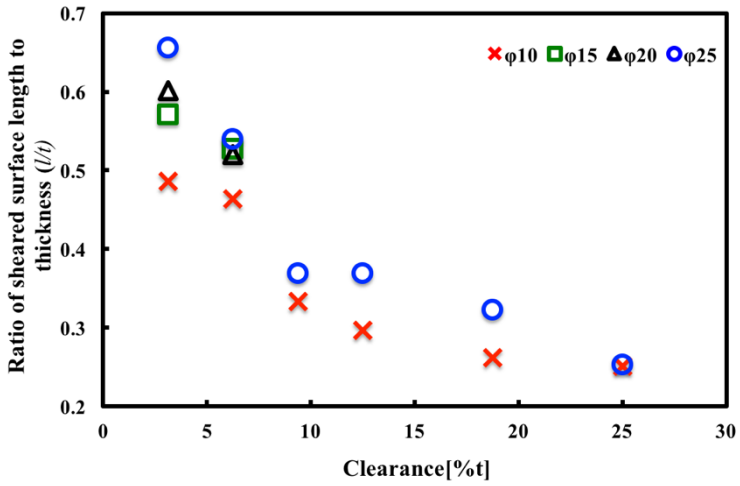

Fig. 3.24 The relationship between the ratio of sheared surface length to thickness and clearance obtained from the punching experiments by using the different punch diameters with the various clearances.

3.5 Experimental results of S45C

3.5.1 The blank thickness after punching

The thickness of the blank after each punching process under each clearance was measured and then the average value was calculated with the same procedure of SPCC. The results for the blank thicknesses of 1.6 mm and 3.2 mm are shown in the Table 3.9 and 3.10.

Table 3.9 Blank thicknesses after punching experiments of S45C (t= 1.6 mm)

Punch diameter [mm]	10			15	20	25		
Clearance [mm]	0.1 6.25 %t	0.3 18.75%t	0.4 25 %t	0.1	0.1	0.1	0.3	0.4
Blank thickness after punching [mm]	1.61	1.65	1.595	1.623	1.626	1.618	1.613	1.61
	1.615	1.605	1.595	1.625	1.621	1.613	1.615	1.61
	1.61	1.605	1.593	1.62	1.62	1.612	1.61	1.612
	1.612	1.60	1.592	1.62	1.62	1.62	1.615	1.615
	1.61	1.605	1.589	1.612	1.611	1.623	1.62	1.616
Average	**1.611**	**1.613**	**1.593**	**1.62**	**1.62**	**1.617**	**1.615**	**1.613**

Table 3.10 Blank thicknesses after punching experiments of S45C (t= 3.2 mm)

Punch diameter [mm]	10			15	20	25		
Clearance [mm]	0.1 3.125%t	0.3 9.375%t	0.4 12.75 %t	0.1	0.1	0.1	0.3	0.4
Blank thickness after punching [mm]	3.251	3.219	3.225	3.231	3.23	3.23	3.215	3.209
	3.251	3.218	3.22	3.238	3.228	3.224	3.217	3.209
	3.255	3.22	3.22	3.235	3.225	3.22	3.219	3.208
	3.25	3.209	3.223	3.231	3.23	3.229	3.213	3.209
	3.239	3.218	3.221	3.231	3.227	3.22	3.215	3.21
Average	**3.249**	**3.217**	**3.222**	**3.233**	**3.228**	**3.225**	**3.216**	**3.209**

3.5.2 The lengths of sheared and fracture surfaces

The minimum and maximum sheared surface lengths obtained from the first time (one time) punching experiment for the blank thicknesses of 1.6 and 3.2 mm and different clearances with the punch diameter of 10 mm are shown in the following Figures.

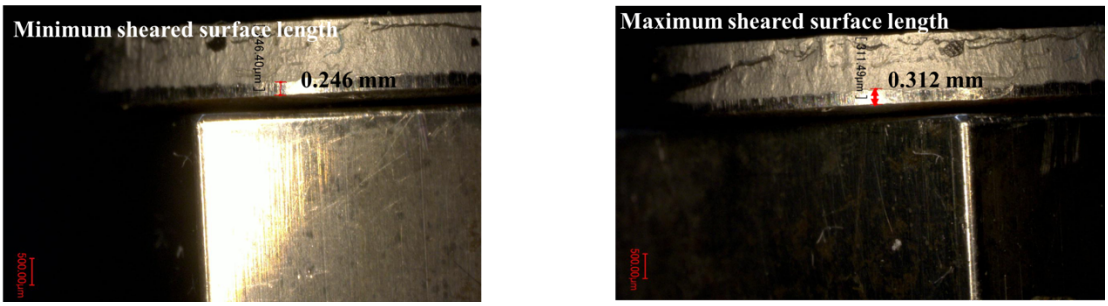

Fig. 3.25 Minimum and maximum sheared surface lengths obtained from the punching experiment with the punch diameter of 10 mm, blank thickness of 1.6 mm and clearance of 0.1 mm (6.25 %t).

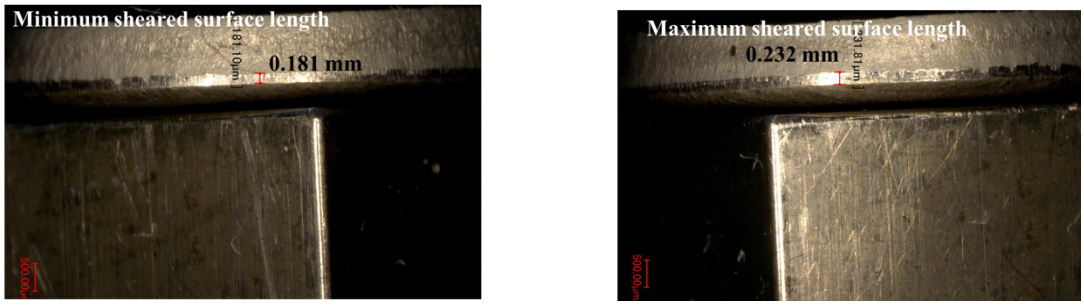

Fig. 3.26 Minimum and maximum sheared surface lengths obtained from the punching experiment with the punch diameter of 10 mm, blank thickness of 1.6 mm and clearance of 0.3 mm (18.75 %t).

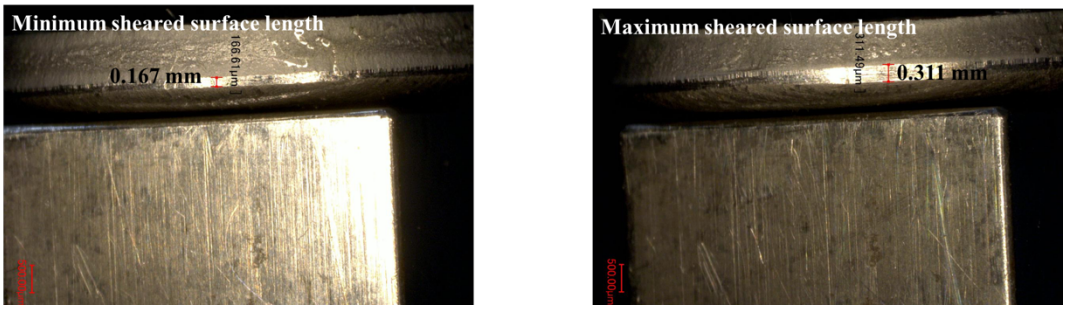

Fig. 3.27 Minimum and maximum sheared surface lengths obtained from the punching experiment with the punch diameter of 10 mm, blank thickness of 1.6 mm and clearance of 0.4 mm (25 %t).

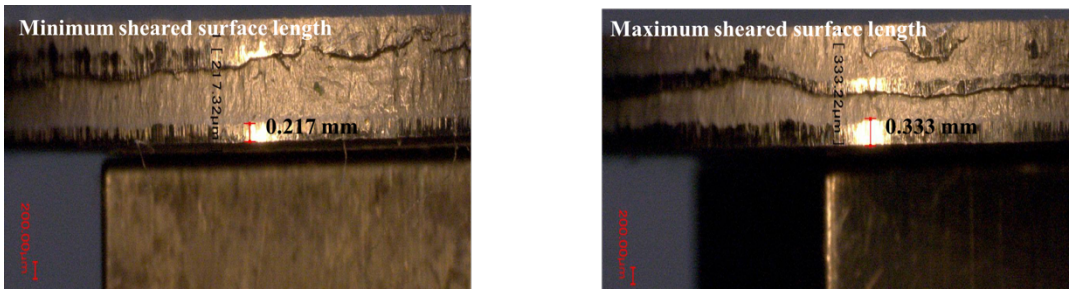

Fig. 3.28 Minimum and maximum sheared surface lengths obtained from the punching experiment with the punch diameter of 15 mm, blank thickness of 1.6 mm and clearance of 0.1 mm (6.25 %t).

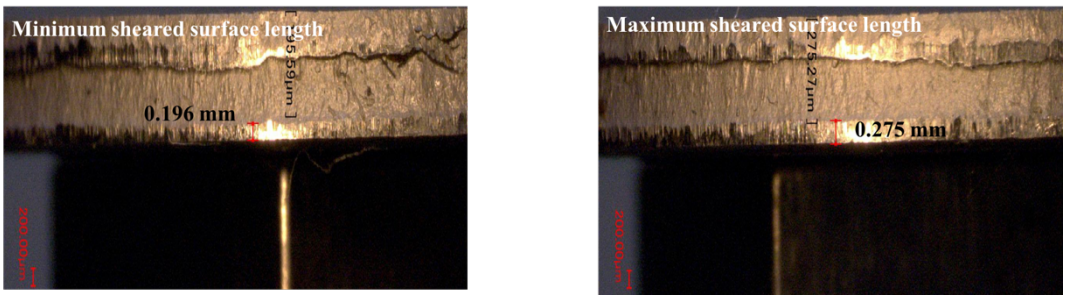

Fig. 3.29 Minimum and maximum sheared surface lengths obtained from the punching experiment with the punch diameter of 20 mm, blank thickness of 1.6 mm and clearance of 0.1 mm (6.25 %t).

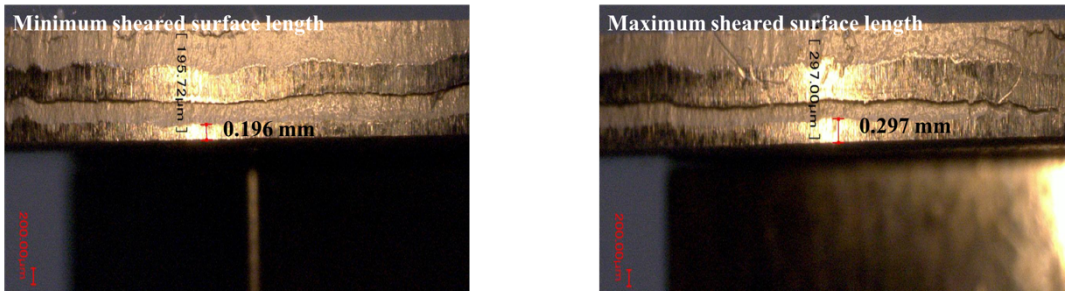

Fig. 3.30 Minimum and maximum sheared surface lengths obtained from the punching experiment with the punch diameter of 25 mm, blank thickness of 1.6 mm and clearance of 0.1 mm (6.25 %t).

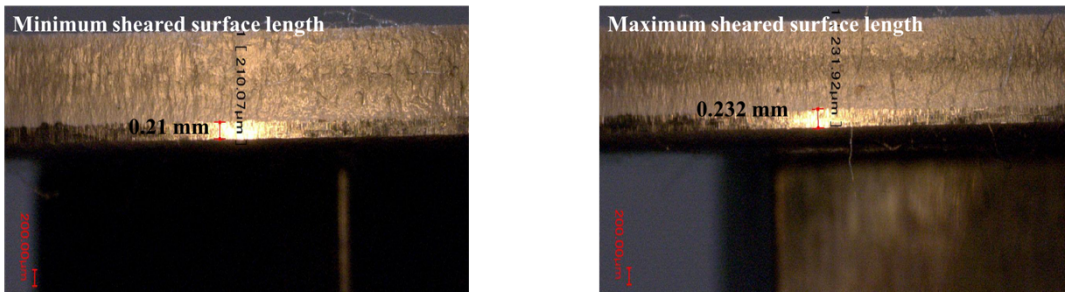

Fig. 3.31 Minimum and maximum sheared surface lengths obtained from the punching experiment with the punch diameter of 25 mm, blank thickness of 1.6 mm and clearance of 0.3 mm (18.75 %t).

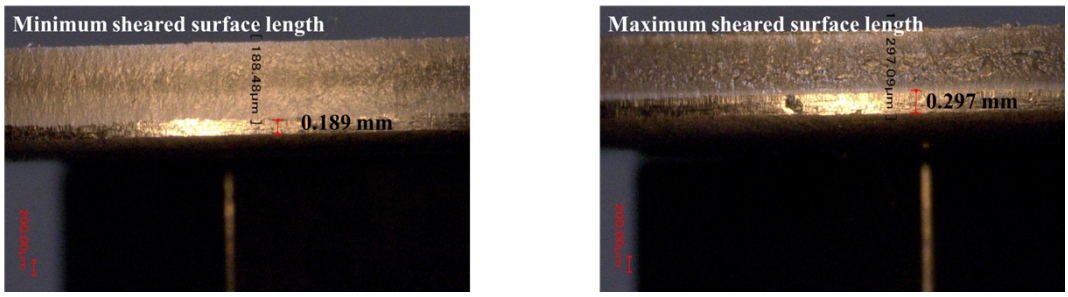

Fig. 3.32 Minimum and maximum sheared surface lengths obtained from the punching experiment with the punch diameter of 25 mm, blank thickness of 1.6 mm and clearance of 0.4 mm (25 %t).

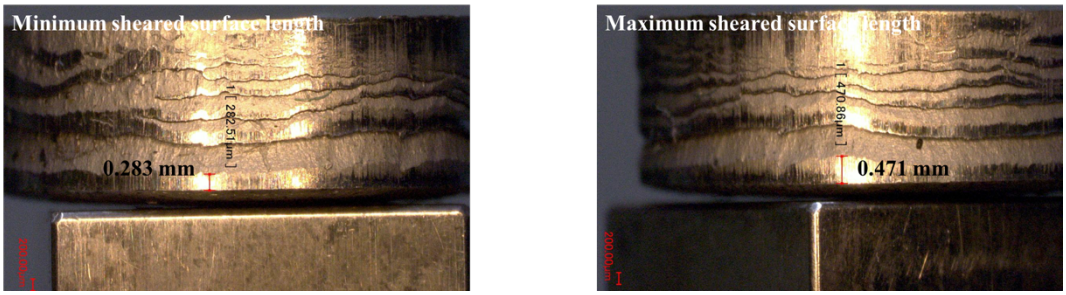

Fig. 3.33 Minimum and maximum sheared surface lengths obtained from the punching experiment with the punch diameter of 10 mm, blank thickness of 3.2 mm and clearance of 0.1 mm (3.125 %t).

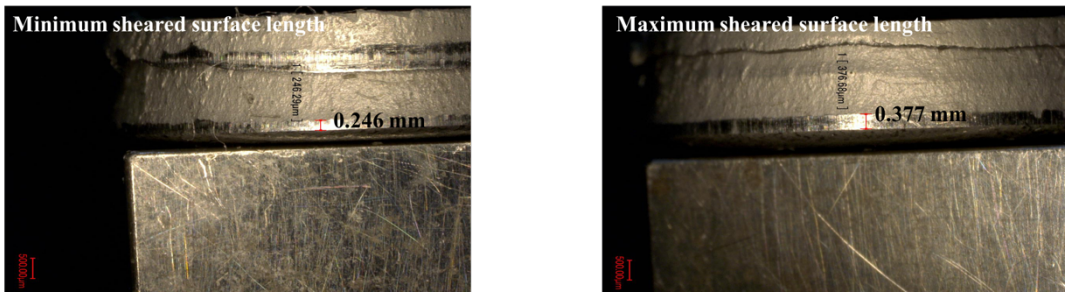

Fig. 3.34 Minimum and maximum sheared surface lengths obtained from the punching experiment with the punch diameter of 10 mm, blank thickness of 3.2 mm and clearance of 0.3 mm (9.375 %t).

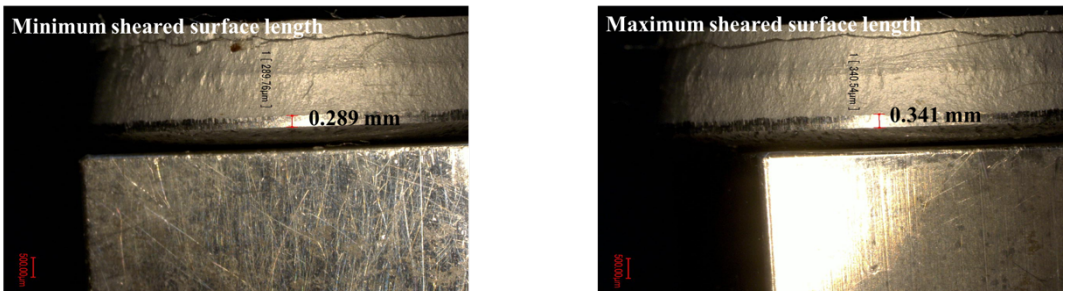

Fig. 3.35 Minimum and maximum sheared surface lengths obtained from the punching experiment with the punch diameter of 10 mm, blank thickness of 3.2 mm and clearance of 0.4 mm (12.5 %t).

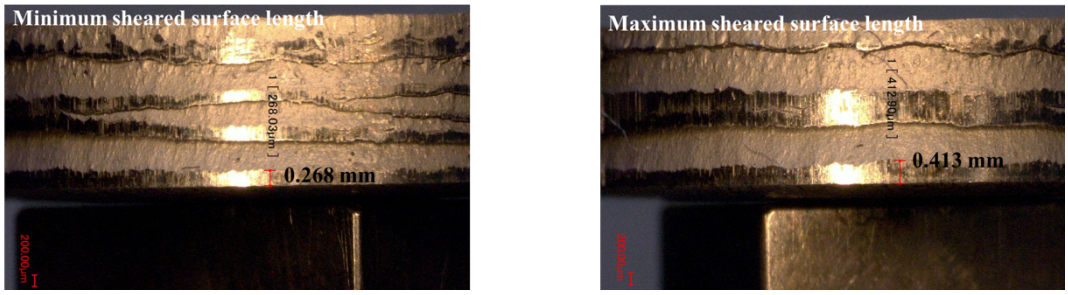

Fig. 3.36 Minimum and maximum sheared surface lengths obtained from the punching experiment with the punch diameter of 15 mm, blank thickness of 3.2 mm and clearance of 0.1 mm (3.125 %t).

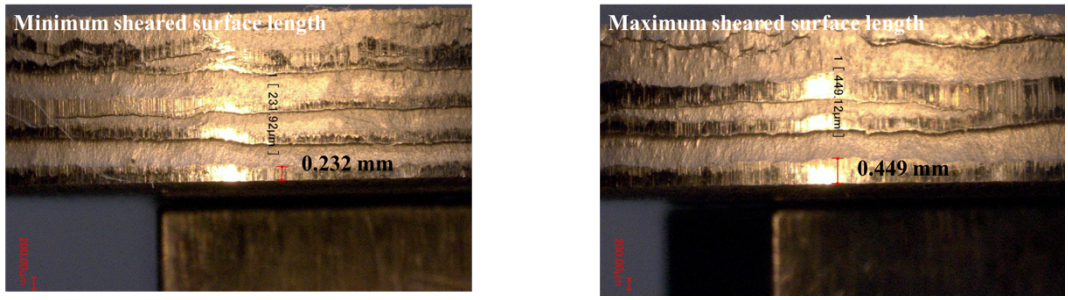

Fig. 3.37 Minimum and maximum sheared surface lengths obtained from the punching experiment with the punch diameter of 20 mm, blank thickness of 3.2 mm and clearance of 0.1 mm (3.125 %t).

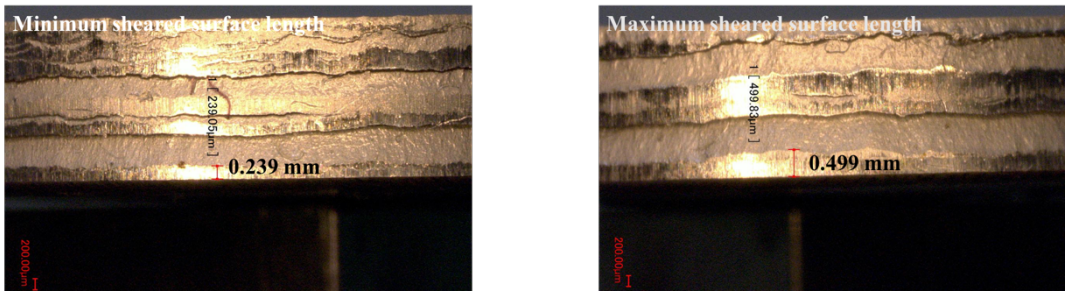

Fig. 3.38 Minimum and maximum sheared surface lengths obtained from the punching experiment with the punch diameter of 25 mm, blank thickness of 3.2 mm and clearance of 0.1 mm (3.125 %t).

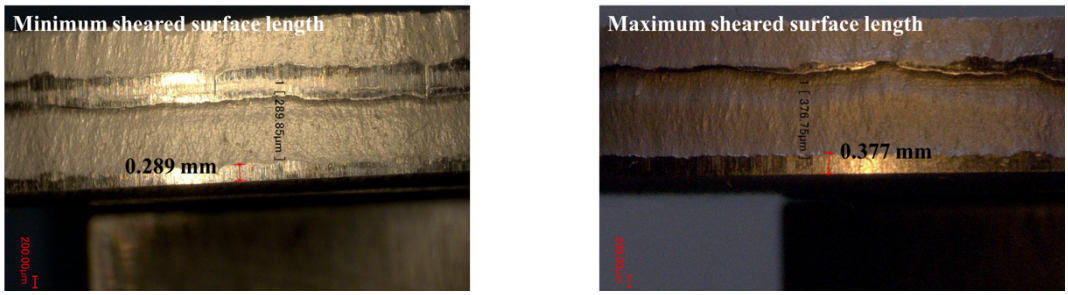

Fig. 3.39 Minimum and maximum sheared surface lengths obtained from the punching experiment with the punch diameter of 25 mm, blank thickness of 3.2 mm and clearance of 0.3 mm (9.375 %t).

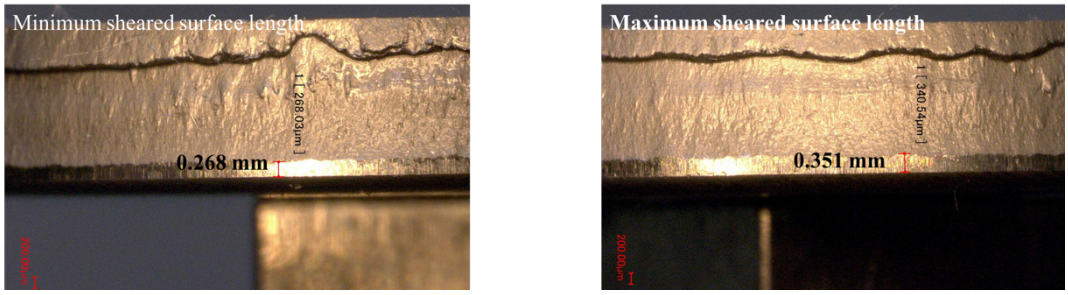

Fig. 3.40 Minimum and maximum sheared surface lengths obtained from the punching experiment with the punch diameter of 25 mm, blank thickness of 3.2 mm and clearance of 0.4 mm (12.5 %t).

The punch diameters and the clearances used in the punching experiments, the number of experiments, the experimental results, such as the value of minimum sheared surfaces, maximum sheared surfaces and the average values for all conditions of S45C are summarized in the Table 3.11 and 3.12.

Table 3.11 Sheared surface lengths obtained from the punching experiments (S45C, 1.6 mm)

Sheared surface lengths for blank thickness of 1.6 mm, (S45C)				
Punch diameter and clearance	No. of experiments	Minimum (mm)	Maximum (mm)	Average (mm)
ϕ10 CL0.1	1	0.246	0.312	0.279
	2	0.217	0.289	0.254
	3	0.232	0.341	0.286
	4	0.232	0.355	0.293
	5	0.239	0.297	0.268
	Average	0.233	0.319	0.276
ϕ10 CL0.3	1	0.181	0.232	0.206
	2	0.174	0.246	0.21
	3	0.188	0.261	0.225
	4	0.203	0.239	0.221
	5	0.188	0.253	0.221
	Average	0.187	0.246	0.217
ϕ10 CL0.4	1	0.167	0.311	0.239
	2	0.174	0.326	0.249
	3	0.188	0.304	0.246
	4	0.174	0.318	0.246
	5	0.167	0.311	0.239
	Average	0.174	0.314	0.244
ϕ15 CL0.1	1	0.217	0.333	0.275
	2	0.203	0.333	0.268
	3	0.217	0.283	0.249
	4	0.217	0.297	0.257
	5	0.196	0.319	0.257
	Average	0.21	0.313	0.262
ϕ20 CL0.1	1	0.196	0.275	0.236
	2	0.188	0.283	0.235
	3	0.181	0.304	0.243
	4	0.196	0.304	0.249
	5	0.225	0.355	0.289
	Average	0.197	0.304	0.251
ϕ25 CL0.1	1	0.196	0.297	0.246
	2	0.21	0.333	0.272
	3	0.21	0.275	0.243
	4	0.21	0.333	0.272
	5	0.21	0.304	0.257
	Average	0.27	0.309	0.258
ϕ25 CL0.3	1	0.21	0.232	0.221
	2	0.225	0.232	0.228
	3	0.188	0.239	0.214
	4	0.21	0.254	0.232
	5	0.196	0.261	0.228
	Average	0.206	0.243	0.225
ϕ25 CL0.4	1	0.189	0.297	0.243
	2	0.188	0.312	0.249
	3	0.203	0.304	0.254
	4	0.225	0.289	0.257
	5	0.196	0.283	0.239
	Average	0.199	0.297	0.248

Table 3.12 Sheared surface lengths obtained from the punching experiments (S45C, t= 3.2 mm)

Sheared surface lengths for blank thickness of 3.2 mm, (S45C)				
Punch diameter and clearance	No. of experiments	Minimum (mm)	Maximum (mm)	Average (mm)
ϕ10 CL0.1	1	0.283	0.471	0.377
	2	0.319	0.442	0.38
	3	0.268	0.529	0.395
	4	0.275	0.499	0.388
	5	0.275	0.449	0.362
	Average	0.284	0.478	0.381
ϕ10 CL0.3	1	0.246	0.377	0.312
	2	0.283	0.406	0.344
	3	0.276	0.369	0.323
	4	0.283	0.413	0.348
	5	0.261	0.369	0.315
	Average	0.269	0.387	0.328
ϕ10 CL0.4	1	0.289	0.341	0.315
	2	0.268	0.319	0.293
	3	0.283	0.348	0.315
	4	0.283	0.341	0.312
	5	0.275	0.348	0.312
	Average	0.279	0.339	0.309
ϕ15 CL0.1	1	0.268	0.413	0.341
	2	0.254	0.391	0.322
	3	0.232	0.427	0.329
	4	0.225	0.406	0.315
	5	0.239	0.413	0.326
	Average	0.243	0.41	0.327
ϕ20 CL0.1	1	0.232	0.449	0.341
	2	0.254	0.456	0.355
	3	0.246	0.369	0.308
	4	0.246	0.507	0.377
	5	0.268	0.384	0.326
	Average	0.249	0.433	0.341
ϕ25 CL0.1	1	0.239	0.499	0.369
	2	0.268	0.485	0.377
	3	0.232	0.485	0.359
	4	0.246	0.652	0.449
	5	0.261	0.456	0.359
	Average	0.249	0.516	0.382
ϕ25 CL0.3	1	0.289	0.377	0.333
	2	0.268	0.406	0.337
	3	0.268	0.427	0.348
	4	0.283	0.413	0.348
	5	0.246	0.42	0.333
	Average	0.271	0.409	0.339
ϕ25 CL0.4	1	0.268	0.351	0.309
	2	0.232	0.369	0.301
	3	0.254	0.333	0.293
	4	0.297	0.312	0.304
	5	0.254	0.333	0.293
	Average	0.261	0.339	0.3

The average of minimum sheared surface lengths, average of maximum sheared surface lengths and average of minimum and maximum sheared surface lengths are calculated by using the average values from the Table 3.11 and 3.12 and the results are shown in the Table 3.13.

Table 3.13 The average values of sheared surface lengths obtained from the punching experiments (S45C)

Average values of sheared surface length			
Punch diameter, blank thickness and clearance	Minimum (mm)	Maximum (mm)	Average (mm)
ϕ10, t1.6, CL 0.1	0.233	0.319	0.276
ϕ10, t1.6, CL 0.3	0.187	0.246	0.217
ϕ10, t1.6, CL 0.4	0.174	0.314	0.244
ϕ15, t1.6, CL 0.1	0.21	0.313	0.262
ϕ20, t1.6, CL 0.1	0.197	0.304	0.251
ϕ25, t1.6, CL 0.1	0.207	0.309	0.258
ϕ25, t1.6, CL 0.3	0.206	0.243	0.225
ϕ25, t1.6, CL 0.4	0.199	0.297	0.249
ϕ10, t3.2, CL 0.1	0.284	0.478	0.381
ϕ10, t3.2, CL 0.3	0.269	0.387	0.328
ϕ10, t3.2, CL 0.4	0.279	0.339	0.309
ϕ15, t3.2, CL 0.1	0.243	0.41	0.327
ϕ20, t3.2, CL 0.1	0.249	0.433	0.341
ϕ25, t3.2, CL 0.1	0.249	0.516	0.383
ϕ25, t3.2, CL 0.3	0.271	0.409	0.339
ϕ25, t3.2, CL 0.4	0.261	0.339	0.3

3.5.3 The ratio of sheared surface length to thickness (*l/t*)

The ratios of sheared surface length to thickness (*l/t*) were also calculated by using the values from the Table 3.13 to compare with the cutting length obtained from the finite element analysis. The results for the sheared surface length or the ratio of shared surface length to thickness are shown in the Table 3.14.

Through the results, the sheared surface length of S45C is smaller than SPCC for same experimental conditions, such as same punch diameter, clearance and blank thickness. The ratio of sheared surface length to thickness were plot against the clearance values and that was shown in the Fig. 3.41.

Table 3.14 The ratios of sheared surface length to thickness obtained from the punching experiments (S45C)

Punch diameter, blank thickness and clearance	Clearance (% thickness)	Minimum (*l*/*t*)	Maximum (*l*/*t*)	Average (*l*/*t*)
ϕ10, t1.6, CL 0.1	6.25	0.146	0.199	0.173
ϕ10, t1.6, CL 0.3	18.75	0.117	0.154	0.135
ϕ10, t1.6, CL 0.4	25	0.109	0.196	0.153
ϕ15, t1.6, CL 0.1	6.25	0.131	0.196	0.163
ϕ20, t1.6, CL 0.1	6.25	0.123	0.19	0.157
ϕ25, t1.6, CL 0.1	6.25	0.129	0.193	0.161
ϕ25, t1.6, CL 0.3	18.75	0.129	0.152	0.14
ϕ25, t1.6, CL 0.4	25	0.125	0.186	0.155
ϕ10, t3.2, CL 0.1	3.125	0.177	0.299	0.238
ϕ10, t3.2, CL 0.3	9.375	0.168	0.242	0.205
ϕ10, t3.2, CL 0.4	12.5	0.175	0.212	0.193
ϕ15, t3.2, CL 0.1	3.125	0.152	0.256	0.204
ϕ20, t3.2, CL 0.1	3.125	0.156	0.271	0.213
ϕ25, t3.2, CL 0.1	3.125	0.156	0.322	0.239
ϕ25, t3.2, CL 0.3	9.375	0.169	0.255	0.212
ϕ25, t3.2, CL 0.4	12.5	0.163	0.202	0.188

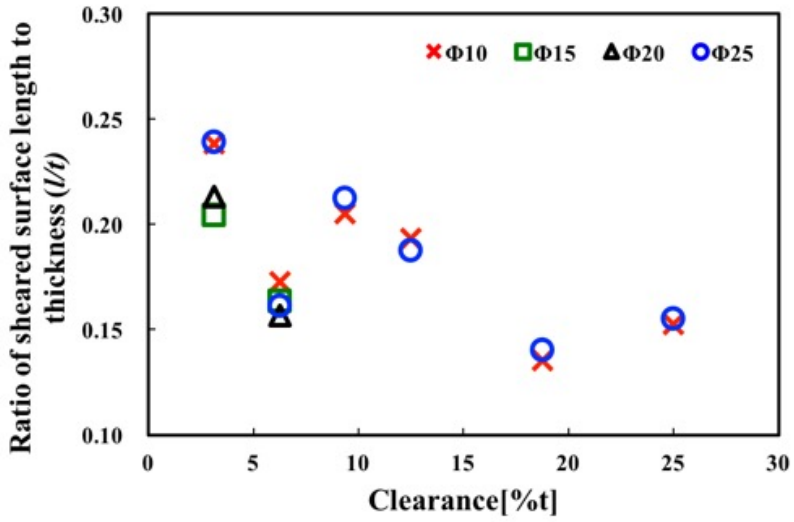

Fig. 3.41 The relationship between the ratio of sheared surface length to thickness and clearance obtained from the punching experiments by using the different punch diameters with the various clearances.

The figure shows the relationship between the ratio of sheared surface length to thickness and the clearance between the punch the die. The increase in the clearance causes a decrease in the ratio of sheared surface length to thickness. For S45C material, the difference between the sheared surface lengths obtained with the punch diameters of 10 mm and 25 mm for the smallest clearance of 3.125 %t are not significant. The sheared surface lengths obtained by different punch diameters for one clearance is the same. As an exceptional case, the sheared surface length obtained under the clearance of 6.25 %t is smaller than the sheared surface lengths obtained at the clearances of 9.375 %t and 12.5 %t. The ratios of sheared surface length to thickness which are used in the FEA to determine the threshold values of ductile fracture criteria are obtained from the Fig. 3.41.

The sheared surface length of SPCC is larger than that of S45C for same experimental conditions. For the smallest clearance of 3.125 %t, the difference between the sheared surface lengths obtained by the different punch diameters is high for the SPCC and it is not significant for S45C. Through the results, it was found that SPCC is higher ductility and secondary shear surface can be found on the cut surface of S45C.

Chapter (4) Ductile Fracture and Ductile Fracture Criteria

4.1 Introduction

Ductile materials usually fail with three stages, formation of a free surface at an inclusion or second-phase particle by either interface decohesion or particle cracking (void nucleation), growth of the void around the particle, by means of plastic strain and hydrostatic stress and the last one is coalescence of the growing void with adjacent voids [29]. The stages of ductile fracture are shown in the following.

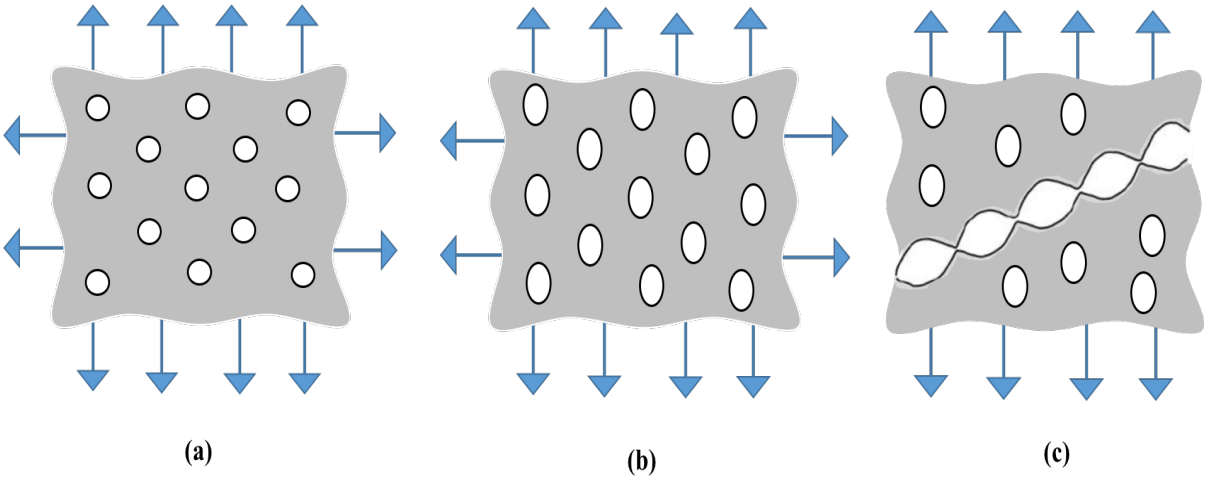

Fig. 4.1 Stages in the ductile fracture process, (a) void nucleation (b) void growth (c) void coalescence and fracture.

The voids can initiate at inclusions, secondary phase particles or at dislocation pile-ups. The growth and coalescence of voids are driven by the plastic deformation and it was taken into account in the deformation history of a ductile fracture model [29].

4.2 Characteristics of stress state

When the material was applied by a load, the stress states are appeared in the material and these stress states lead elastic deformation, plastic deformation and failure. In elastic deformation, the deformation under tensile load is characterized by Hooke`s law and the state of stress and strain depend on Young`s modulus and Poisson`s ratio. However, plastic deformation is described by hardening curves and different plasticity models. The stress states can be expressed by various formulas and their associated geometrical interpretations. The homogeneous and isotropic material can take the form of three stress invariants [30]. The three invariants of the stress tensor are shown below.

$$J_1 = \sigma_1 + \sigma_2 + \sigma_3 = 3\sigma_m \tag{4-1}$$

$$J_2 = \frac{1}{6}[(\sigma_1 - \sigma_2)^2 + (\sigma_1 - \sigma_3)^2 + (\sigma_2 - \sigma_3)^2] \tag{4-2}$$

$$J_3 = (\sigma_1 - \sigma_m)(\sigma_2 - \sigma_m)(\sigma_3 - \sigma_m) \tag{4-3}$$

where, σ_1, σ_2, σ_3 and σ_m are three principal stresses and hydrostatic stress or mean stress, respectively. J_1, J_2 and J_3 are first stress invariant, second stress invariant and third stress invariant and the von Mises stress $\bar{\sigma}$ is defined as the function of second invariant and can be expressed as below.

$$\bar{\sigma} = \sqrt{3J_2} \tag{4-4}$$

The researchers use some special parameters such as stress triaxiality η, maximum shear stress ratio ϕ, normalized third stress invariant ξ, and lode angle θ, parameters to study the behavior of ductile fracture. The definition of these parameters are described below [31].

$$\eta = \frac{\sigma_m}{\bar{\sigma}} \tag{4-5}$$

$$\phi = \frac{\tau_{max}}{\bar{\sigma}} = \frac{\sigma_1 - \sigma_3}{2\bar{\sigma}} \tag{4-6}$$

$$\xi = \frac{27J_3}{2\bar{\sigma}^3} \tag{4-7}$$

$$\bar{\theta} = 1 - \frac{6\theta}{\pi} = 1 - \frac{2}{\pi} arccos\xi \tag{4-8}$$

The above mentioned parameters and formulas are used depending on the coordinate system. Bai and Wierzbicki [32] built the deviatoric plane (p plane) with three coordinate systems in the principal stress space. The mean stress, von Mises stress and lode angle parameters are for the cylindrical coordinate system and mean stress, stress triaxiality and lode angle parameters are for the spherical coordinate system.

4.3 Ductile fracture criteria

The choice of the appropriate fracture criterion is important in the prediction of ductile fracture initiation in the metal forming processes. Ductile fracture criteria are implemented by using the physical and mathematical models based on experimentally-gathered data. Factors such as the the stress and strain path, hydrostatic stress, and the stress triaxiality have a major impact on the material failure. Generally, a fracture indicator can be viewed as an integral over an interval from zero to the maximum plastic strain which leads to fracture [30] and If the deformation and loading reach a critical value, the material will start to fracture. The fracture criteria can be divided into two groups such as coupled and uncoupled models. The coupled models can be divided into mechanism based models and continuum damage mechanics (CDM) based models. The uncoupled models are also known as phenomenological models.

4.3.1 Mechanism based models

From the microscopic point of view, the effects of micro-voids in the ductile fracture were studied by McClintock and Rice and Tracey [1,3]. Gurson and Tvergaard analyzed the plastic flow in porous medium by assuming that the material behaves as a continuum. Gurson and Tvergaard studied the effect of hydrostatic stress on the yield surface although the classical plasticity assumes that yielding surface is independent of hydrostatic stress [5,6]. Tvergaard and Needleman replaced void volume fraction with an effective void volume fraction. GTN model approaches for describing the ductile fracture behavior as a consequence of micro-void nucleation, growth and coalescence [33]. Gurson model can be described as the following.

$$\phi = (\frac{\bar{\sigma}}{\sigma_0})^2 + 2f cosh\left(-\frac{3\sigma_m}{2\sigma_0}\right) - 1 - f^2 = 0 \qquad (4\text{-}9)$$

where, σ_0 is the flow stress of the material, f is the void volume fraction , $\bar{\sigma} = \sqrt{\frac{3}{2}\boldsymbol{s}:\boldsymbol{s}}$ is the von Mises equivalent stress, $\boldsymbol{s}$ is the deviatoric part of the stress tensor and σ_m =- *trace(σ)/3* is the hydrostatic stress.

The equation (4-9) was modified by Tvergaard and Needleman and they introduced two constitutive coefficients q_1 and q_2 for the interaction effects between the voids. The modified version was shown in the bellow.

$$\phi = (\frac{\bar{\sigma}}{\sigma_0})^2 + 2q_1 f^* cosh\left(-\frac{3q_2\sigma_m}{2\sigma_0}\right) - (1 + {q_1}^2 {f^*}^2) = 0 \qquad (4\text{-}10)$$

Here, f^* is the effective void volume fraction, the relation between f^* and f was introduced by Tvergaard and Needleman for the simulation of the coalescence between the voids and its function is shown below.

$$f^* = \begin{cases} f & for\ f \le f_c \\ f_c + (f - f_c)\dfrac{f_u - f_c}{f_f - f_c} & for\ f > f_c \end{cases} \tag{4-11}$$

Here, f_c is the critical value of the void volume fraction, $f_u = {}^1/_{q_1}$ is ultimate void volume fraction and f_f is the void volume fraction at fracture. The evolution of voids ($\dot{f}$) includes existing voids growth ($\dot{f}_{growth}$) and new voids nucleation ($\dot{f}_{nucleation}$).

$$\dot{f} = \dot{f}_{growth} + \dot{f}_{nucleation} \tag{4-12}$$

The growth of voids was described in the equation (4-13) and the new void nucleation was described in the equation (4-14).

$$\dot{f}_{growth} = (1 - f)\dot{\varepsilon}_v \tag{4-13}$$

$$\dot{f}_{nucleation} = \frac{f_N}{S_n\sqrt{2\pi}} exp\left[-\frac{1}{2}\left(\frac{\varepsilon_M^p - \varepsilon_n}{S_n}\right)\right]\dot{\varepsilon}_M^p \tag{4-14}$$

In the above equations, $\dot{\varepsilon}_v$ is the volume strain-rate, f_N is the void volume fraction for nucleation of new void, S_n is the standard deviation of the distribution, $\dot{\varepsilon}_M^p$ is the equivalent plastic strain rate and ε_n is mean nucleating strain.

The predictive accuracy of the mechanism based model depends on the material constants involved in the model. There are nine material constants in the model and the values of parameters are determined by experimentally.

4.3.2 Continuum damage mechanics model

Continuum Damage Mechanics (CDM) approaches the failure process in a given material from a local point of view. Damage takes into account the progressive degradation of the material properties and the loss of stiffness due to the irreversible process of void nucleation and growth [34].

N. Bonora derived the damage model to predict the ductile fracture. It is derived in the continuum damage mechanics framework and the stress is replaced by the effective stress although the constitutive equations for the damaged material and undamaged material are same. The formulation differs from others for the following features: damage reduces material stiffness only, no softening of the flow curve, damage accumulates only under tensile (positive stress triaxiality) state of stress, damage effects are temporarily restored under compression and damage evolution with plastic strain is characterized by only four parameters [35]. Bonora model can be described with the following equation.

$$dD = \alpha \frac{(D_{cr}-D_0)^{1/\alpha}}{\ln(\varepsilon_{cr})-\ln(\varepsilon_{th})} f\left(\frac{\sigma_H}{\sigma_{eq}}\right)(D_{cr}-D_0)^{\alpha-1/\alpha}\frac{dp}{p} \tag{4-15}$$

Here, D_0 is the initial amount of damage, ε_{th} is plasticity damage occurred only after a specific strain level, ε_{cr} is strain at failure, D_{cr} is critical damage value, α is the damage exponent, p is effective equivalent plastic strain.

The predictive accuracy of the CDM based models also depends on the material constants involved in the model. Four parameters are involved in this model and these parameters are determined by experimentally.

4.3.3 Phenomenological models

The uncoupled models are also known as the phenomenological models. These models are based on the geometry of defects (enlargement of voids), growth mechanism and material behavior. The phenomenological ductile fracture criteria can be considered as a process of damage accumulation without an actual damage parameter. In these criteria, the critical ductile fracture criteria can be determined by a combination of known deformation quantities such as stress and strain. The uncoupled ductile fracture criterion was written as an integral of stress and strain history over plastic strain (ε_p) up to fracture of a certain function of the stress state.

The criteria can also be easily implemented in the commercial finite element codes. Some phenomenological models [36] are described below.

Cockcroft-Latham

$$\int_0^{\varepsilon_R} \frac{\sigma_{max}}{\sigma_{eq}} d\varepsilon_{eq} = C_1 \tag{4-16}$$

Oyane

$$\int_0^{\varepsilon_R} (\alpha + \frac{\sigma_H}{\sigma_{eq}}) d\varepsilon_{eq} = C_2 \tag{4-17}$$

Ayada

$$\int_0^{\varepsilon_R} (\frac{\sigma_H}{\sigma_{eq}}) d\varepsilon_{eq} = C_3 \tag{4-18}$$

Rice and Tracey

$$\int_0^{\varepsilon_R} \exp\left(1.5 \frac{\sigma_H}{\sigma_{eq}}\right) d\varepsilon_{eq} = C_4 \tag{4-19}$$

Freudenthal

$$\int_0^{\varepsilon_R} \sigma_{eq} d\varepsilon_{eq} = C_5 \tag{4-20}$$

Brozzo

$$\int_0^{\varepsilon_R} \frac{2}{3} (\frac{\sigma_{max}}{\sigma_{max} - \sigma_H}) d\varepsilon_{eq} = C_6 \tag{4-21}$$

Norris

$$\int_0^{\varepsilon_R} (\frac{1}{1 - c\sigma_H}) d\varepsilon_{eq} = C_7 \tag{4-22}$$

Atkins

$$\int_0^{\varepsilon_R} (\frac{1 + {}^1\!/_{2L}}{1 - c\sigma_H}) d\varepsilon_{eq} = C_6 \tag{4-23}$$

In the above expressions, σ_{max} is maximum principal stress, hydrostatic stress $\sigma_H = 1/3(\sigma_1 + \sigma_2 + \sigma_3)$, equivalent von Mises stress $\sigma_{eq} = ({}^{1}/_{2}\,[(\sigma_1 - \sigma_2)^2 + (\sigma_2 - \sigma_3)^2 + (\sigma_3 - \sigma_1)^2])^{0.5}$, ε_R is the strain at fracture, equivalent plastic strain $\varepsilon_{eq} = ({}^{2}/_{3}\,({\varepsilon_1}^2 + {\varepsilon_2}^2 + {\varepsilon_3}^2))^{0.5}$, triaxiality ${}^{\sigma_H}/_{\sigma_{eq}}$, $L = {}^{d\varepsilon_1}/_{d\varepsilon_2}$, α and C are material constants.

The coupled models have parameters that require calibration. In order to implement the coupled constitutive models, long duration experimental data are required for the model parameter calibration and is computationally expensive. On the other hand, the existing phenomenological models have an acceptable accuracy in the prediction of ductile fracture initiation in the conventional punching and fine blanking processes.

In this research, phenomenological ductile fracture criteria were used to predict fracture initiation and to determine the values of critical ductile fracture criteria. The common phenomenological criteria, Cockcroft-Latham shown in the equation (4-16), Oyane shown in the equation (4-17) and Ayada shown in the equation (4-18) chosen from the literature and aforementioned research were used in this research. There are no constant values in the Cockcroft-Latham and Ayada criteria. The Cockcroft-Latham criterion considers the effect of the maximum principal stress over the plastic strain path, whereas the Ayada model is based on the stress triaxiality. Meanwhile, the Oyane criterion is derived from the plasticity theory of porous materials; in that criterion, the value of parameter α can be varied to obtain a valid ductile fracture model.

Chapter (5) Finite Element Analysis (FEA) of Punching Processes

5.1 Introduction

Numerical simulations are widely used to optimize the metal forming processes. The prediction and understanding of the nature of sheet metals in the metal forming process can be obtained by numerical analysis. The finite element method has been applied to the analysis of the behavior of the cut surfaces in conventional punching, fine blanking and other metal forming processes.

In this research, the commercial FEM codes MSC.Marc.Mentat and MSC.Marc were used to create FEA model of the punching process to analyze the punching process, respectively. The axisymmetric model of the blank and punch-die set is shown in the Fig. 5.1.

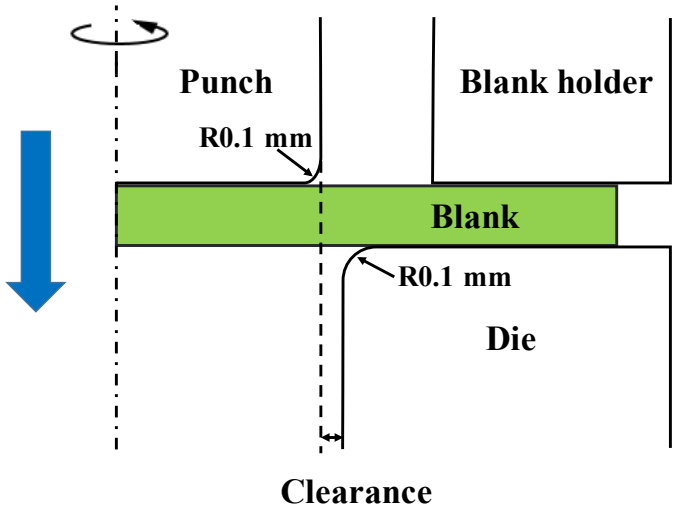

Fig. 5.1 Axisymmetric model of the blank and punch-die set with the values of punch and die corner radii used in the finite element analysis of punching process.

The FEA model of the test specimens is rectangular in shape, with an outside diameter of 40 mm and thicknesses of 1.6 and 3.2 mm. The radii of the cutting edges of the punch and die are 0.1 mm. The punch diameters and the clearances for the numerical analysis are the same with the values used in the experiments.

5.2 Conditions of FEA model

The conditions of the FEA model, initial contact region, local refinement region and boundary conditions are depicted in the Fig. 5.2

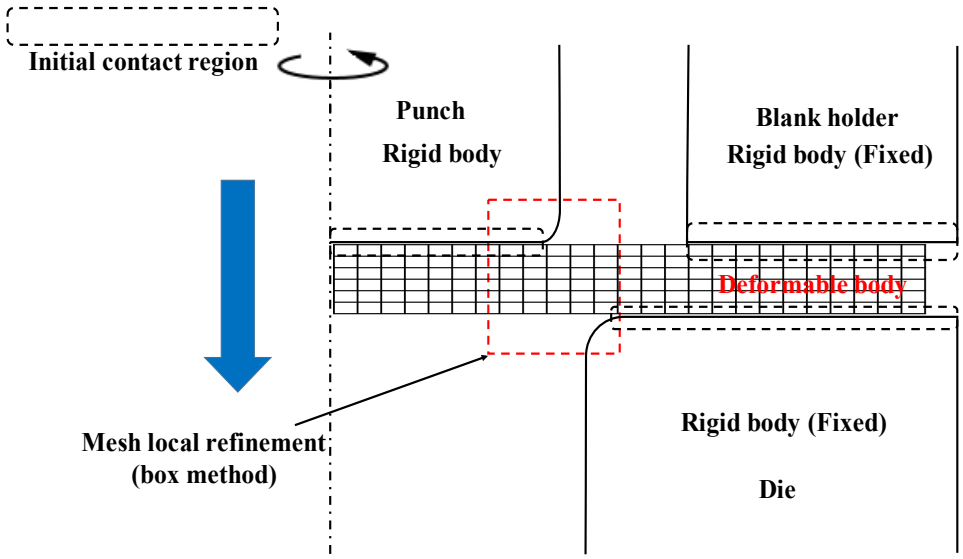

Fig. 5.2 Axisymmetric model of the blank and punch-die set with the mesh local refinement region, initial contact region and boundary conditions, used in the finite element analysis of punching process.

Axisymmetric four-node linear elements were used in the analysis. The punch and the die were considered to be rigid bodies and the blank was considered to be deformable elastic-plastic body. The automatic remeshing function with the advancing front-quad and the box method for the mesh local refinement were applied. The element length was changed to 0.01 mm after remeshing. The contact type of node to segment contact was applied by assuming no friction between the rigid bodies and deformable elastic-plastic one.

The yield criterion for the plasticity property, Von Mises yield criterion with table input method was used to predict the fracture initiation in the punching process. The isotropic hardening rule with piecewise linear strain rate method was used. The conditions of FEA model are shown in the Table 5.1.

Table 5.1 Blank thickness, number of elements, number of nodes and initial element length of finite element analysis model for punching process.

	Blank thickness	
	1.6 mm	3.2 mm
Initial number of elements	5000	10000
Initial number of nodes	5271	10291
Initial element length [mm]	0.08	0.08
Minimum element length after remeshing [mm]	0.01	0.01

5.3 Prediction of fracture initiation

The user subroutines ELEVAR (which makes element quantities available at the end of each increment) and plotv (which is used to capture the mean stress in MSC.Marc) were used to create the program with ductile fracture criteria proposed by Cockcroft-Latham, Oyane and Ayada. The distributions of ductile fracture criteria, (C) values were calculated along the cutting length obtained from the numerical analysis of punching process. The value of fracture criterion (C) which shows the shear limit point or fracture initiation point was determined by using the ratio of sheared surface length to thickness (l/t) obtained from the punching experiments. The results for SPCC are shown in the Fig. 5.3 and Fig. 5.4.

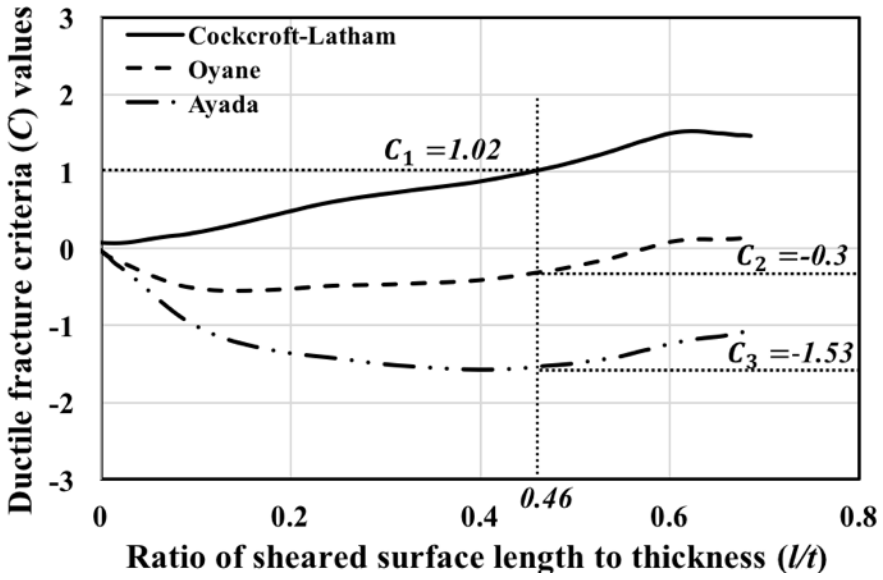

Fig. 5.3 The relationships between the fracture criteria (C) values and ratio of sheared surface length to thickness (punch diameter 10 mm, blank thickness 1.6 mm and clearance of 6.25 %t).

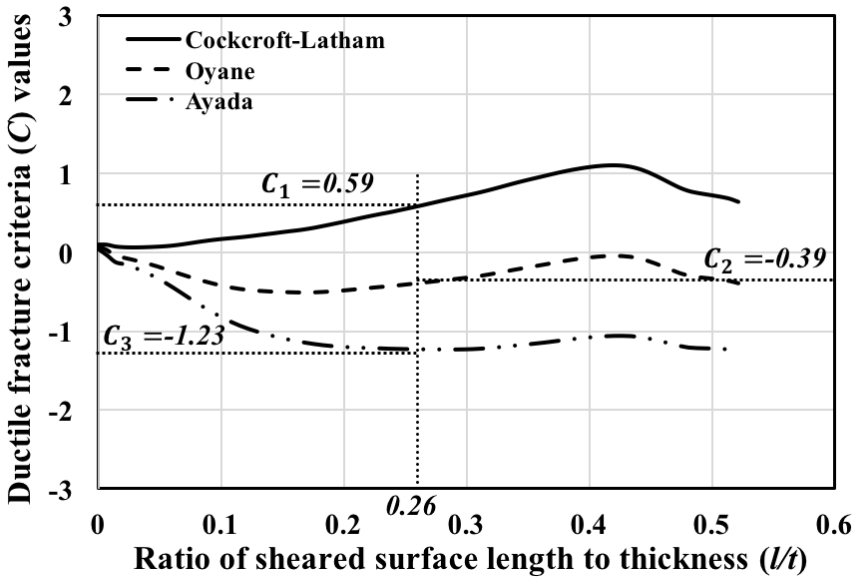

Fig. 5.4 The relationships between the fracture criteria (*C*) values and ratio of sheared surface length to thickness (punch diameter 10 mm, blank thickness 1.6 mm and clearance of 18.75 %t).

The figures show the results for the blank thickness of 1.6 mm, the punch diameter of 10 mm and clearances of 6.25 %t and 18.75 %t, respectively. The value of the ductile fracture criterion proposed by Cockcroft-Latham tended to increase monotonically during the punching process. The threshold value can be determined from a particular deformation path. The threshold values of Cockcroft-Latham (C_1) are 1.02 for the clearance of 6.25 %t and 0.59 for the clearance of 18.75 %t. The hydrostatic stress in the criteria of Oyane and Ayada is negative during punching process and hence the criteria (C_2) and (C_3) are negative values.

The threshold values for other cases were also calculated and the values of critical ductile fracture criteria for all punch diameters and clearances were plotted against the ratio of sheared surface length to thickness (*l/t*) obtained from the experiments and the clearance (%t) between the punch and the die. The results for SPCC are shown in the Fig. 5.5 and Fig. 5.6.

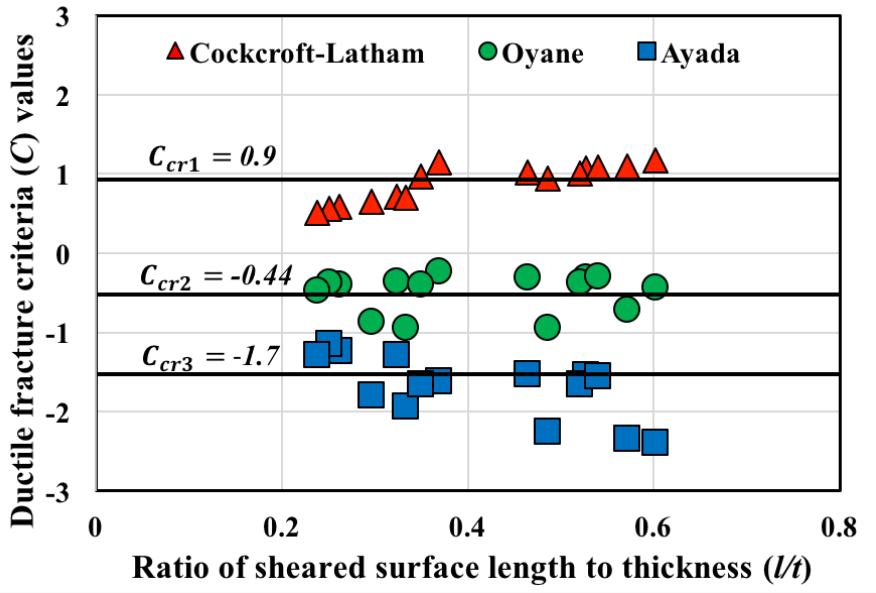

Fig. 5.5 Determination of the value of critical ductile fracture criteria from the relationship between the ratio of sheared surface length to thickness and ductile fracture criteria (C) values (SPCC).

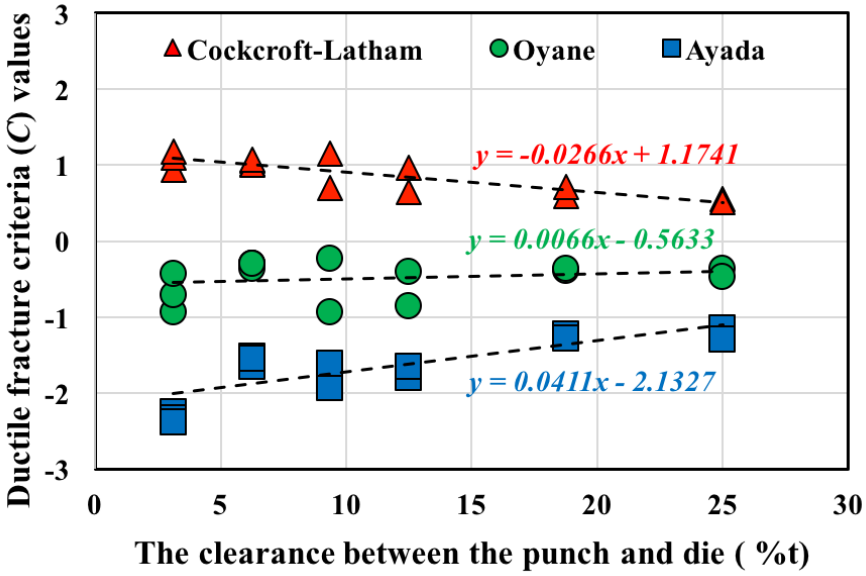

Fig. 5.6 Determination of the value of the critical ductile fracture criteria from the relationship between the ductile fracture criteria and the clearance between the punch and the die (SPCC).

The average value of threshold values, which show the shear limit point for each clearance and punch diameter is assumed to be the critical value of each criterion for the material SPCC. However, the difference between the threshold values obtained by Oyane

criterion is minimum for all the ratios of sheared surface length to thickness than other two criteria of Cockcroft-Latham and Ayada. Through the results from the Fig. 5.6, it is found that the threshold values obtained by Cockcroft-Latham criterion decrease with increasing the clearance between the punch and the die. The threshold values obtained by Ayada criterion increase with the increasing the clearance between the punch and the die. The minimum difference between each threshold values can be obtained by Oyane criterion and through the results it can not be assumed that the critical ductile fracture criterion value is material constant.

The same procedure was performed for S45C to determine the values of critical ductile fracture criteria which can be used in the actual punching process and the results are shown in the following.

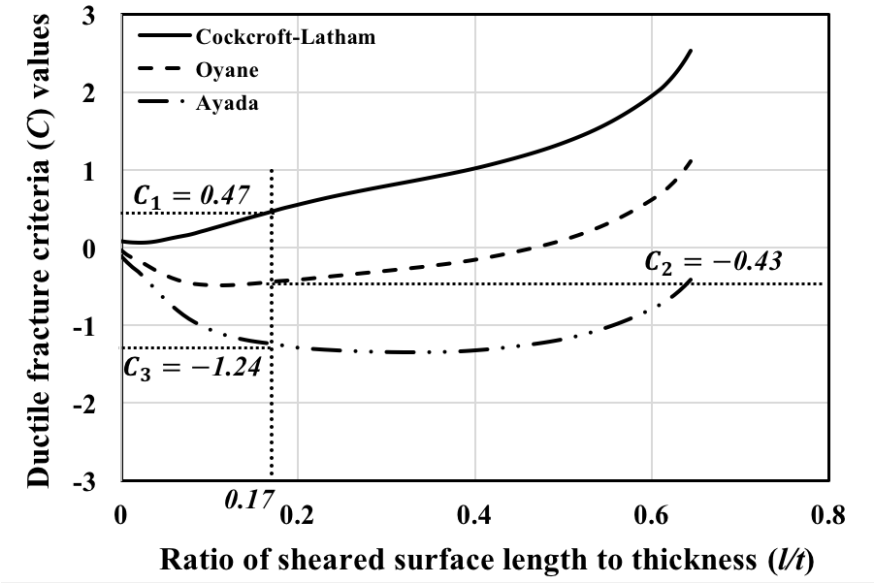

Fig. 5.7 The relationships between the fracture criteria (C) values and ratio of sheared surface length to thickness (punch diameter 10 mm, blank thickness 1.6 mm and clearance of 6.25 %t, S45C).

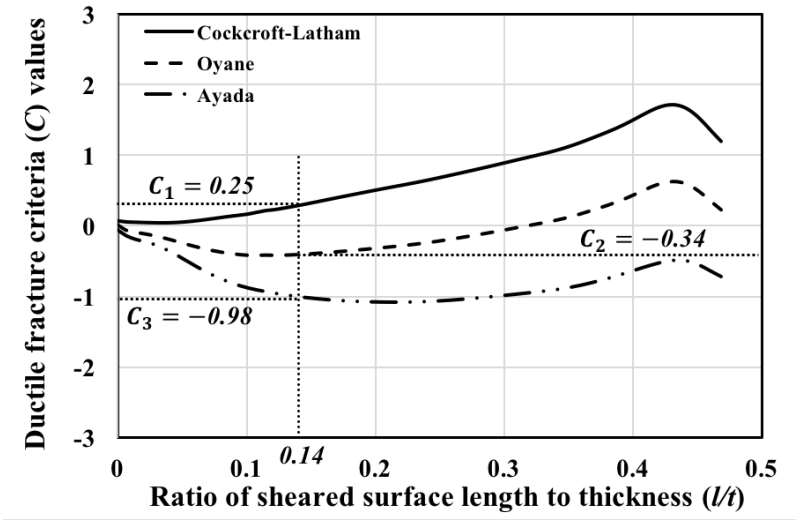

Fig. 5.8 The relationships between the fracture criteria (C) values and ratio of sheared surface length to thickness (punch diameter 10 mm, blank thickness 1.6 mm and clearance of 18.75 %t, S45C).

The Figures 5.7 and 5.8 show the results obtained by the punch diameter of 10 mm, the blank thickness of 1.6 mm and the clearances of 6.25 %t and 18.75 %t. It can be found that the threshold value which shows the shear limit point decreases with the decreasing the sheared surface length and increasing the clearance. The variation of damage distribution is same as SPCC. The value of the ductile fracture criterion proposed by Cockcroft-Latham tended to increase monotonically during the punching process. The threshold value can be determined from a particular deformation path and the criteria (C_2) and (C_3) are negative values because of negative hydrostatic stress during punching process. The threshold values for all cases were plotted against the ratio of sheared surface length to thickness and the clearance between the punch and the die and the relationships are shown in the Fig. 5.9 and Fig. 5.10.

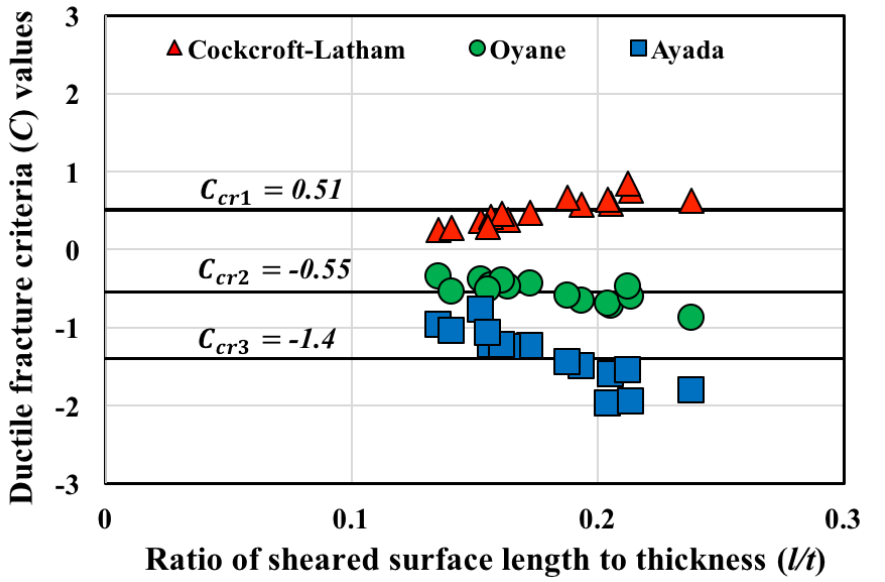

Fig. 5.9 Determination of the value of critical ductile fracture criteria from the relationship between the ratio of sheared surface length to thickness and ductile fracture criteria (C) values (S45C).

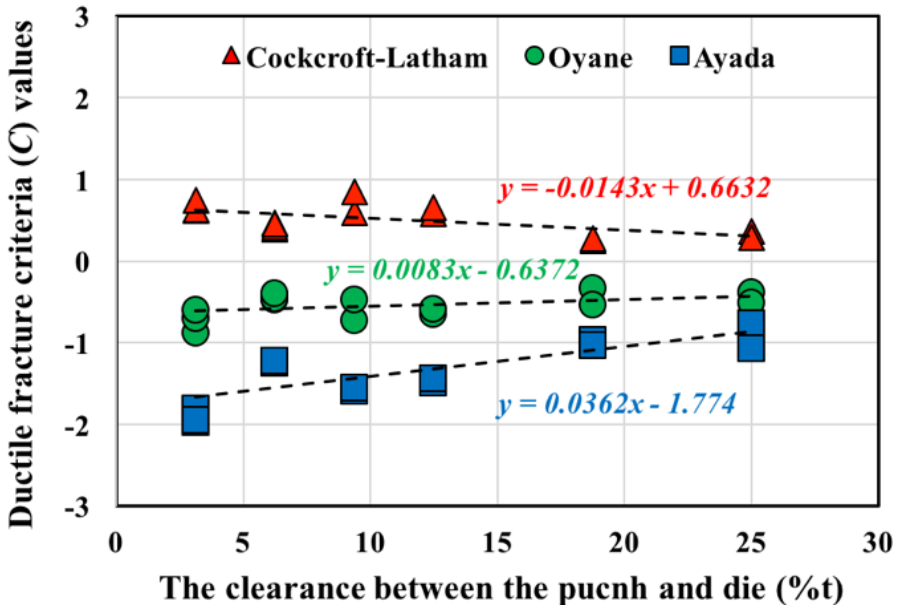

Fig. 5.10 Determination of the value of the critical ductile fracture criteria from the relationship between the ductile fracture criteria and the clearance between the punch and the die (S45C).

The same procedure like SPCC, the average values of threshold values, which show the shear limit point for each clearance and punch diameter are assumed to be the critical values of fracture criteria for the material S45C. The variation of three criteria for the different ratios

of sheared surface length to thickness and for the different clearances are similar. The minimum difference between each value can be obtained from the Oyane criterion. However, the difference between each value in Oyane criterion makes difficult to assume that the critical ductile fracture criterion (C) is constant for one material. The Cockcroft-Latham and Ayada criteria show that the critical ductile fracture criteria vary with the clearance. The Oyane parameter, α value used in the above analysis (0.32) is the value of S35C. Hence, the appropriate Oyane parameter, α value for SPCC and S45C will be calculated and the relationship between the clearance and the critical ductile fracture criteria (C) values will be determined.

5.4 Determination of Oyane parameter

The Oyane parameter, α value is material-dependent and it is important to use an appropriate value to get valid ductile fracture criterion for one material. The appropriate α value was chosen according to the following procedure. The value was chosen so that the same value of the Oyane criterion (C) was determined for both the punching process and uniaxial tensile test. Firstly, the distribution of (C) along the cutting length obtained from the simple punching process was calculated by FEA in MSC.Marc for different α values. The distributions of Oyane criterion for SPCC and S45C are shown in the Fig. 5.11 and Fig. 5.12.

The figures show the distribution of Oyane ductile fracture criteria (C) values for the different α values obtained from the FEA of punching process with the blank thickness of 1.6 mm, the punch diameter of 10 mm and the clearance of 6.25 %t.

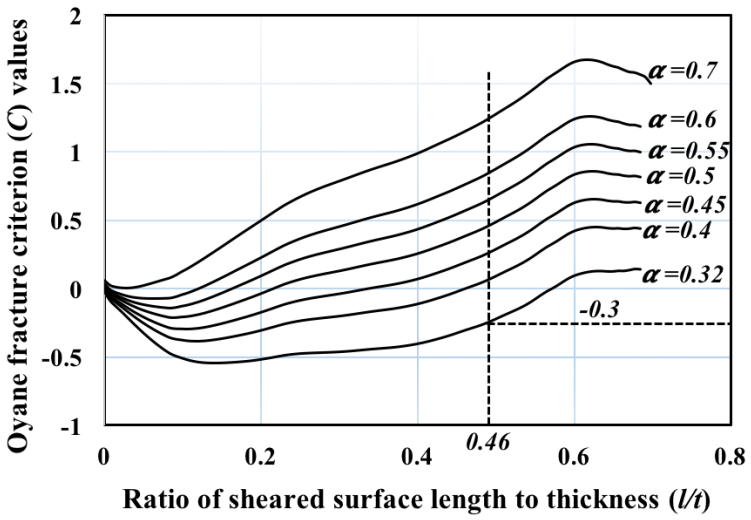

Fig. 5.11 The distribution of Oyane fracture criterion (C) values along the cutting length of punched surface for different α values (SPCC).

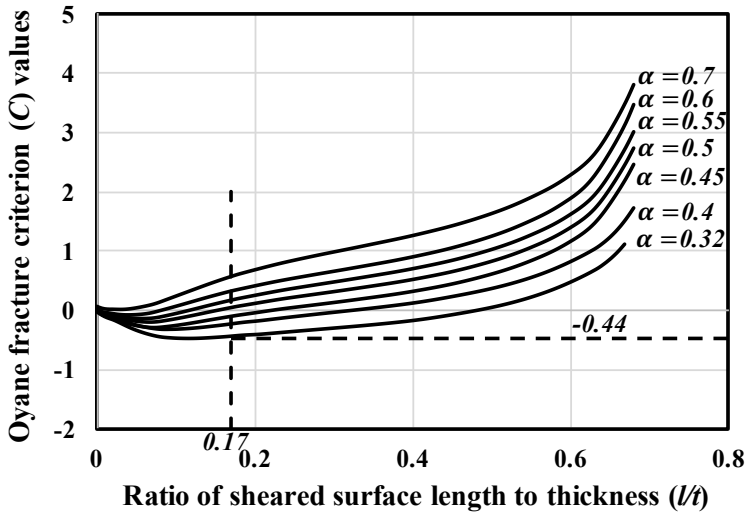

Fig. 5.12 The distribution of Oyane fracture criterion (C) values along the cutting length of punched surface for different α values (S45C).

The figures show the influences of α values on the Oyane fracture criterion. The values of critical ductile fracture criteria (C) for all α values were determined by comparing the cutting lengths obtained from the FEA with the ratios of sheared surface length to thickness obtained from the punching experiments. The critical value of Oyane criterion with α=0.32 is -0.44 for S45C and -0.3 for SPCC and the critical values for other cases were also determined.

Hence, the values of critical ductile fracture criteria of SPCC and S45C for different values of α are obtained from the Fig. 5.11 and Fig. 5.12.

Secondly, the values of critical ductile fracture criterion, Oyane for the uniaxial tensile case were calculated according to the following procedure. The fracture strain value obtained from the uniaxial tensile test and the same α (0.32-0.7) values like the punching process analysis were used in the Oyane model. The stress triaxiality, $\frac{\sigma_H}{\sigma_{eq}}$ in the model is equal to 1/3 in the case of uniaxial loading. The values of critical ductile fracture criteria, (C) values were obtained by inserting the fracture strain, 1/3 in the place of $\frac{\sigma_H}{\sigma_{eq}}$, and α values in the Oyane fracture criterion equation. The appropriate value of Oyane parameter (α= 0.55) for SPCC and (α= 0.6) for S45C were then selected from the best fits to the two (C) values. The new Oyane parameters were used to investigate the relationships between the fracture criteria and the clearances between the punch and the die.

5.5 Determination of the value of critical ductile fracture criterion, (C) value (SPCC)

The predictions of fracture initiation point in punching process were performed to determine the value of critical ductile fracture criteria (C) values of SPCC by using the new chosen Oyane parameter in the Oyane criterion. The results are shown in the Figures 5.13-5.17.

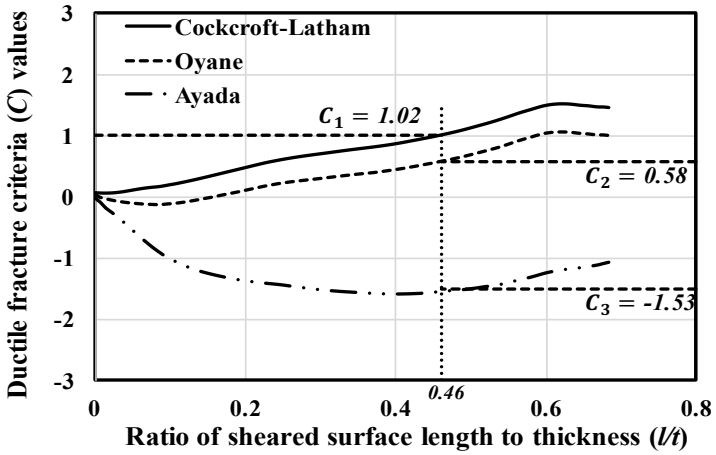

Fig. 5.13 The relationships between the fracture criteria (C) values and ratio of sheared surface length to thickness (punch diameter 10 mm, blank thickness 1.6 mm and clearance of 6.25 %t).

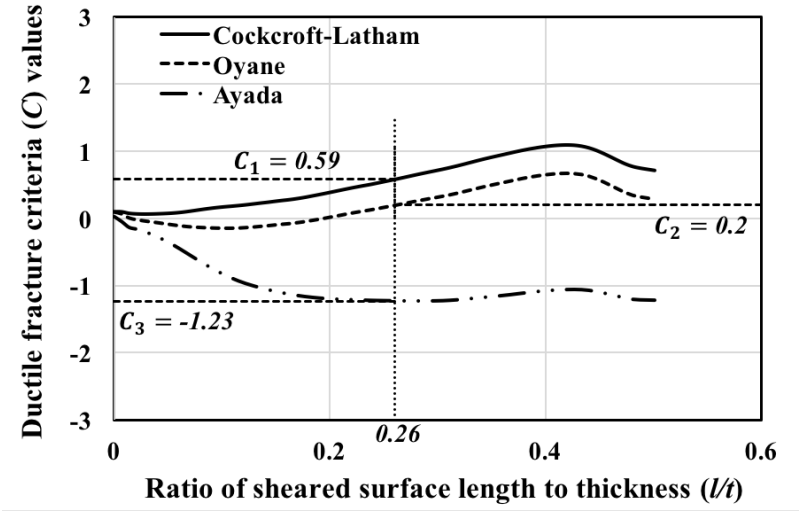

Fig. 5.14 The relationships between the fracture criteria (*C*) values and ratio of sheared surface length to thickness (punch diameter 10 mm, blank thickness 1.6 mm and clearance of 18.75 %t).

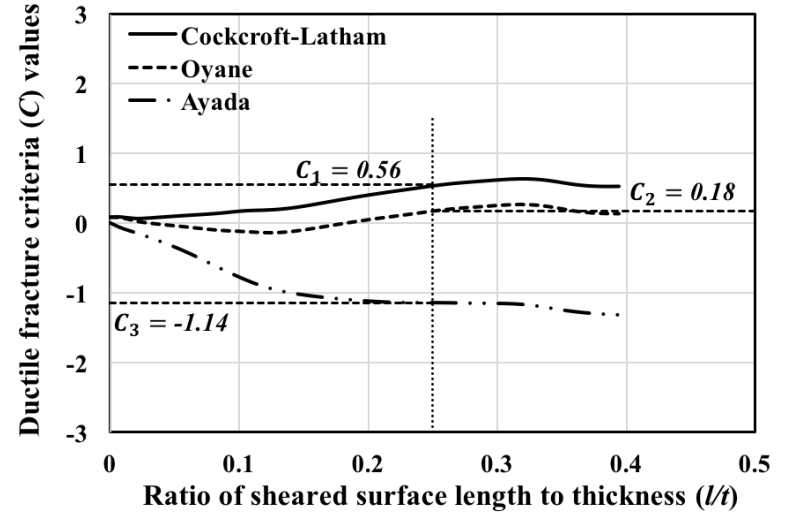

Fig. 5.15 The relationships between the fracture criteria (*C*) values and ratio of sheared surface length to thickness (punch diameter 10 mm, blank thickness 1.6 mm and clearance of 25 %t).

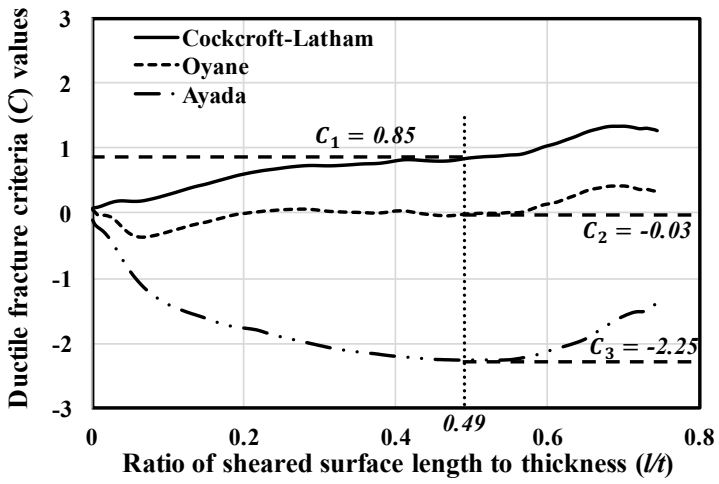

Fig. 5.16 The relationships between the fracture criteria (C) values and ratio of sheared surface length to thickness (punch diameter 10 mm, blank thickness 3.2 mm and clearance of 3.125 %t).

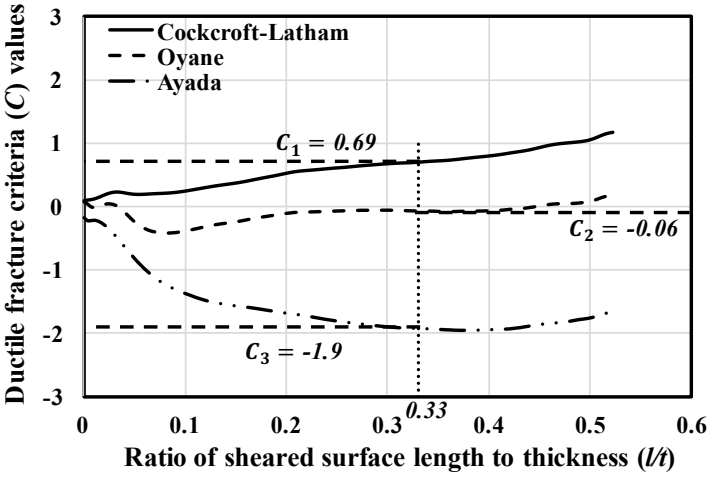

Fig. 5.17 The relationships between the fracture criteria (C) values and ratio of sheared surface length to thickness (punch diameter 10 mm, blank thickness 3.2 mm and clearance of 9.375 %t).

The figures show that the criteria obtained from Ayada model decrease during punching and increase again after fracture initiation point. The threshold values which show fracture initiation point obtained from the Ayada model are negative because the compressive hydrostatic stress along the cutting surface is negative. Through the results, it is found that the value of the ductile fracture criterion tended to increase monotonically during the punching process in the Cockcroft-Latham and Oyane criteria for the blank thickness of 1.6 mm.

However, the monotonically tended increasing is not obtained from the Oyane criterion for the blank thickness of 3.2 mm and the threshold values are still negative. Hence, 5000 elements were used for both thicknesses to achieve reasonable approximation during remeshing, especially for the Oyane criterion and the critical ductile fracture criteria (*C*) values were determined. The results are shown in the Figures 5.18-5.20.

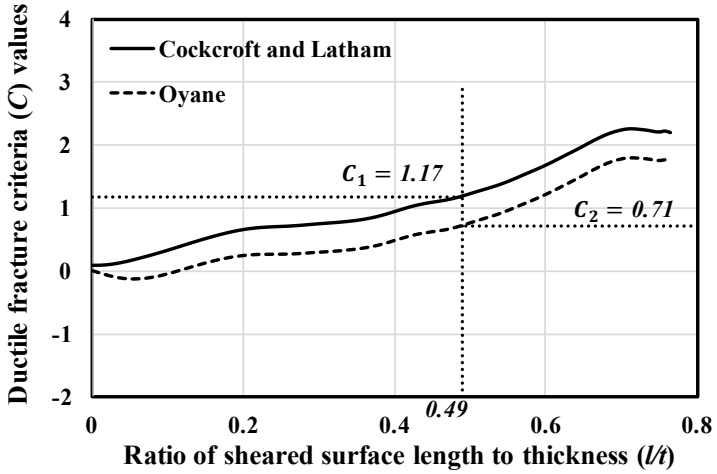

Fig. 5.18 The relationships between the value of ductile fracture criteria and the ratio of sheared surface length (t=3.2, punch diameter 10, clearance 0.1, numbers of element 5000).

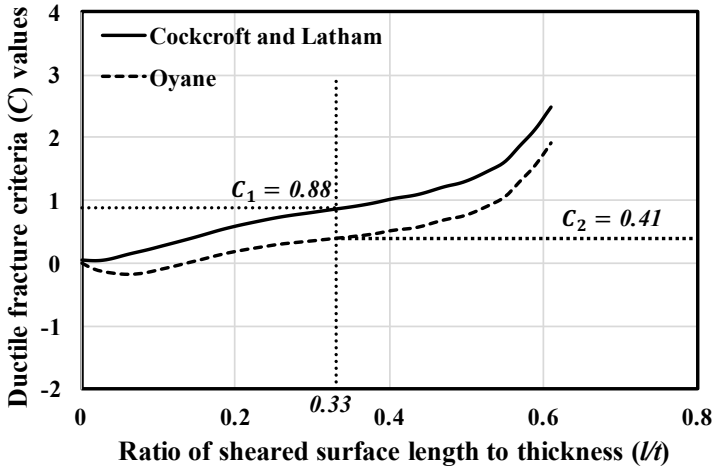

Fig. 5.19. The relationships between the value of ductile fracture criteria and the ratio of sheared surface length (t=3.2, punch diameter 10, clearance 0.3, numbers of element 5000).

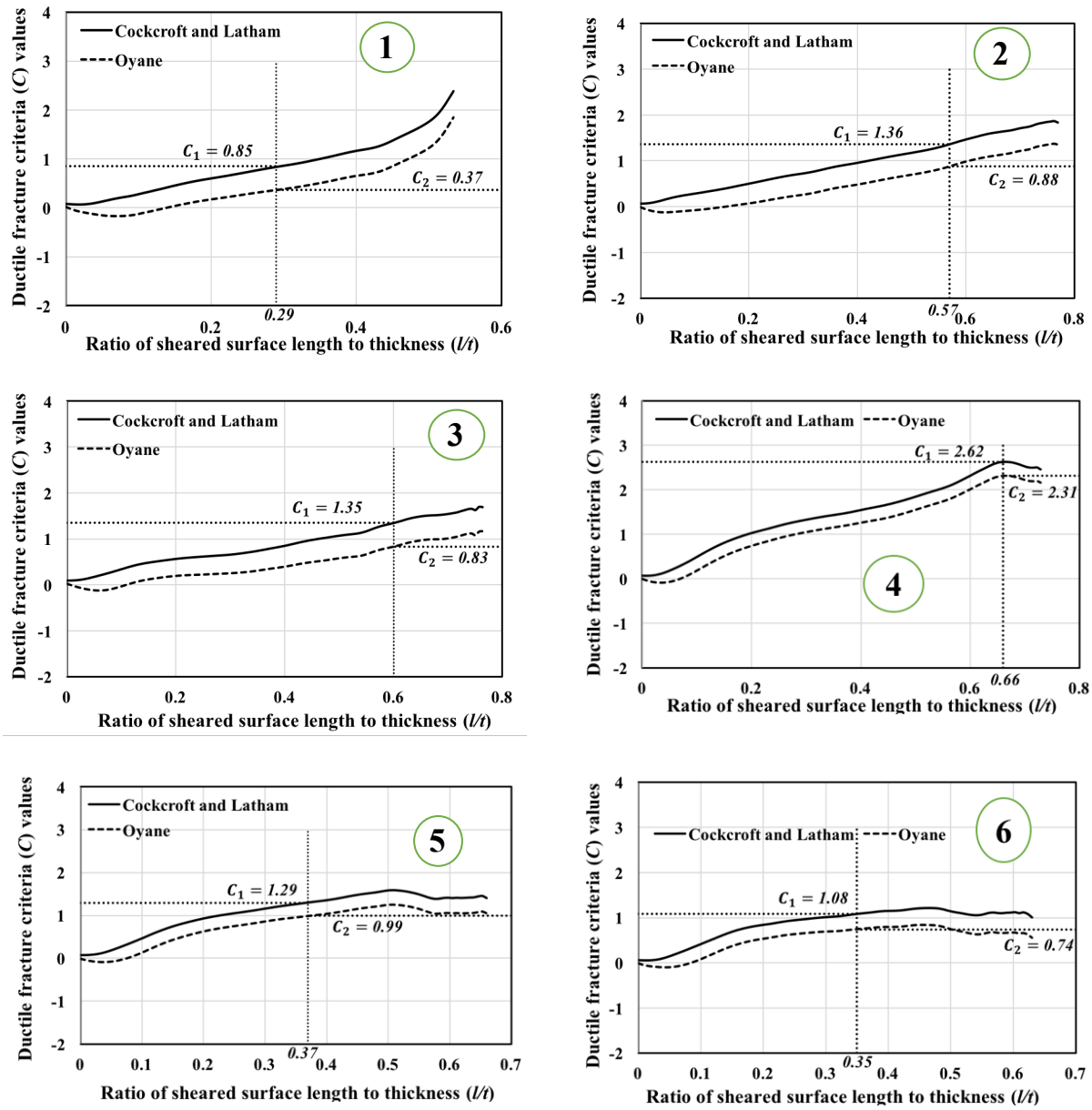

Fig. 5.20. The relationships between the value of ductile fracture criteria and the ratio of sheared surface length to thickness (*l/t*) for the different punch diameters, clearance with the blank thickness of 3.2 mm (1) Punch diameter 10 mm, clearance 0.4 mm (2) punch diameter 15 mm, clearance 0.1 mm (3) punch diameter 20 mm, clearance 0.1 mm (4) punch diameter 25 mm, clearance 0.1 mm (5) punch diameter 25 mm, clearance 0.3 mm (6) punch diameter 25 mm, clearance 0.4 mm.

The threshold values which show the shear limit point, obtained for all conditions were plotted against the ratio of sheared surface length to thickness and the clearance to determine the values of critical ductile fracture criteria of the material. The relationships between the ductile fracture criteria and the ratios of sheared surface length to thickness and the clearances are shown in the Fig. 5.21 and Fig. 5.22.

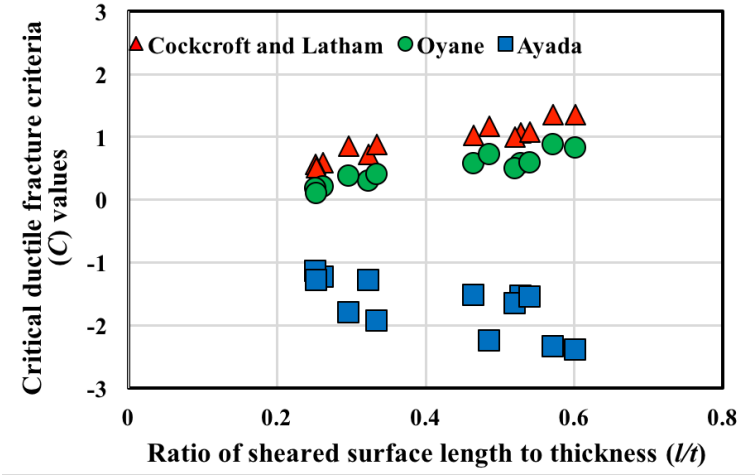

Fig. 5.21 Comparison of the variation of three ductile fracture criteria against the ratio of sheared surface length to thickness for different punch diameters and clearances for the blank thicknesses of 1.6 mm and 3.2 mm.

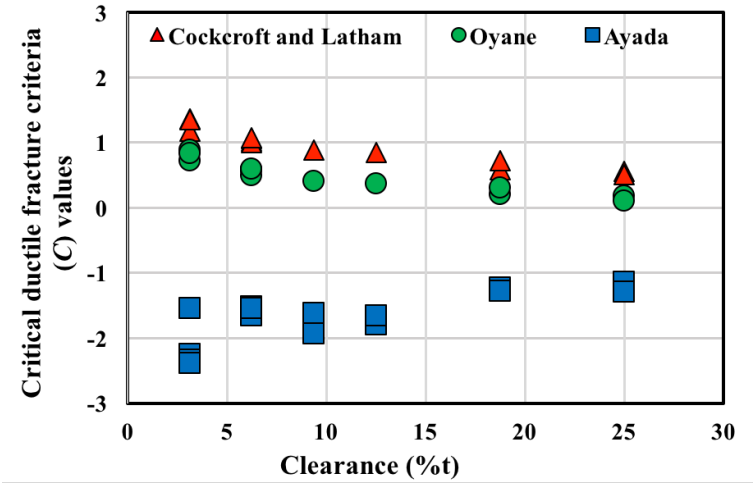

Fig. 5.22 Comparison of the variation of three ductile fracture criteria against the ratio of sheared surface length to thickness for different punch diameters and clearances for the blank thicknesses of 1.6 mm and 3.2 mm.

Fig. 5.21 shows the relationships between the sheared surface length to thickness ratio and fracture criteria (*C*) values. The increase in the ratio of sheared surface length to thickness causes an increase the fracture criteria in the Cockcroft-Latham and Oyane models and causes a decrease in the Ayada model. Fig. 5.22 shows that at the shear limit point (*l/t*), each ductile fracture criterion value (*C*) obtained by FEA depends on the clearance (%t). When the clearance is increased, (*C*) values of Cockcrfot-Latham and Oyane decrease but increase in the Ayada criterion.

Through the results, it is found that the value of ductile fracture criterion varies with the clearance between the punch and the die and it is not a material unique constant. Hence, the relationships between the values of critical ductile fracture criteria and the clearances were determined and that relations are shown in the Fig. 5.23.

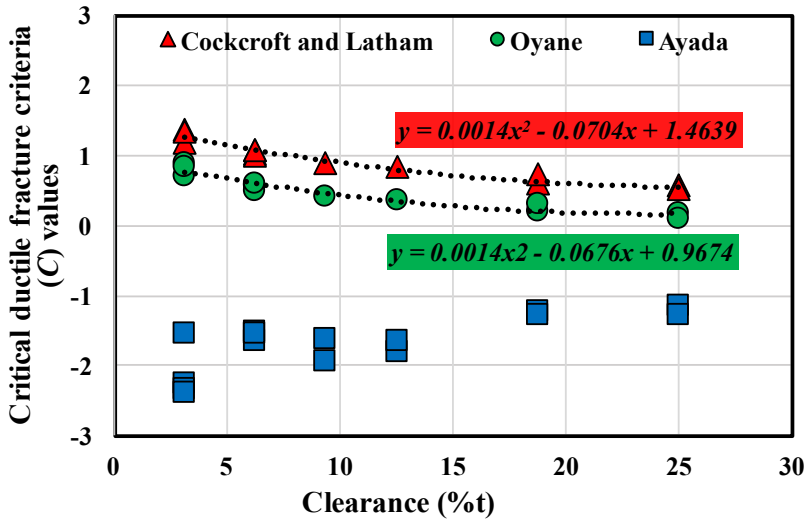

Fig. 5.23 The relationships between the value of critical ductile fracture criteria (*C*) values and clearance (% t).

The Fig. 5.23 shows the relationships between the critical ductile fracture criteria and the clearances. The accurate polynomial line fitting to the data (including all result data) was obtained from the Cockcroft-Latham and Oyane criteria. The polynomial line fitting to the data (including all result data) cannot be obtained from the Ayada model as it is based on Mode I

tensile crack opening mechanism but Cockcroft-Latham criterion performs well. The relationships (polynomial line fitting) between the critical ductile fracture criteria and clearances obtained from the Fig. 5.23 are written as Cockcroft-Latham in equation 5-1 and Oyane in equation 5-2.

$$C_{cr} = 0.0014(x)^2 - 0.0704(x) + 1.4639 \qquad Cockcroft - Latham \qquad 5\text{-}1$$

$$C_{cr} = 0.0014(x)^2 - 0.0676(x) + 0.9674 \qquad Oyane \qquad 5\text{-}2$$

where, C_{cr} is the clearance-dependent critical ductile fracture criterion (C) value and x is the clearance between the punch and the die (% t). The value of critical ductile fracture criterion that can be used in an actual punching process can be obtained by fitting a second-order polynomial to the data. The most reliable fracture criteria that can be used in a real punching process are the Cockcroft-Latham and Oyane criteria. The clearance-dependent critical ductile fracture criteria of SPCC can be obtained from the Fig. 5.23 and from the equations 5-1 and 5-2. It can be used to predict fracture initiation in the punching process to reduce time and costs for experiments before producing the punch and die set.

5.6 Effect of stress triaxiality on the sheared surface length

The ductile fracture strongly depends on the stress triaxiality [36]. The critical damage value is largely affected by the stress state [37]. The punching process consists of different loading conditions such as compression, shear and tension. The values of stress triaxiality vary from negative to positive values (low stress triaxiality to high stress triaxiality) during punching process. The equivalent plastic strain at the fracture is related in terms of the stress triaxiality. The fracture is controlled by shear mode at negative stress triaxiality, void growth plays important at large stress triaxiality values and the combination of shear and void growth modes

controls the fracture process at low stress triaxialities. The equivalent strain at the fracture decreases with the stress triaxiality, in the range of negative stress triaxiality (between -1/3 and 0, compression), reaches minimum at the zero of stress triaxiality (pure shear), increases with the low stress triaxiality in the range of low stress triaxiality (between 0 and 1/3), it reaches peak value at the value of stress triaxiality 1/3 (tension) and decreases with the stress triaxiality in the range of high stress triaxiality (between 1/3 and 2/3). Hence it was found that the fracture lines are curved if the triaxiality space was used [38,39].

The effect of stress triaxiality which is control parameter for the fracture initiation, on the punched cut surface was studied. The distribution of stress triaxiality during the punching process and the relationship between the clearances, shear limit point and the stress triaxiality were shown in the Fig. 5.24 and Fig. 5.25.

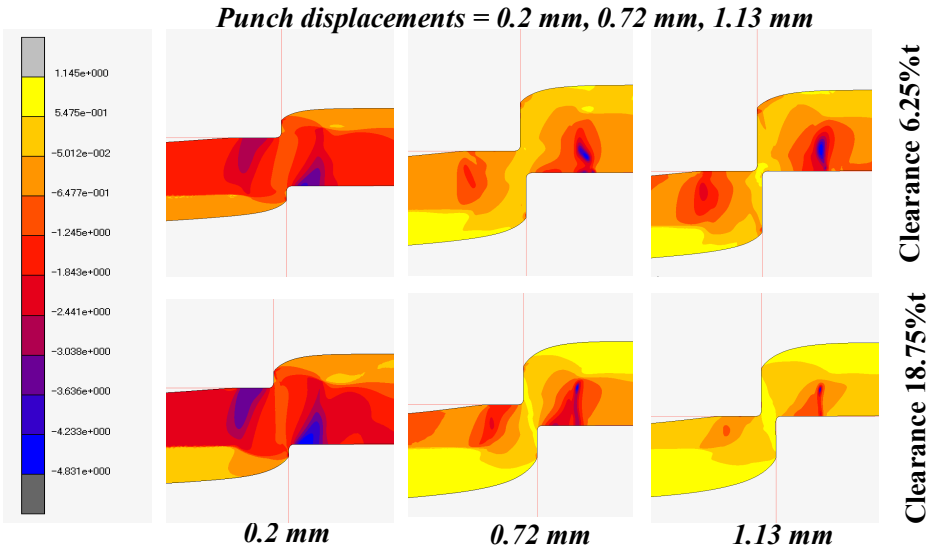

Fig. 5.24 The distribution of stress triaxiality, $(\frac{\sigma_H}{\sigma_{eq}})$ at the different punch displacements for the blank thickness of 1.6 mm, diameter of 10 mm and the clearances of 6.25 %t and 18.75 %t.

Fig. 5.24 shows the distribution of stress triaxiality at the different punch displacements. At the early stage of punch displacement 0.2 mm, negative stress triaxiality is generated in the clearance zone for both clearances. At the stage of punch displacement 0.72 mm, the value of stress triaxiality in the clearance zone increases for the clearance of 18.75 %t.

However, the value of stress triaxiality is still negative (compressive) for the clearance of 6.25 %t. The negative stress triaxiality, the hydrostatic compressive stress acting on the cut surface delays the fracture initiation. The higher stress triaxiality has developed in the clearance zone at the end of punch penetration for the clearance of 18.75 %t. The lower stress triaxiality, the higher hydrostatic compressive stress is generated in the smaller clearance case and it postpones the formation of the fracture initiation at early stages. The comparison of the distribution of stress triaxiality at the fracture initiation point (shear limit point) for the blank thickness of 1.6 mm, punch diameter of 10 mm, clearances of 6.25 %t and 18.75 %t is shown in the Fig. 5.25.

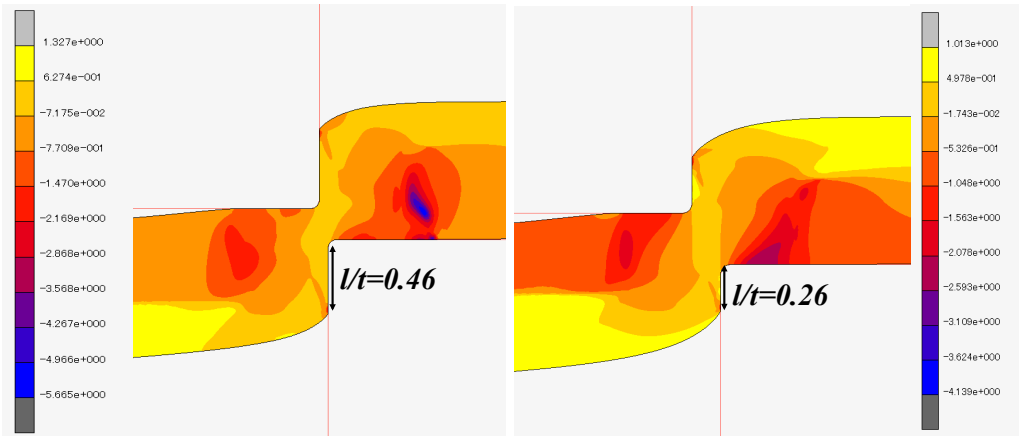

Fig. 5.25 The distribution of stress triaxiality at the fracture initiation point for the blank thickness of 1.6 mm, punch diameter of 10 mm and the clearance of 6.25 %t and 18.75 %t.

The figure shows that the low stress triaxiality, high compressive stress is acting on the cut surface in the clearance of 6.25 %t and larger sheared surface (l/t = 0.46 mm) can be obtained. The high stress triaxiality is localized near the cutting edge of the tool and acting on the cut surface in the clearance of 18.75 %t and it starts fracturing at the early stage of the punch displacement. Hence, the sheared surface obtained from the larger clearance is small and it was found that the value of the critical ductile fracture criterion (C) is affected by the stress triaxiality and punch-die clearance and it is not a material constant.

5.7 Effect of equivalent plastic strain

The ductile fracture criteria used in the determination of critical values are based on the stress triaxiality and equivalent plastic strain. Hence, the effect of equivalent plastic strain or evolution of equivalent plastic strain in the punching process was also studied. The distribution of equivalent plastic strain for the different punch displacements during the punching process with the different clearance is shown in the Fig. 5.26.

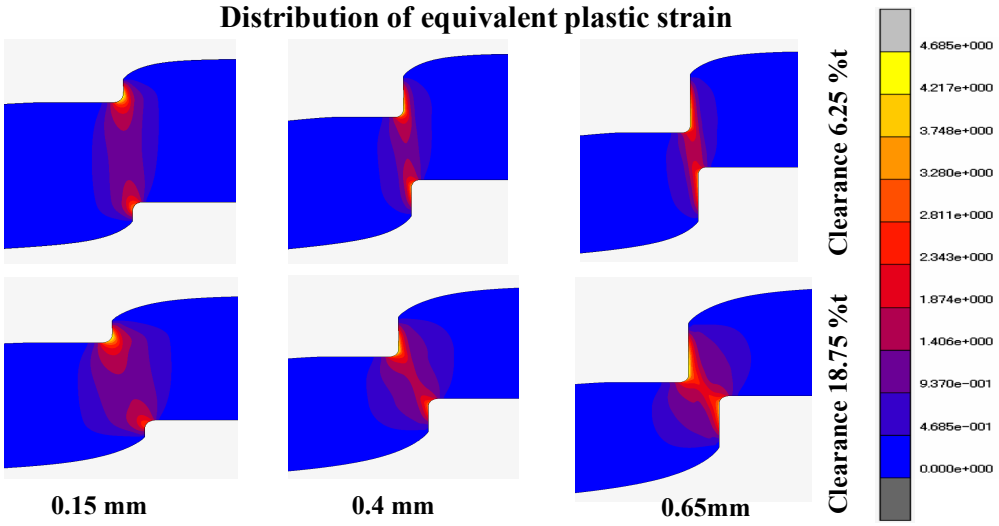

Fig. 5.26 The distribution of equivalent plastic strain during the punching process with different clearances.

The figure shows the distribution of the equivalent plastic strain for the different punch displacements during the punching process. The localized plastic strain is formed at the contact between the punch, the die and the sheet and the equivalent plastic strain at the punch size is higher than the die size. When the punch displacement is increased, localized band from the both sides propagates into the blank. Through the results, it is found that the localized band size depends on the clearance between the punch and the die. The highest equivalent plastic strain is occurred at the largest punch displacement and at the smaller clearance. The highest value of equivalent plastic strain region is defined as the region with high hardening before fracturing starts.

The investigation on the relationship between the micro-hardness and the equivalent plastic strain affected region of the punched profile proved that the ductile fracture initiation depends on hardness the level in the clearance zone and the hardness depends on the equivalent plastic strain affected region [40]. The relationships between the clearance, evolution of equivalent plastic strain and fracture initiation of SPCC in the punching process were investigated and the results are shown in the Fig. 5.27.

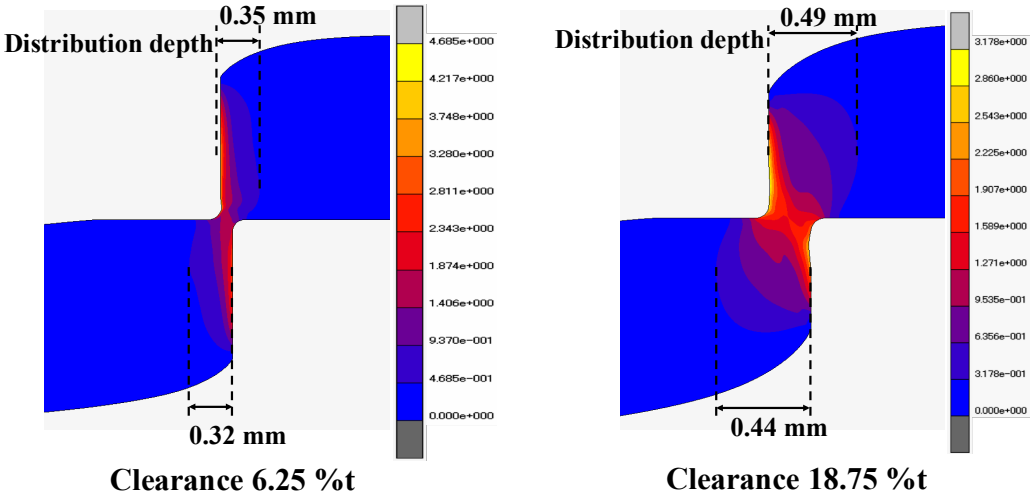

Fig. 5.27 The variation of distribution depth of equivalent plastic strain for different clearances of 6.25 %t and 18.75 %t.

The figure shows that the equivalent plastic strain decreases from the surface of the punched profile to the inside of the sheet. The distribution depth is affected by the clearance. The increase in the clearance causes a larger equivalent plastic strain distribution depth. The equivalent plastic strain distribution depth is 0.32 mm for the clearance of 6.25 %t and it is 0.44 mm for the clearance of 18.75 %t. The highest value of equivalent plastic strain in the clearance of 6.25 %t is larger than that of 18.75 %t. The decrease in the clearance causes more localization of equivalent plastic strain near the punched cut surface. This reduces early crack initiation and postpones early fracture initiation. Hence, the length of sheared surface obtained from the small clearance is larger than the length of sheared surface obtained from the large clearance.

5.8 Effect of punch diameter on the sheared surface length

The experiments were performed by using the punch diameters of 10, 15, 20 and 25 mm under the different clearances. The values of critical ductile fracture criteria were determined by comparing the ratios of sheared surface length to thickness (*l*/*t*) obtained from the experiments with the cutting lengths obtained from the FEA. In this research, the effect of punch diameter on the sheared surface length was also considered. Hence, the sheared surface lengths of blank thickness of 1.6 mm under the clearances of 1 %t and 0.2 %t with the different punch diameters (10, 13, 15, 20 and 25 mm) were also predicted by using the values of critical fracture criteria obtained from the Cockcroft-Latham and Oyane models. The values of critical ductile fracture criteria (*C*) were calculated from the polynomial equation for the clearances of 1 %t and 0.2 %t and these values were used to predict the sheared surface lengths. The results are shown in the Figs. 5.28 to 5.30, respectively.

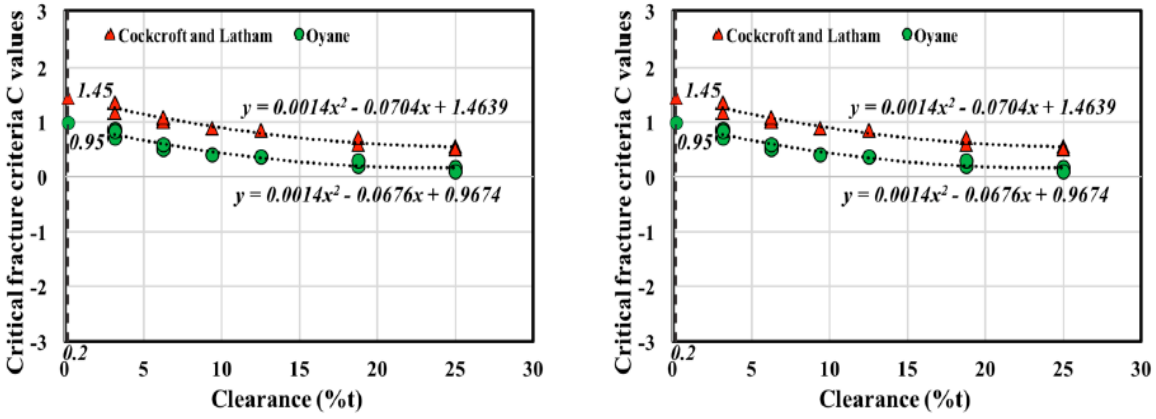

Fig. 5.28 The values of critical ductile fracture criteria for the Cockcroft-Latham and Oyane models for the clearances (a) 1 %t (b) 0.2 %t.

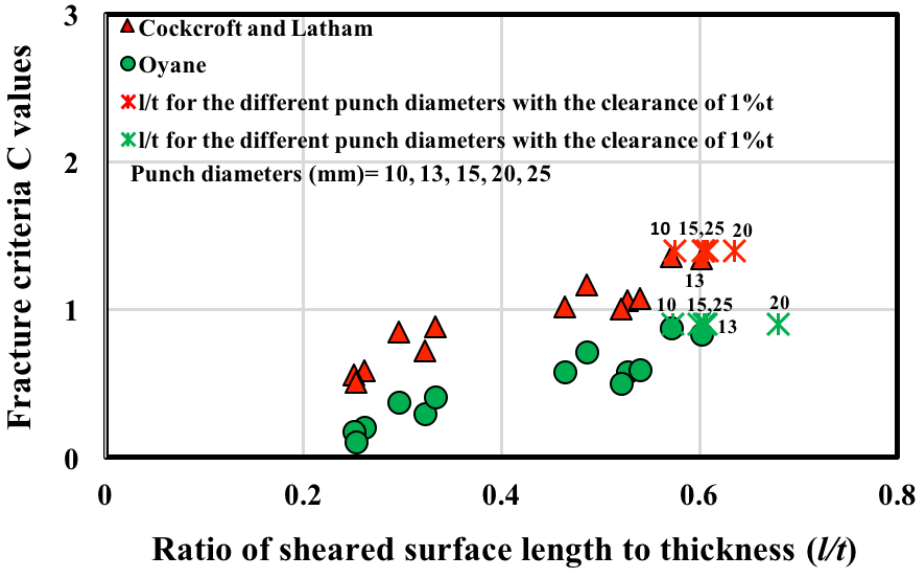

Fig. 5.29 Relationships between the values of fracture criteria and the ratio of sheared surface length to thickness predicted by the punch diameters of 10, 13, 15, 20 and 25 mm for the clearance of 1 %t.

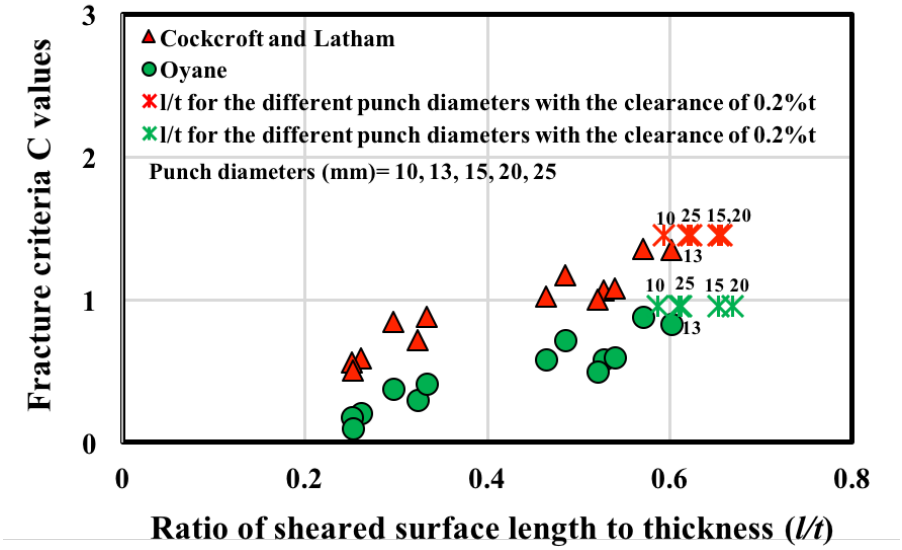

Fig. 5.30 Relationships between the values of fracture criteria and the ratio of sheared surface length to thickness predicted by the punch diameters of 10, 13, 15, 20 and 25 mm for the clearance of 0.2 %t.

The figures show that the sheared surface lengths obtained from the clearances of 3.125 %t and 1%t with the different punch diameters are equal. However, for a punch diameter of 20

mm, the sheared surface length increases. The maximum and minimum differences between the sheared surface lengths predicted by Oyane critical fracture criterion are higher than the differences predicted by Cockcroft-Latham critical value. The maximum difference between the sheared surface lengths predicted by the Cockcroft-Latham critical value is 0.06 mm and the minimum difference is 0.002 mm for both cases. A larger sheared surface length can be obtained for the clearance of 0.2 %t. A clearance of less than 1 %t is preferable for achieving a larger sheared surface for SPCC, and the fracture surface is very short.

The blank thickness of 1.6 mm with the punch diameter of 30 mm was also considered to clear the effect of punch diameter on the sheared surface length. The values of critical ductile fracture criteria (C) of Cockcroft-Latham and Oyane were calculated for the different clearances and these values were used to predict the sheared surface length or (l/t) with the punch diameter of 30 mm and the results are shown in the Table 5.2.

Table 5.2 The values of critical ductile fracture criteria (C) for the different clearances and sheared surface lengths predicted by the punch diameter of 30 mm for the blank thickness of 1.6 mm

Punch diameter (mm)	Clearance [%t]	Cockcroft-Latham		Oyane	
		Critical value (C)	Predicted l/t	Critical value (C)	Predicted l/t
30	0.2	1.45	0.45	0.95	0.36
	1	1.39	0.43	0.90	0.34
	5	1.15	0.35	0.66	0.27
	10	0.89	0.28	0.43	0.23
	15	0.72	0.25	0.27	0.21

The results indicate that the lengths of sheared surfaces predicted by the punch diameter of 30 mm are smaller than the lengths of sheared surfaces predicted by the punch diameter of 10, 13, 15, 20 and 25 mm for the same clearances of 0.2%t and 1 %t. This is the fact that the higher stress triaxiality has developed in the clearance zone at the early stages of the punch displacement and the high stress triaxiality leads to an earlier fracture.

The values of critical ductile fracture criteria (C) which show the fracture initiation were determined by using the punch diameters of 10, 15, 20 and 25 mm. Hence, the values of critical ductile fracture criteria obtained from the figure 5-23 can be used for the prediction of fracture initiation in punching processes with the punch diameters of less than 25 mm. Through the results, it is found that the effect of the punch diameter on the sheared surface length also should be taken into account for the prediction of fracture initiation point in the punching processes.

5.9 Determination of the value of critical ductile fracture criterion, (C) value (S45C)

The predictions of fracture initiation point in punching processes were performed to determine the values of critical ductile fracture criteria (C) of S45C with the same procedure like SPCC by using the new chosen Oyane parameter ($\alpha = 0.6$) in the Oyane criterion. The conditions for FEA are the same as previous cases. The relationship between the fracture criteria (C) values and the ratio of sheared surface length to thickness obtained by the punch diameter of 10 mm under the clearances of 6.25 %t and 18.75 %t are shown in the Fig. 5.31 and Fig. 5.32.

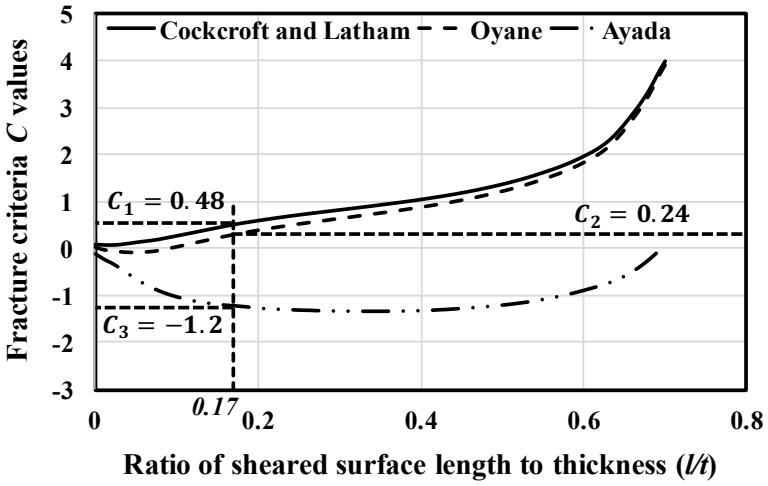

Fig. 5.31 The relationships between the values of fracture criteria and the ratio of sheared surface length to thickness predicted by the punch diameter of 10 mm under the clearance of 6.25 %t (S45C).

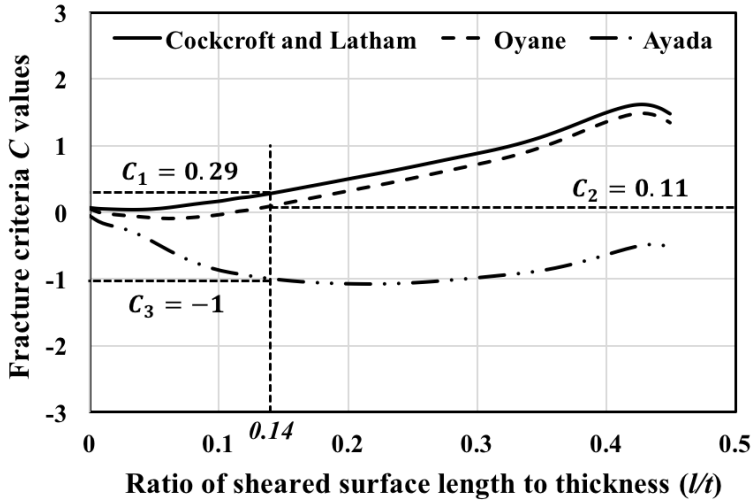

Fig. 5.32 The relationships between the values of fracture criteria and the ratio of sheared surface length to thickness predicted by the punch diameter of 10 mm under the clearance of 18.75 %t (S45C).

The figures show that the distributions of damage values predicted by Cockcroft-Latham and Oyane criteria increase monotonically but different situation is occurred in the Ayada criterion. Through the results, it is found that the value of critical ductile fracture criterion (*C*) obtained from the Oyane criterion for each clearance becomes positive value and

the damage value obtained from Ayada model is still negative. Then, the values of critical ductile fracture criteria for other conditions are calculated by using Cockcroft-Latham and Oyane criteria because these two criteria can predict fracture initiation properly and accurate results were obtained in the previous case of SPCC. These fracture criteria (*C*) values were plotted against the ratio of sheared surface length to thickness and the clearance so as to find the relationship between the values of ductile fracture criteria (*C*) and the clearances for the S45C. The results are shown in the following.

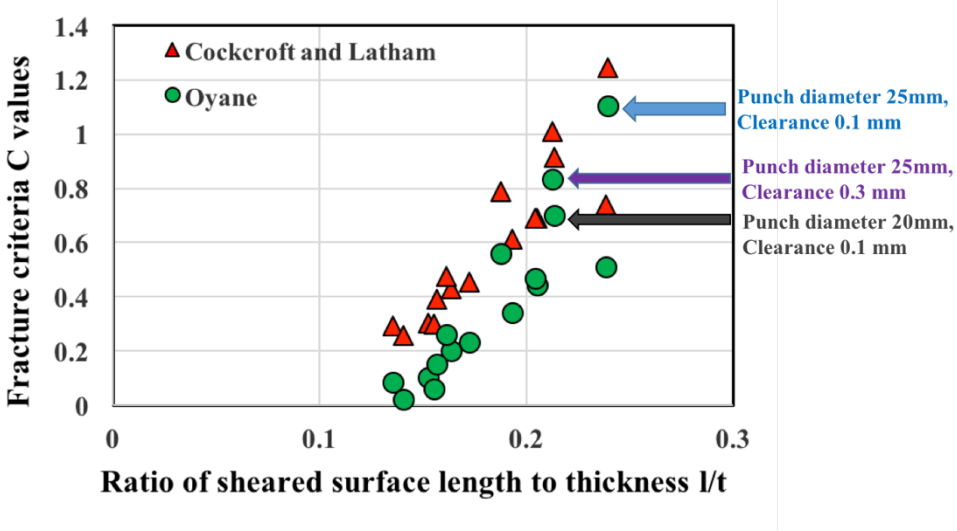

Fig. 5.33 The relationships between the values of Cockcroft-Latham and Oyane fracture criteria and the ratio of sheared surface length to thickness obtained from the punching experiments (S45C).

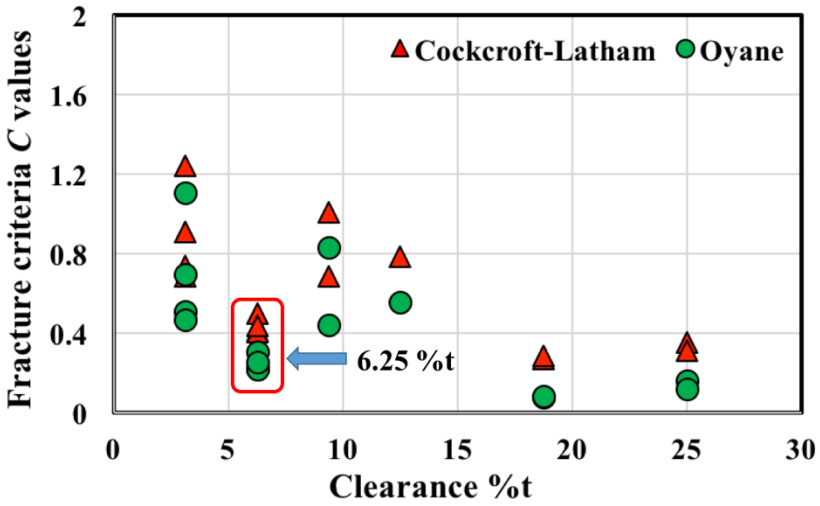

Fig. 5.34 The relationships between the values of Cockcroft-Latham and Oyane fracture criteria and the clearance between the punch and the die (S45C).

The figures show that the value of critical ductile fracture criterion varies with the ratio of sheared surface length to thickness and the clearance. However, the gap between predicted values of criteria is high. The significant difference between the predicted values of fracture criteria by the punch diameters of 20 mm and 25 mm under the same clearance of 0.1 mm can be found in the Fig. 5.33. The Fig. 5.34 shows the relationship between the value of fracture criterion and the clearance between the punch and die. The effect of punch diameter on the cut surface is more significant in S45C than SPCC. This effect can be found under the clearances of 3.125 %t and 9.375 %t. The values of critical ductile fracture criteria were determined by comparing the cutting length obtained from FEA and the ratio of sheared surface length to thickness obtained from the punching experiments. Hence, the values of critical ductile fracture criteria for the clearance of 6.25 %t is lower than the values for the clearance of 9.375 %t because the sheared surface length obtained under the clearance of 6.25 %t is smaller than the sheared surface length under the clearance of 9.375 %t. Through the results, it is found that the accurate line fitting for the relationship between the fracture criteria and the clearances cannot be obtained for S45C. Hence, the variation of fracture criteria with the clearance was

investigated by changing the conditions of FEA (considering the mesh dependence) to verify the above mentioned results. The number of elements is 10000 for both thicknesses of 1.6 mm and 3.2 mm and the results are shown in the Fig. 5.35 and Fig. 5.36.

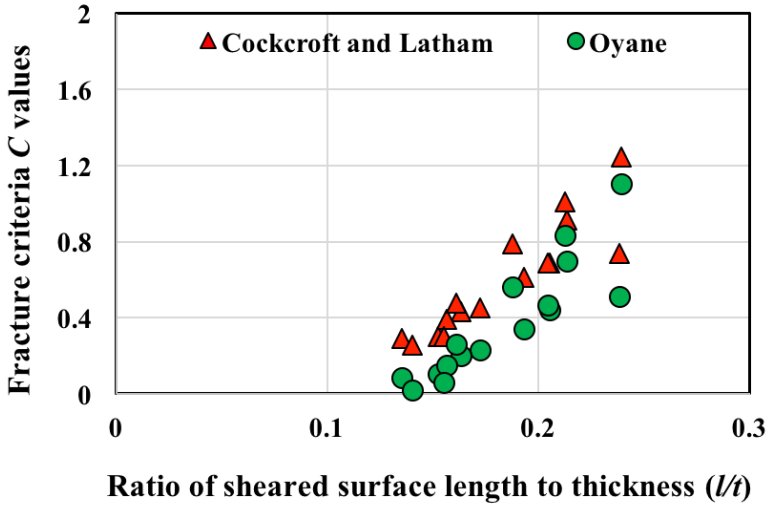

Fig. 5.35 The relationships between the values of Cockcroft-Latham and Oyane fracture criteria and the ratio of sheared surface length to thickness (S45C).

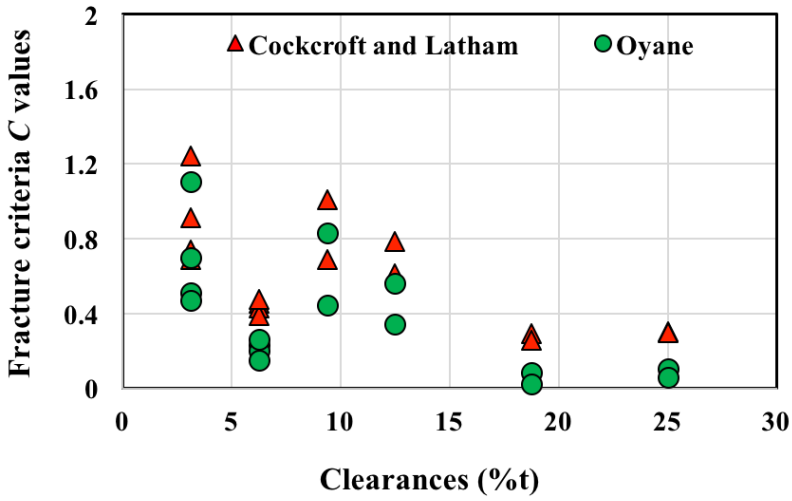

Fig. 5.36 The relationships between the values of Cockcroft-Latham and Oyane fracture criteria and the clearance between the punch and the die (S45C).

The figures show that changing the FEA conditions has no effect on the relationship between the values of ductile fracture criteria and the ratio of sheared surface length to thickness and the clearance between the punch and die. The results indicate that the accurate line fitting (including all result data) for the relationship between the fracture criteria and the clearance cannot be obtained for S45C.

5.10 Effect of stress triaxiality

The effect of stress triaxiality on the fracture initiation point was also studied as it plays important role in ductile fracturing. The results are shown in the Fig. 5.37.

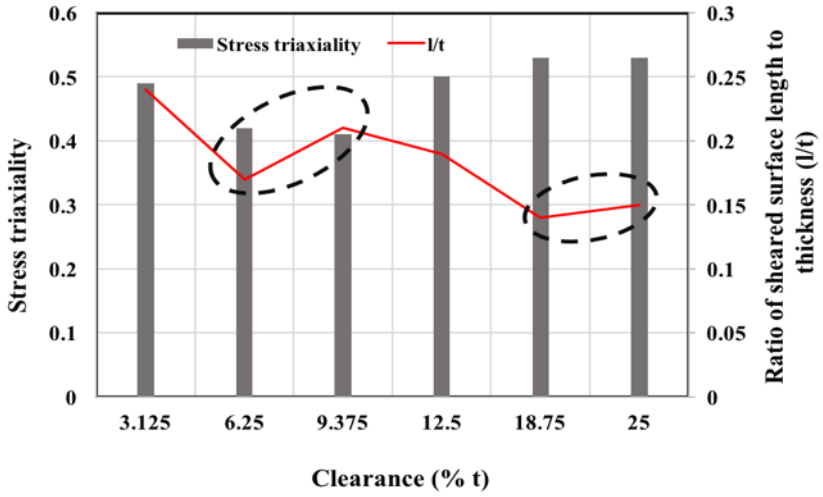

Fig. 5.37. The relationships between stress triaxiality, ratio of sheared surface length to thickness and the clearance between the punch and the die (S45C).

The Fig. 5.37 shows the relationship between the shear limit point (*l/t*) obtained from the experiments and the value of stress triaxiality at that shear limit point for the different clearances. The stress triaxiality influences the fracture initiation point in the punching process. The decrease in the clearance causes a decrease in the range of stress triaxiality in the clearance zone and larger sheared surface can be obtained. However, the different conditions can be occurred through the results from the Fig. 5.37. The ratio of sheared surface length to thickness obtained from the clearance of 6.25 %t is smaller than the value which was obtained from the

clearance of 9.375 %t at the same value of stress triaxiality and similar condition can be occurred for the clearances of 18.75 %t and 25 %t. Hence, the accurate prediction of fracture initiation in punching process cannot be obtained by the criterion which is based only on the stress triaxiality for the low ductility material such as S45C.

Chapter (6) Fine Blanking Process

6.1 Introduction

The precision sheet metal working method or fine blanking process was introduced by Fritz Schiess and patented in Germany around year 1925. The process was then developed and applied in the late 50s. The first of special machinery, named the fine blanking press had been designed by H.Schmid and manufactured in his company in 1952[41].

The fine blanking process is sheet metal forming process producing fine sheared surface. It is used in the manufacturing of high quality and precision metal components, such as automobile and aircraft parts and small precision parts. The fine blanking process is high-precision shearing process where a blank is placed under pressure and the malleability of the material is improved through the effects of hydrostatic stress. The fine blanking process can produce the parts which have high accuracy and fully-fine sheared surface reducing secondary operations.

6.2 Characteristics of fine blanking process

The characteristics of fine blanking process are initial compression, V-ring indenter, small clearance between the punch and the die which is less than one percent of blank thickness (1 %t), the counter punch its force holds the sheet to prevent from bending of the sheet during the blanking process. The fine blanking process consists of four steps of punch movements, contact of the blank with V-ring indenter, the V-ring indenter was pressed into the blank for hydrostatic compressive stress, the step of initial compression and the final one is the step of shearing process. The four steps of punch movements in the fine blanking process are shown in the Fig. 6.1.

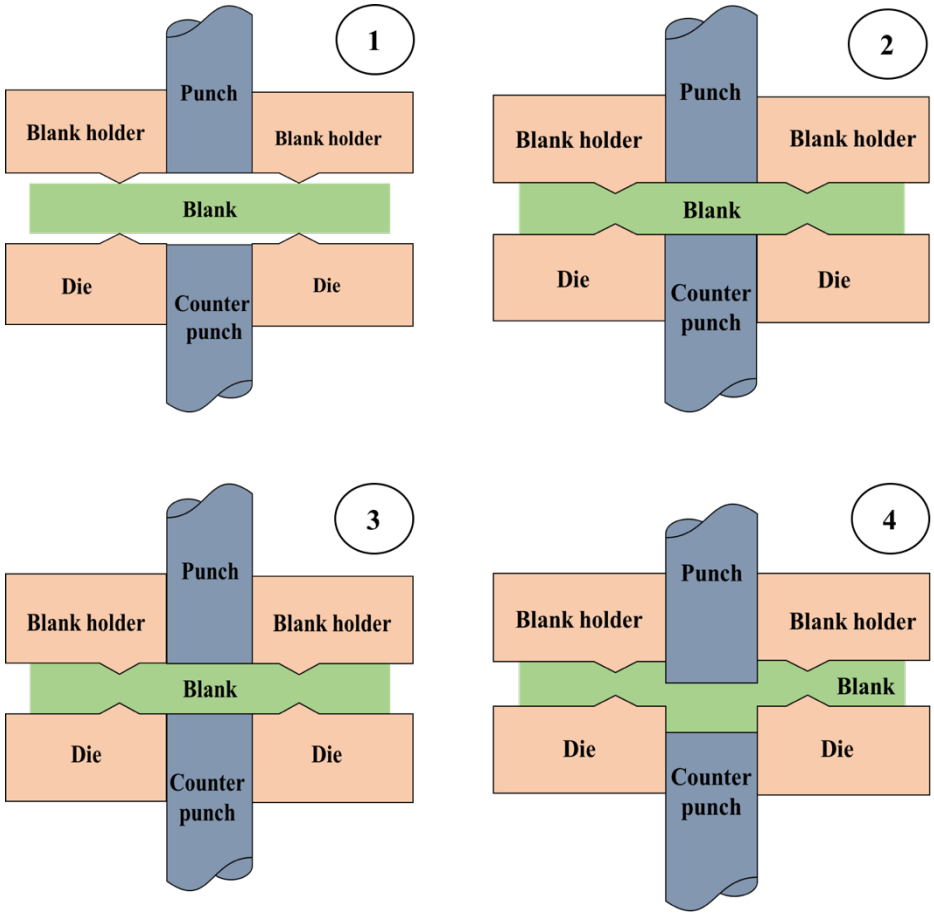

Fig. 6.1 The steps of punch movement in the fine blanking process (1) Contact of the punch with the blank (2) V-ring indenter was pressed into the blank (3) Step of initial compression (4) Step of shearing process.

6.3 Literature review of fine blanking process

Researchers used various criteria by taking into account different influenced parameters in the prediction of the nature of cut surface produced by the conventional punching and fine blanking process. Lee et al. presented theoretical analysis of FEM deformation in the fine blanking process with rigid plastic model and the results on the distribution of effective stress and strain were described [41]. Hambli used pressure dependent damage model for the fine blanking processes and the results showed that the exponential damage evolution model was the good one [42]. The finite element method together with the void damage was developed by

Yu-min Li et al. to study the influences of process parameters in the fine blanking processes [43].

Thipprakmas analyzed the V-ring indenter mechanism in the fine blanking processes and the effects of V-ring on the compressive stress and material flow during cutting phase were described [44]. Tanaka et al. used Cockcroft-Latham, Oyane and Rice and Tracey criteria to study shear droop on the punched surface in the fine blanking process and found that the differences between the shear droop obtained from FEM simulation and experimental values can be reduced by implementing remeshing function [45]. The forming quality of part shape in the fine blanking process with Oyane fracture criterion was studied by Liu et al. and the relationship between the part shape and the die roll height and crack surface height were described [46].

The V-ring was replaced by a trough and the conditions of cut surfaces were studied by Wang et al. and the results showed that a fully sheared surface was obtained with a trough on the die [47]. Mao et al. investigated the discontinuous dot indenter effect in the fine blanking process to reduce the difficulties in the manufacturing of V-ring indenter and the machining accuracy. Oyane fracture criterion was used and clean cut surface part was obtained with the discontinuous dot indenter blank holder [48]. Oyane criterion was used to propose a new die design by Tang et al. and it has to known that the size of die-roll was reduced with the proposed die design [49].

The nesting strategy was used by Voigts et al. in the fine blanking processes to investigate the height of die-roll [50]. Luo et al. used Oyane fracture criterion and proposed a method to minimize the length of die roll in the fine blanking process. In that work, the method which is easier than negative clearance blanking and counter shearing cutting was proposed [51].

In the above mentioned research, the critical damage value or critical fracture criterion was determined by experimentally. It was set to be constant for one material and used in the fracture initiation analysis. Hence, long duration experiments are required to obtain the critical damage value and experimental costs are high.

In this study, the values of clearance-dependent critical ductile fracture criteria (C) obtained from the relationship between critical ductile fracture criteria and clearances, Fig. 5-23, were used to predict the nature of cut surface of SPCC in the fine blanking process. Hence, the time and costs for experiments to obtain the values of critical ductile fracture criteria can be reduced. The influences punch and die corner radii on the sheared surface length, the influences of initial compression and V-ring indenter on the sheared surface length were studied for the clearances of 1 %t and 0.15 %t. The values of critical ductile fracture criteria are calculated from the polynomial equation in the Fig. 5-23 [54] for the clearances of 1 %t and 0.15 %t. These critical values were used to predict the nature of cut surface. The values of critical ductile fracture criteria are 1.39 and 1.5 (Cockcroft-Latham), 0.9 and 0.96 (Oyane) for the clearances of 1 %t and 0.15 %t.

6.4 Finite Element Analysis of fine blanking process

The schematic diagram of the simulation model created for the analysis of fine blanking process is shown in the Fig. 6.2. The FEA model of the test specimen is rectangular shape, with outside diameter of 20 mm and thickness of 4 mm. The punch diameter of 10 mm was used.

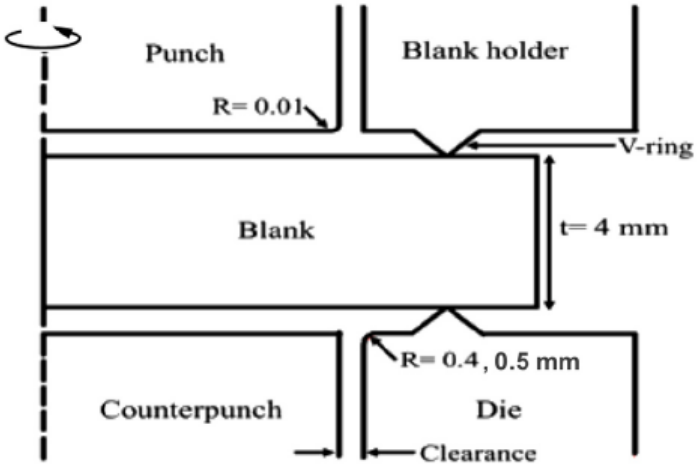

Fig. 6.2 The axisymmetric model of the blank, the blank holder with V-ring, punch, counter punch used for the finite element analysis of the fine blanking process.

The radii of the cutting edges of the punch and die are 0.01 mm, 0.4 and 0.5 mm. Axisymmetric four node quadrilateral elements were used in this analysis. The punch and die were considered to be rigid bodies and the blank material was considered to be a deformable elastic-plastic body. The automatic remeshing function with advancing front-quad was used. After remeshing, the element length was changed to 0.01 mm and quasi-static phenomenon was used and the initial compression for hydrostatic compressive stress is initially set to 0.01 mm. The initial number of elements are 6250 and initial element length is 0.08 mm.

6.4.1 Effect of initial compression on the sheared surface length

The effects of initial compressions on the fracture initiation under the clearance of 1 %t were studied. The ratio of sheared surface length to thickness obtained by FEA of fine blanking process was predicted by using the critical ductile fracture criteria of Cockcroft-Latham and Oyane. The results are shown in the Fig. 6.3 and Fig. 6.4.

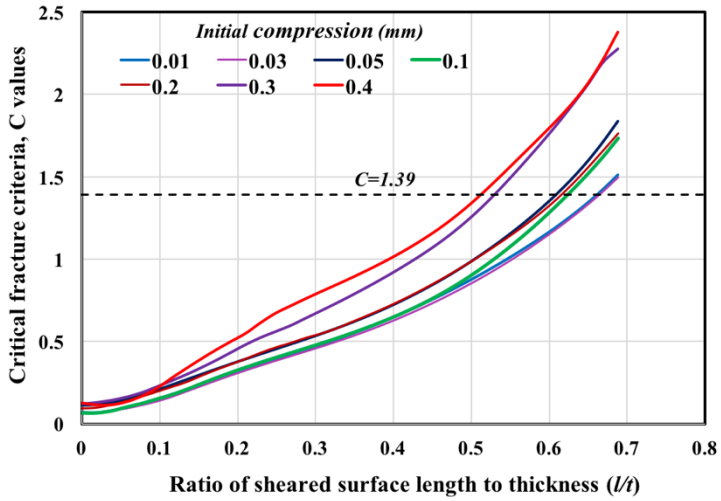

Fig. 6.3 The ratios of sheared surface length to thickness predicted by the value of Cockcroft-Latham critical ductile fracture criterion under the different value of initial compressions under the clearance of 1 %t.

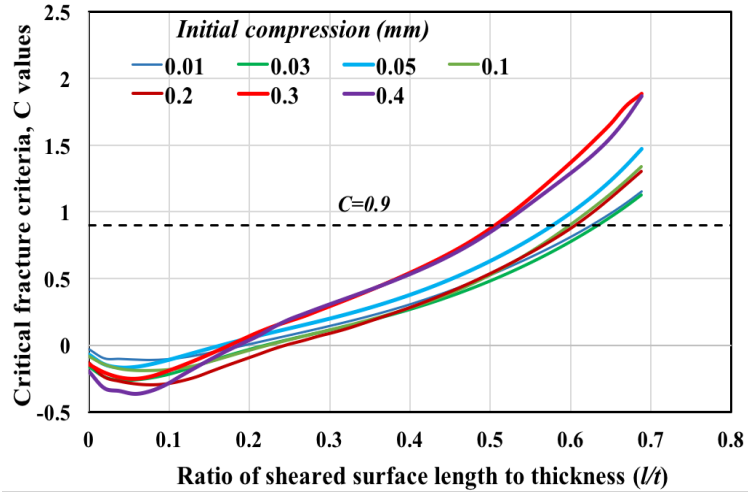

Fig. 6.4 The ratios of sheared surface length to thickness predicted by the value of Cockcroft-Latham critical ductile fracture criterion under the different value of initial compressions under the clearance of 1 %t.

The increase in the initial compression causes an increase in the hydrostatic compressive stress and it postpones the fracture initiation point. From the other side, the increase in the initial compressive stress changes the material flow and the state of stress and early fracture initiation can be found. This means that the increase in the hydrostatic stress

causes an increase in the range of stress triaxiality and leads to an earlier fracture initiation. Hence, the right choice of the initial compression is important in the fine blanking process. The figures show that the larger sheared surface can be obtained from the cases of initial compressions of 0.01 mm and 0.03 mm and the minimum sheared surface lengths were obtained with the initial compressions of 0.3 and 0.4 mm. The results indicate that there is a threshold value of initial compression to obtain larger sheared surface under the same value of critical ductile fracture criterion and under the same clearance in the fine blanking process. Hence, the initial compression of 0.03 mm was chosen to study the effects of other process parameters on the fracture initiation point without choosing initial compression of 0.01 mm to reduce difficulties in measuring.

6.4.2 Effect of punch corner radius on the sheared surface length

The effect of tool geometry on the fracture initiation point was also studied. The tool designs from the economical point of view and the wear point of view are not considered. In this study, the effect of punch corner radius on the cut surface was studied for the clearance of 1 %t. The ratio of sheared surface length to thickness was predicted by using Cockcroft-Latham and Oyane critical ductile fracture criteria with the different punch corner radii. The relationships between punch corner radius and the sheared surface length to thickness ratio are depicted in the Fig. 6.5 and Fig. 6.6.

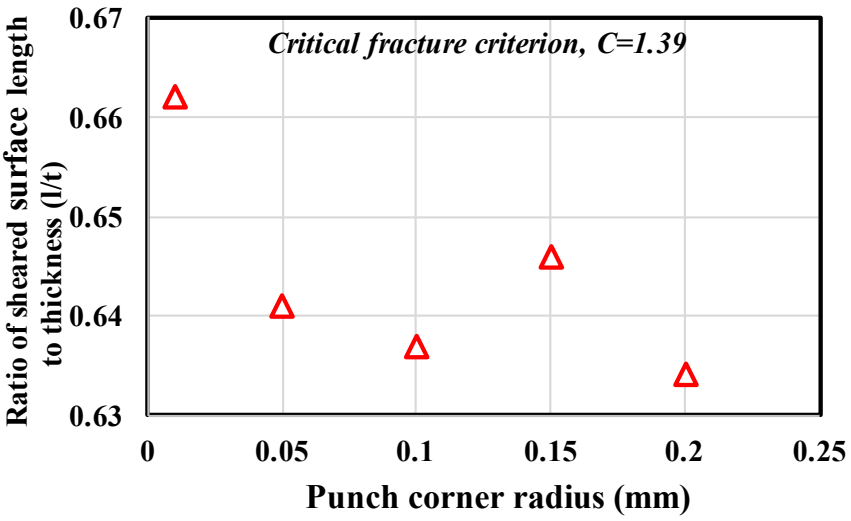

Fig. 6.5 The relationships between the ratio of sheared surface length to thickness and punch corner radius predicted by using the value of Cockcroft-Latham critical ductile fracture criterion for the clearance of 1 %t.

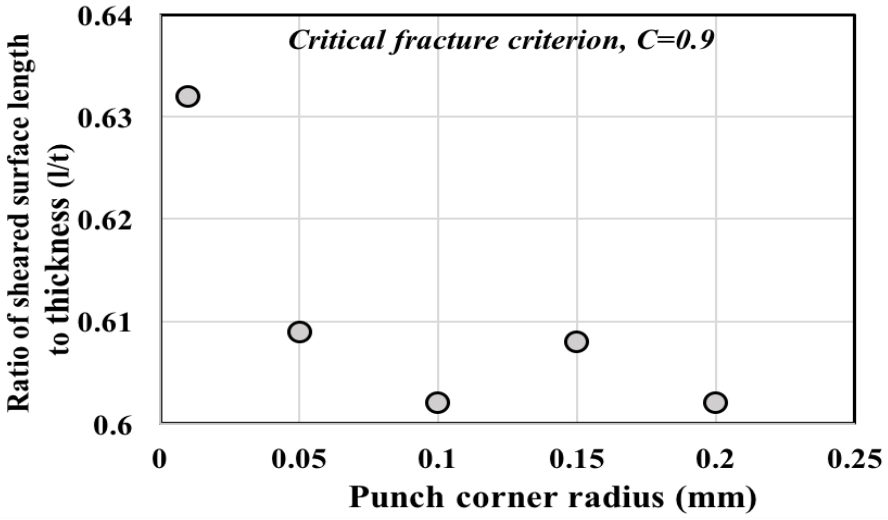

Fig. 6.6 The relationships between the ratio of sheared surface length to thickness and punch corner radius predicted by using the value of Oyane critical ductile fracture criterion for the clearance of 1 %t.

The condition of cut surface also depends on the punch corner radius. Fig. 6.5 and 6.6 illustrate that the larger sheared surface can be obtained by smaller punch corner radius. The largest sheared surface is obtained by the punch corner radius of 0.01 mm and the ratio of sheared surface length to thickness is decreased in increasing the punch corner radius. The stress and strain values are decreased when the punch corner radius increases. The sheared surface length decreases in increasing the punch corner radius. The smaller punch corner radius causes the higher compressive stress in the sheet. The high compressive stress postpones the early fracture initiation and causes an increase in the sheared surface length [53]. From the wear point of view, the researchers have found that the punch corner radius have a significant influence on the punch stress. The increase in the punch corner radius causes a decrease in punch stress and an increase in tool life.

6.4.3 Effects of V-ring indenter on the sheared surface length

The blank holder with the V-ring indenter was used in the fine blanking process. The effect of V-ring indenter parameters, such as height and position and V-ring indenter angle are important in the fine blanking process. The V-ring height should be chosen depending on the thickness of the blank to get fully fine sheared surface. In this study, the effect of V-ring height on the sheared surface length was studied with the heights of 0.35 mm and 0.7 mm. The V-ring indenter angle for both cases was set to 90 and the distance from the punch side was 1 mm for both the blank holder and the die.

The ratios of sheared surface length to thickness with the V-ring indenter heights of 0.35 mm and 0.7 mm for the clearance of 1 %t were predicted by using the values of Cockcroft-Latham and Oyane critical criteria. The results are shown in the Figs. 6.7 and 6.8.

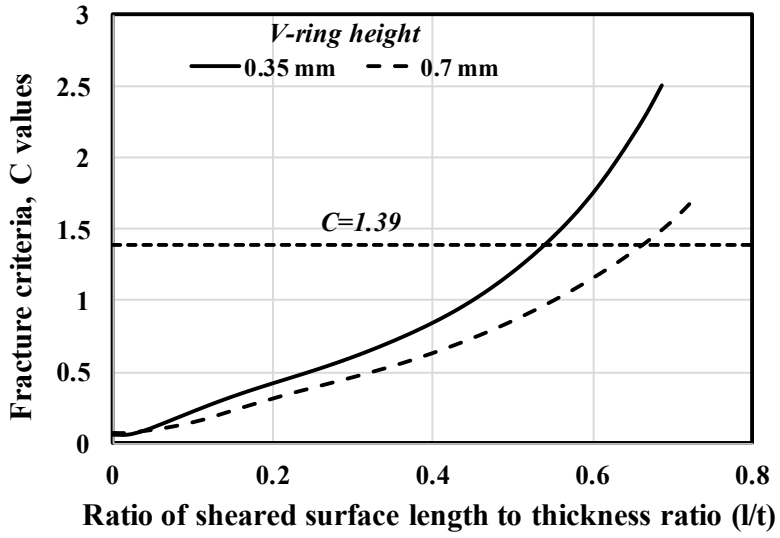

Fig. 6.7 The ratios of sheared surface length to thickness obtained by the V-ring indenter heights of 0.3 and 0.7 mm by using the value of Cockcroft-Latham critical ductile fracture criterion for the clearance of 1 %t.

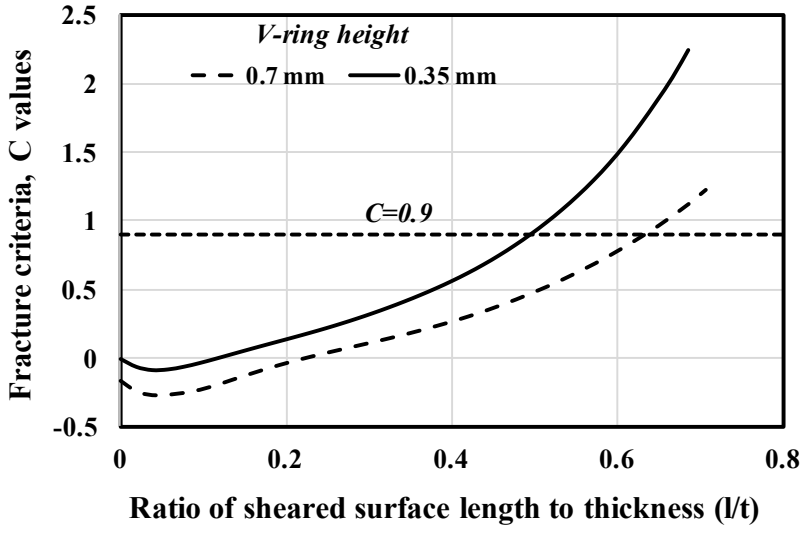

Fig. 6.8 The ratios of sheared surface length to thickness obtained by the V-ring indenter heights of 0.3 and 0.7 mm by using the value of Oyane critical ductile fracture criterion for the clearance of 1 %t.

The figures illustrate that the right choice of the V-ring indenter is also important to obtain larger fine sheared surface in the fine blanking process. The ratio of sheared surface length to thickness was affected by the V-ring indenter height. The sheared surface length by the V-ring indenter height of 0.7 mm is larger than the sheared surface length by the V-ring indenter height of 0.35 mm. This shows that the higher V-ring indenter height increases the hydrostatic pressure around shear band and this leads to the high ductility and postpones the early fracture initiation [54]. The results indicate that the height of V-rig indenter 0.7 mm is more reliable for the blank thickness of 4 mm.

6.4.4 Effect of stress triaxiality

The effect of stress triaxiality on the sheared surface length in the fine blanking process was also studied. The distribution of stress triaxiality under the V-ring indenter heights of 0.35 mm and 0.7 mm are shown in the Fig. 6.9.

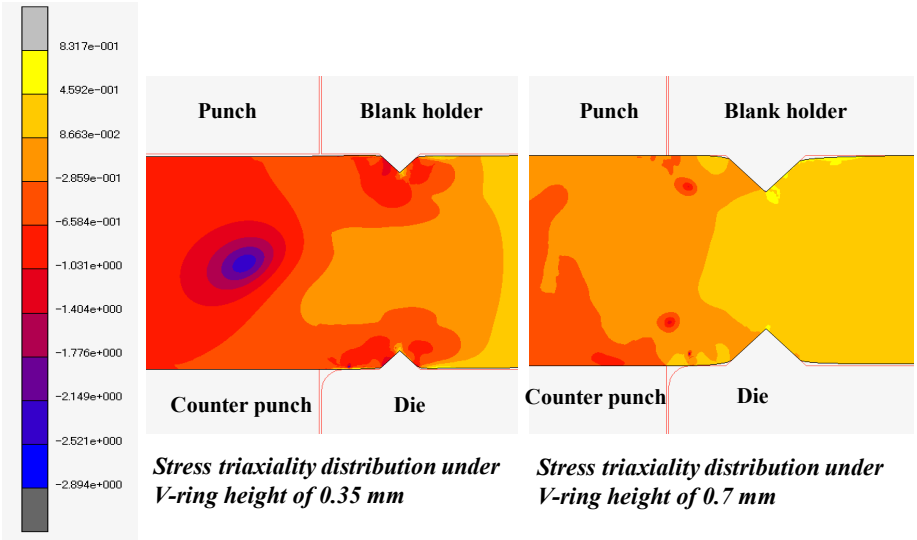

Fig. 6.9 The distribution of stress triaxiality after V-ring was totally immersed in the blank (before cutting phase) for the V-ring heights of 0.35 and 0.7 mm with the clearance of 1 %t.

The high stress triaxiality was generated around the V-ring indenter. The higher stress triaxiality has developed under the V-ring height of 0.7 mm. It decreased toward the inside of

the blank and in the shearing zone. The V-ring indenter increased the compressive stress in the blank before cutting and it causes material flow rotation resulting in the increase of hydrostatic compressive stress [46]. Hence, the sheared surface length is affected also by the V-ring indenter which increases the hydrostatic stress before cutting phase.

The distribution of stress triaxiality during punching process and at the fracture initiation point or shear limit point (*l/t*) is shown in the Fig. 6.10.

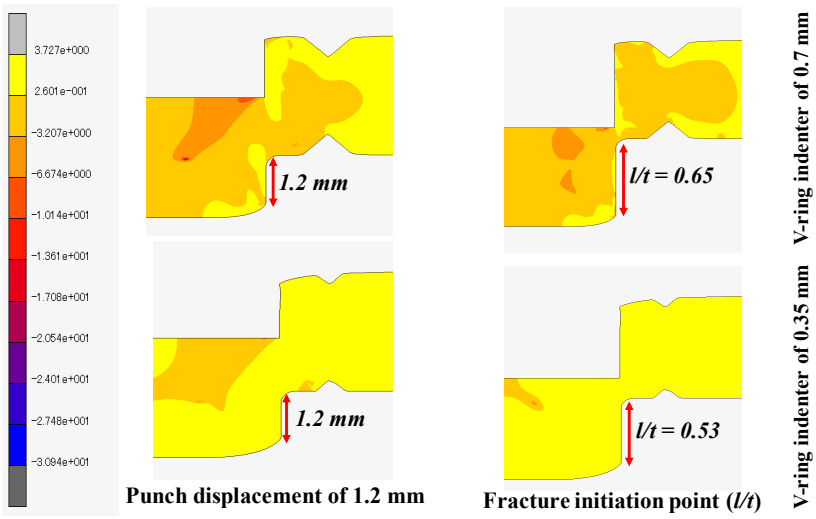

Fig. 6.10 The distribution of stress triaxiality during the punch displacement (1.2 mm) and the fracture initiation point or shear limit point (*l/t*) with the V-ring indenter heights of 0.35 mm and 0.7 mm.

The distribution of stress during the process of blanking under the different V-ring indenter heights for the same clearance of 1 %t was studied. The results from the Fig. 6.10 show the distribution of stress triaxiality at the punch displacement of 1.2 mm and the fracture initiation or shear limit point (*l/t*) with the different V-ring indenters. For the V-ring indenter height of 0.7 mm, at the stage of punch displacement of 1.2 mm, the higher stress triaxiality is developed around the V-ring and negative stress triaxiality is generated in the clearance zone, at the middle of the blank. The lower stress triaxiality, the higher hydrostatic compressive stress is generated in the clearance zone at the middle of the blank and it postpones the formation of the fracture initiation at early stages. When the punch reaches to the shear limit point (*l/t*), the

high stress triaxiality is acting along the cutting surface. The negative stress triaxiality in the middle is decreased with the decrease in the thickness. The stress triaxiality around the V-ring is decreased, the high stress triaxiality is developed in the clearance zone and it leads to fracturing. For the V-ring indenter height of 0.35 mm, the distribution of stress triaxiality is significantly different from the case of V-ring indenter height of 0.7 mm. The high stress triaxiality is developed at the stage of punch displacement of 1.2 mm and the high stress triaxiality is generated in the whole blank at the fracture initiation or shear limit point. The high stress triaxiality leads to an earlier fracture and hence the sheared surface length under the V-ring height of 0.35 mm is small.

6.5 Optimization of parameters for fine blanking process

The process parameters which give the larger sheared surface were selected through the results obtained from the case of clearance of 1 %t and were used to predict the condition of the cut surface under the clearance of 0.15 %t. The height of V-ring indenter 0.7 mm, the initial compression of 0.01 and 0.03 mm, the punch corner radius of 0.01 mm were selected. The ratio of sheared surface length to thickness with the selected parameter values for the clearance of 0.15 %t was predicted by using Cockcroft-Latham and Oyane critical criteria of 1.5 and 0.96. The result with Cockcroft-Latham criterion is shown in the Fig. 6.11 and the result with Oyane criterion is shown in the Fig. 6.12.

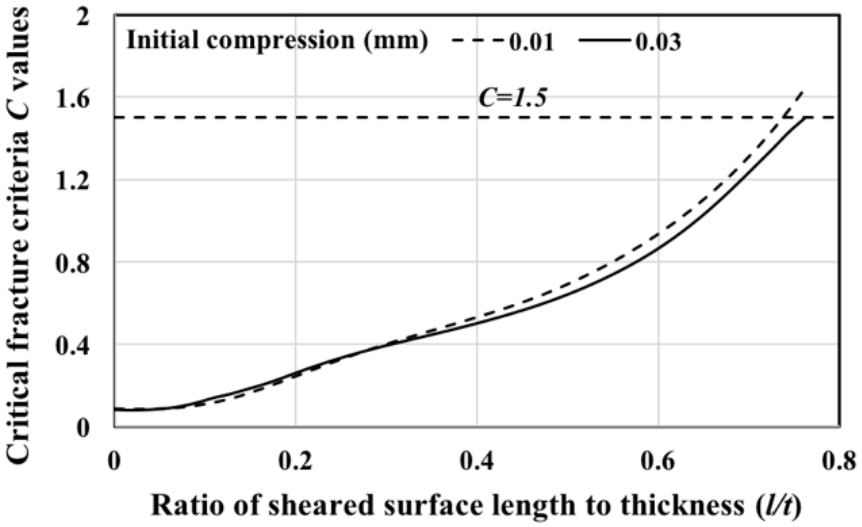

Fig. 6.11 The ratio of sheared surface length to thickness predicted by using the selected parameters under the clearance of 0.15%t and punch diameter of 10 mm for the initial compressions of 0.01 mm and 0.03 mm. (Cockcroft and Latham).

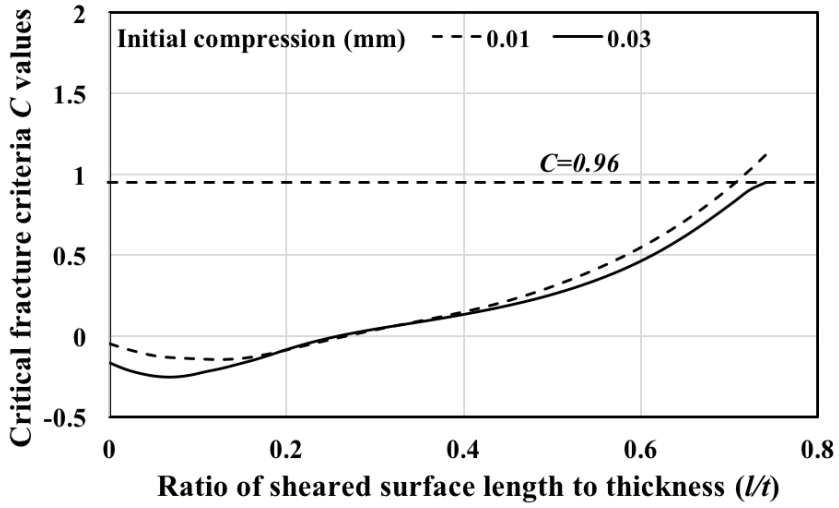

Fig. 6.12 The ratio of sheared surface length to thickness predicted by using the selected parameters under the clearance of 0.15%t and punch diameter of 10 mm for the initial compressions of 0.01 mm and 0.03 mm. (Oyane).

The distribution of damage value along the cutting length is above the critical fracture criteria (C) value for the initial compression of 0.01 mm. However, it is under the threshold value 1.5 (Cockcroft-Latham) and 0.96 (Oyane) for the initial compression of 0.03 mm which means that the cut surface is fully sheared. The figures show that the fully sheared surface can

be obtained by the selected optimized parameters of initial compression of 0.03 mm, punch corner radius of 0.01 mm V-ring indenter height of 0.7 mm under the clearance of 0.15 %t. The results indicate the importance of choosing appropriate process parameters.

6.6 Verification of optimized parameters

The parameters which give fully sheared surface of SPCC in the fine blanking process were selected by using the punch diameter of 10 mm and the blank diameter of 20 mm. The predictions of the behavior of cut surfaces were performed under the same clearance of 0.15 %t by using the blank diameter of 100 mm and the punch diameters (10,15,20,30,40 and 50 mm) to verify whether the optimized parameters can be used for other conditions such as larger blank diameter and larger punch diameter. The initial element length and the element length after remeshing are same with former case of blank diameter of 20 mm and the values are 0.08 mm and 0.01 mm. The total number of element is 31250. The predicted cut surfaces for the blank diameter of 100 mm and punch diameters of 10, 15 and 20 mm under the clearance of 0.15 %t by using the optimized parameters are shown in the Fig. 6.13 and Fig. 6.14.

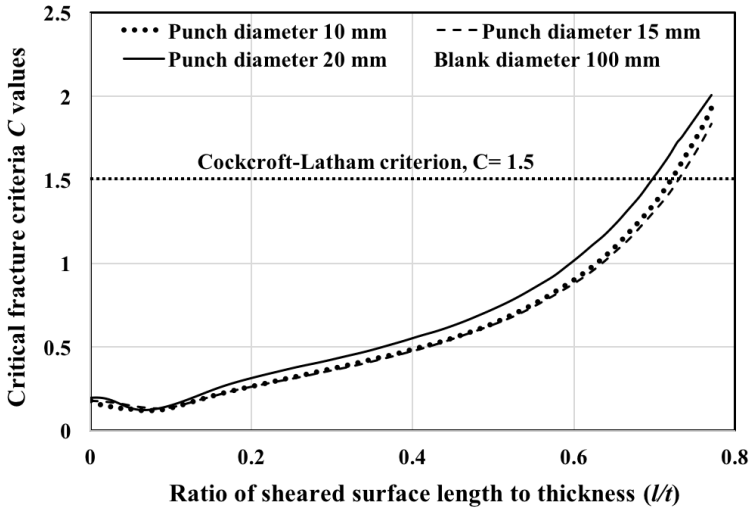

Fig. 6.13 The ratios of sheared surface length to thickness predicted by the punch diameters of 10, 15 and 20 mm with the blank diameter of 100 mm using the optimized parameters under the clearance of 0.15 %t (Cockcroft-Latham).

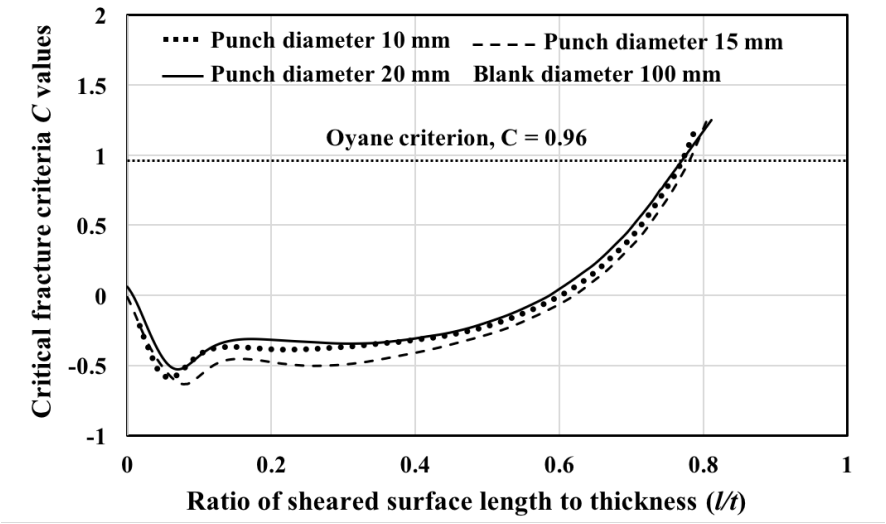

Fig. 6.14 The ratios of sheared surface length to thickness predicted by the punch diameters of 10, 15 and 20 mm with the blank diameter of 100 mm using the optimized parameters under the clearance of 0.15 %t (Oyane).

The figures show the condition of cut surfaces predicted by Cockcroft-Latham and Oyane criteria. The results obtained from both criteria describe that the predicted cut surfaces are not fully sheared in all cases of punch diameters of 10, 15 and 20 mm for the blank diameter of 100 mm under the same clearance. Through the results, it is found that the right choice of process parameters to obtain fully sheared surface is important in the fine blanking process. The nature of cut surfaces in the fine blanking process with larger punch diameters were also studied by using punch diameters of 30, 40 and 50 mm under the clearance of 0.15 %t. The results are shown in the Fig. 6.15 and Fig. 6.16.

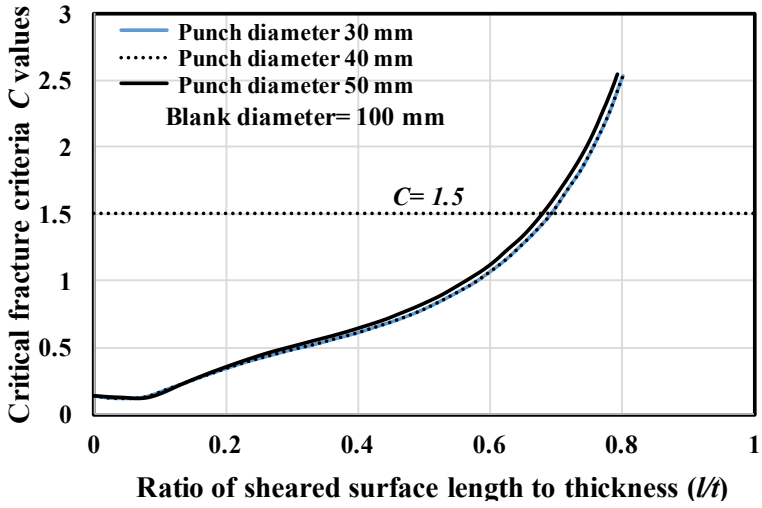

Fig. 6.15 The ratios of sheared surface length to thickness predicted under the clearance of 0.15 %t, blank diameter of 100 mm and punch diameters of 30, 40 and 50 mm by using selected parameters (Cockcroft-Latham).

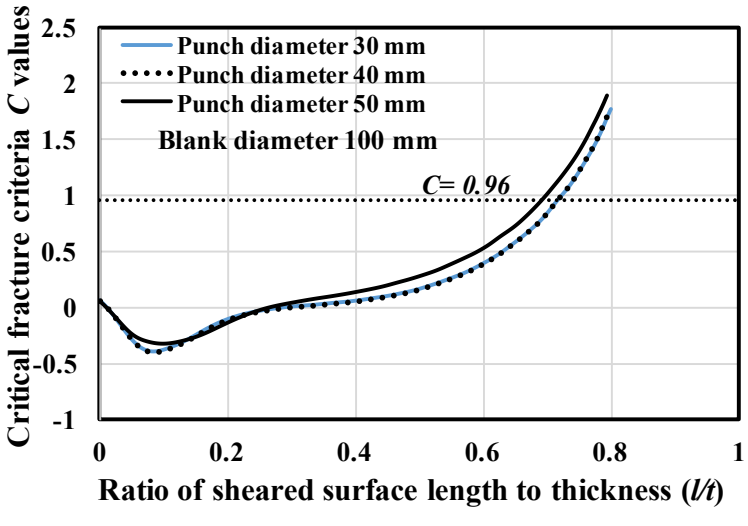

p

Fig. 6.16 The ratios of sheared surface length to thickness predicted under the clearance of 0.15 %t, blank diameter of 100 mm and punch diameters of 30, 40 and 50 mm by using selected parameters (Oyane).

The figures describe that the predicted cut surfaces by Cockcroft-Latham and Oyane critical criteria are not fully sheared. The damage distribution along the cutting plane is larger than the threshold value. The die corner radius used in the above predictions was 0.4 mm. Hence, the die corner radius was changed to 0.5 mm to study the nature of cut surfaces in the

fine blanking process by using the clearance dependent critical ductile fracture criteria. The predicted cut surfaces are shown in the following.

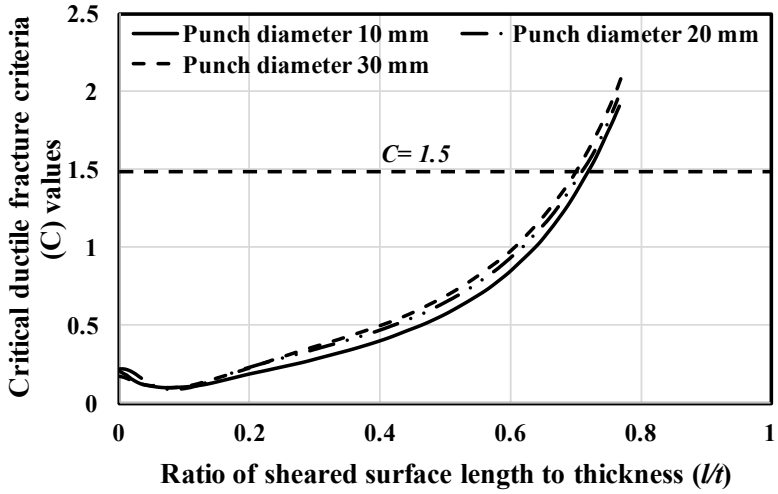

Fig. 6.17 The ratios of sheared surface length to thickness predicted under the clearance of 0.15 %t and blank diameter of 100 mm, die corner radius of 0.5 mm and punch diameters of 10, 20 and 30 mm by using selected parameters (Cockcroft-Latham).

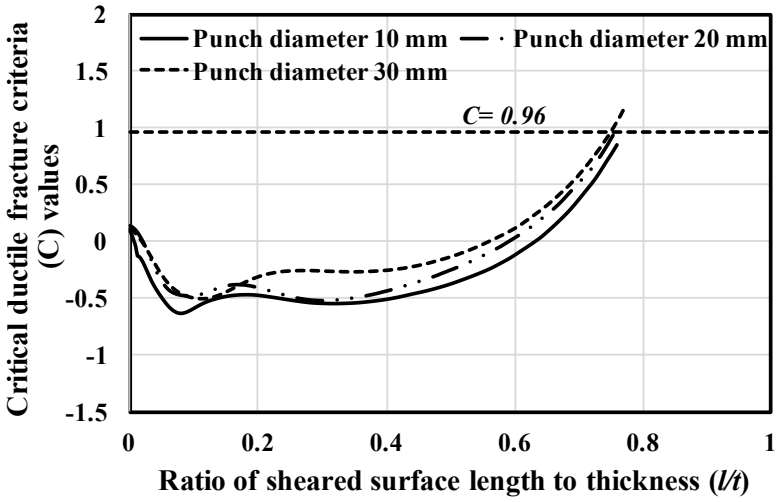

Fig. 6.18 The ratios of sheared surface length to thickness predicted under the clearance of 0.15 %t and blank diameter of 100 mm, die corner radius of 0.5 mm and punch diameters of 10, 20 and 30 mm by using selected parameters (Oyane).

The results show that the larger sheared surface can be obtained with the die corner radius of 0.5 mm for the different diameters under the same clearance of 0.15 %t. The Fig. 6.17 shows the predicted cut surface with the Cockcroft-Latham criterion. The distribution of damage is above the critical value of 1.5 and the predicted cut surfaces are not fully sheared. The Fig. 6.18 shows the predicted cut surfaces with the Oyane criterion. The distribution of damage along the cutting length is under the threshold value for the punch diameters of 10 and 20 mm. However, it is above the threshold value for the punch diameter of 30 mm. The predicted cut surfaces by the punch diameter of 30 mm are not fully sheared surface for the die corner radius of 0.4 mm and 0.5 mm but the sheared surface length obtained with 0.5 mm is larger than the sheared surface length obtained with 0.4 mm.

Through the results, it is found that the fully sheared surface can be obtained by using the optimized parameters: initial compression of 0.03 mm, punch corner radius of 0.01 mm, die corner radius of 0.5 mm and the V-ring height of 0.7 mm. The figures also indicate that the clearance dependent critical ductile fracture criteria can be used to predict fracture initiation in the conventional punching and fine blanking processes with the punch diameters of less than 25 mm.

Chapter (7) Summary and Future Work

7.1 Summary of research

In the conventional punching and fine blanking processes, if the value of critical ductile fracture criterion is known, the ductile fracture initiation can be predicted by using the critical ductile fracture criterion value. Critical ductile fracture criteria obtained by performing complicated tests and long duration of experiments were used in numerical simulations to optimize metal forming processes. This study is based on the experiment-simulation coupled approach by performing punching experiments. The following summary can be drawn from this research.

Punching experiments were performed for SPCC and S45C with different punch diameters, blank thicknesses and clearances. The minimum and maximum sheared surface lengths were measured for all cases and the average values were calculated for all experiments. The ratios of sheared surface length to thickness (l/t) were calculated and they were plotted against the clearances between the punch and the die and the relationship between the ratio of sheared surface length to thickness and clearance was obtained.

FEA for the punching processes were performed to determine the values of critical ductile fracture criteria and to predict the fracture initiation in the conventional punching and fine blanking processes. Three phenomenological models for ductile fracture were used in this research: Cockcroft-Latham, Oyane and Ayada models. The value of critical ductile fracture criterion (C), which gives the shear limit point for each model, was obtained through a best-fit of the experimental data.

When the clearance is increased, the sheared surface length decreases for all punch diameters. The Cockcroft–Latham and Oyane criteria are suitable because both critical fracture criteria (C) increase monotonically. The α value which gives the same value of (C) for the uniaxial tensile test and punching process was selected as Oyane parameter. The value of

critical fracture criterion (C) depends on the clearance (%t) and varies with the ratio of sheared surface length to thickness and it is not a material constant. The value of critical ductile fracture criterion that can be used in an actual punching process can be obtained by fitting a second-order polynomial to the data in Cockcroft-Latham and Oyane models. The polynomial line fitting to the data (including all result data) cannot be obtained from the Ayada model as it is based on Mode I tensile crack opening mechanism.

The effect of stress triaxiality on the value of critical fracture criterion was studied and it was found that the critical fracture criterion is affected by the stress triaxiality and it is not a material unique constant. The effect of punch diameter on the sheared surface length was also studied with different punch diameters and the results indicated that the effect of punch diameter also should be taken into account for the prediction of fracture initiation in the punching processes. A clearance of less than 1%t is preferable for longer sheared surfaces. The values of critical fracture criteria (C) that can be used in the prediction of fracture initiation of SPCC for the different clearances can be obtained from this research.

The stress triaxiality influences the fracture initiation point in the punching process. The decrease in the clearance causes a decrease in the range of stress triaxiality in the clearance zone and larger sheared surface can be obtained. In the case of S45C, the ratio of sheared surface length to thickness obtained from the clearance of 6.25 %t is smaller than the value which is obtained from the clearance of 9.375 %t at the same value of stress triaxiality. The similar condition can be occurred for the clearances of 18.75 %t and 25 %t. Hence, the accurate prediction of fracture initiation in punching process cannot be obtained by the criterion which is based only on the stress triaxiality for the low ductility material such as S45C.

The clearance-dependent critical ductile fracture criteria were used to study the influences of process parameters on the cut surface in the fine blanking process. In the fine blanking process, the sheared surface length is affected by the clearance between the punch

and the die, the punch corner radius, the die corner radius, the initial compression and V-ring indenter. The correct choice of the process parameters plays important role to predict the condition of cut surface in the fine blanking process. The increase in the punch corner radius decreases the sheared surface length of the blank. The results described that the increase in initial compression decreases the length of sheared surface and the correct choice of the initial compression is crucial for compressive hydrostatic stress which postpones the fracture initiation point.

The sheared surface length in the fine blanking process is also significantly affected by the V-ring indenter. The results indicated that the sheared surface length obtained with the V-ring indenter height of 0.7 mm is larger than that of 0.35 mm. The V-ring indenter height of 0.7 mm is appropriate for the blank thickness of 4 mm. The variations of stress triaxiality under the different V-ring heights were also studied and the results showed that V-ring increases the compressive stress in the blank before cutting. The increased compressive stress affects on the sheared surface length and larger sheared surface length can be obtained.

The results proved that the fully sheared surface can be obtained in the fine blanking process by using the optimized parameters: initial compression of 0.03 mm, punch corner radius of 0.01 mm, die corner radius of 0.5 mm and the V-ring height of 0.7 mm.

The values of the critical ductile fracture criteria obtained from this research can be used for the prediction of fracture initiation in the conventional punching process and fine blanking process with the punch diameters of less than 25 mm. Hence, experimental costs and time to obtain critical fracture criterion (C) or critical damage value can be reduced. Through the results, it is found that the effect of punch diameter also should be taken into account for the prediction of fracture initiation in the conventional punching and the fine blanking processes.

7.2 Limitations and future work

The value of critical ductile fracture criterion for the low ductility material S45C cannot be determined by the fracture criterion which is based only on the stress triaxiality.

As a future work, the mechanism based ductile fracture criteria and continuum damage mechanics based ductile fracture criteria will be considered to predict the fracture initiation in the punching and to determine the value of critical ductile fracture criteria. The lode angle effect also will be taken into account to determine the critical damage value and to predict fracture initiation of low ductility material.

References:

1. McClintock, F.A.; Kaplan, S.M.; Berg, C.A. Ductile fracture by hole growth in shear bands. *Int. J. Fract. 1966, 2, 614-627*.
2. Cockcroft, M.G.; Latham, D.J. Ductility and the workability of metals. *J. Inst. Metals. 1968, 96, 33-39*.
3. Rice, J.R.; Tracey, D.A. On the ductile enlargement of voids in triaxial stress fields. *J. Mech. Phys. Solids. 1969, 17, 201-217*.
4. Oyane, M.; Sato, T.; Okimoto, K.; Shima, S. Criteria for ductile fracture and their applications. *J. Mech. Working. Tech. 1980, 4, 65-81*.
5. Gurson, A.L. Continuum theory of ductile rapture by void nucleation and growth: part 1-yield criteria and flow rules for porous ductile media. *J. Eng. Mater. Technol. 1977, 99, 2-15*.
6. Tvergaard, V. Material failure by void growth to coalescence. *J. Appl. Mech. 1989, 27, 83-151*.
7. Stoughton, T.B.; Yoon, J.W. A new approach for failure criterion of sheet metals. *Int. J. Plasticity. 2011, 27, 440-459*.
8. Khan, A.S.; Liu, H. A new approach for ductile fracture prediction on Al 2024-T351 alloy. *Int. J. Plasticity. 2012, 35, 1-12*.
9. Lou, Y.S.; Huh, H. Extension of a shear controlled ductile fracture model considering the stress triaxiality and the lode parameter. *Int. J. Solids. Struct. 2013, 50, 447-455*.
10. Goijaerts, A.M.; Govaert, L.E.; Baaijens, F.P.T. Prediction of ductile fracture in metal blanking. *J. Manuf. Sci. E-T. ASME. 2000, 122, 476-483*.
11. Brokken, D.; Brekelmans, W.A.M.; Baaijens, F.P.T. Predicting the shape of blanked products: a finite element approach. *J. Mater. Process. Tech. 2000, 103, 51-56*.

12. Hambli, R.; Reszka, M. Fracture criteria identification using an inverse technique method and blanking experiment. *Int. J. Mech. Sci. 2002, 44, 1349-1361*.
13. Kwak, T.S.; Kim, Y.J.; Bae, W.B. Finite element analysis on the effect of die clearance on shear planes in fine blanking. *J. Mater. Process. Tech. 2002, 130-131, 462-468*.
14. Shim, K.H.; Lee, S.K.; Kang, B.S.; Hwan, S.M. Investigation on blanking of thin sheet metal using the ductile fracture criterion and its experimental verification. *J. Mater. Process. Tech. 2004, 155-156, 1935-1942*.
15. Komori, K. Ductile fracture criteria for simulating shear by node separation method. *J. Theor. Appl. Fract. Mech. Sci. 2005, 43, 101-114*.
16. Tanaka, T.; Hagihara, S.; Tadano, Y.; Inada, T.; Mori, T.; Fuchiwaki, K. Application of finite element method to analysis of ductile fracture criteria for punched cutting surfaces. *JSTP. 2013, 54, No.9, 1697-1702*.
17. Xu, J.; Guo, B.; Shan, D.; Wang, C.; Wang, Z. Surface quality improvements of WC-Co micro-punch finished by ion beam irradiation for micro-punching process of metal foil. *J. Surf. Coat. Tech. 2013, 235, 803-810.*
18. Kals, T.A. Miniaturization in sheet metal working. *J. Mater. Process. Tech. 2000, 103, 95-101.*
19. Xu, J.; Guo, B.; Wang, C.; Shan, D. Blanking clearance and grain size effects on micro deformation behavior and fracture in micro-blanking of brass foil. *Int. J. Mach. Tool. Manuf. 2012, 60, 27-34*.
20. Subramonian, S.; Altan, T.; Ciocirlan, B.; Campbell, C. Optimum selection of variable punch-die clearance to improve tool life in blanking non-symmetric shapes. *Int. J. Mach. Tool. Manu. 2013, 75, 63-71.*
21. Yu, S.; Zhao, J. Investigation on blanking of thick sheet metal using the ductile fracture initiation and propagation criterion. *J. Shanghai Jiaotong Univ. Sci. 2012, 17(5), 531-536*.

22. Mohr, D.; Marcadet, J.S. Micromechanically-motivated phenomenological Hosford-coulomb model for predicting ductile fracture initiation at low stress triaxialities. *Int. J. Solids. Struct. 2015, 67-68, 40-55.*
23. Meng, B.; Fu, M.W.; Fu, C.M.; Chen, K.S. Ductile fracture and deformation behavior in progressive microforming. *J. Mater. Design. 2015, 83, 14-25.*
24. Boljanovic, V. Sheet metal forming processes and die design. 2004, ISBN-13:978-0-8311-3182-1.
25. Altan, T.; Tekkaya, A.E. Metal forming processes in manufacturing. *Sheet metal forming fundamentals*, 2012, ISBN-13:978-1-61503-842-8.
26. Subramonian, S. Blanking, *Sheet metal forming processes and application, edited by Altan, T and Tekkaya*, *A.E. 2012, 1-17, ISBN-10-0-61503-844-2*.
27. Taupin, E.; Breitling, J.; Wu, W-T.; Altan, T. Material fracture and burr formation in blanking results of FEM simulations and comparison with experiments. *J. Mater. Process. Tech. 1996, 59, 68-78.*
28. William D. Callister, Jr. Materials science and engineering, an introduction, ISBN-13:978-0-471-73696-7.
29. Anderson, T.L. Fracture mechanics, fundamentals and applications, 3rd edition, ISBN-13: 978-1-4200-5821-5 (29).
30. Urbanek, M.; Dzuagan, J.; Prantl, A. Evaluation of ductile fracture model in bulk forming. *ICPNS 16. 2016, 201, 14-17.*
31. Zhu, Y.; Engelhardt, M. D. Prediction of ductile fracture for metal alloys using a shear modified void growth model. *J Engineering fracture mechanics* (2018), *doi.org/10.1016/j.engfracmech.2017.12.042.*
32. Bai, Y.; Wierzbicki, T. A new model of metal plasticity and fracture with pressure and lode dependence. *Int. J plasticity. 2008, 24, 1071-1096*.

33. Zhang, Z.L.; Hauge, M. On the Gurson micro-mechanical parameters. *J. Fatigue and Fracture Mechanics. 1999, 29, ASTM STP 1332*.

34. Broggiato, G.B.; Campana, F.; Cortese, L. Identification of Material Damage Model Parameters: An inverse approach using digital image processing. *Meccanica. 2007, 42, 9-17*.

35. Bonora, N. A nonlinear CDM model for ductile failure. *J. Engineering Fracture Mechanics. 1997, 58, 11-28*.

36. Bao, Y.; Wierzbicki, T. On the cut-off value of negative triaxiality for fracture. *J. Eng. Fract. Mech*. *2005, 72, 1049-1069*.

37. Yoshida, Y.; Ishikawa, T. Determination of ductile damage parameters by notched plate tensile test using image analysis. *J. Mater. Res. Innov*. *2011, 15, s422-425*.

38. Martins, P.A.F.; Bay, N.; Tekkaya, A.E.; Atkins, A.G. Characterization of fracture loci in metal forming. *Int. J. Mech. Sci. 2014, 83, 112-123*.

39. Bao, Y.; Wierzbicki, T. On fracture locus in the equivalent strain and stress triaxiality space. *Int. J. Mach. Sci. 2004, 46, 81-98*.

40. Achouri, M.; Germain, G.; Santo, P.D.; Saidane, D. Experimental and numerical analysis of micromechanical damage in the punching process for high-strength low-alloy steels. *J. Materials and Design. 2014, 56, 657-670*.

41. Lee, T.C.; Chan, L.C.; Zheng, P.F. Application of the finite element deformation in the fine blanking process. *J. Mater. Process. Tech. 1997, 63, 744-749*.

42. Hambli, R. Finite element simulation of fine blanking processes using a pressure dependent damage model. *J. Mater. Process. Tech. 2001, 116, 252-264*.

43. Li, Y.; Peng, Y. Fine-blanking process simulation by rigid viscous-plastic FEM coupled with void damage. *J. Finite. Elem. Anal. Des*. *2003, 39, 457-472*.

44. Thipprakmas, S. Finite element analysis of V-ring indenter mechanism in fine blanking process. *J. Mater. Des. 2008*, doi: 10.1016/j.matdes.2008.05.072.

45. Tanaka, T.; Hagihara, S.; Tadano, Y.; Yoshimura, S.; Inada, T.; Mori, T.; Fuchiwaki, K. Analysis of shear droop on cut surface of high-strength steel in fine blanking process. *Materials Transactions, JSTP. 2011, 52, 447-451.*

46. Liu, Y.; Hua, L.; Mao, H.; Feng, W. Finite element simulation of effect of part shape on forming quality in fine blanking process. *Procedia Engineering. 2014, 81, 1108-1113.*

47. Wang, J.P. A novel fine blanking approach. *Int. J. Adv. Manuf. Technol. 2015, 78, 1015-1019.*

48. Mao, H.; Zhou, F.; Liu, Y.; Hua, L. Numerical and experimental investigation of the discontinuous dot indenter in the fine blanking process. *J. Manuf. Process. 2016, 24, 90-99.*

49. Tang, B.; Liu, Y.; Mao, H. Investigation of a novel modified die design for fine-blanking process to reduce the die-roll size. *Procedia Engineering. 2017, 20, 1546-1551.*

50. Voigt, H.; Trauth, D.; Feuerhack, A.; Mattfeld, P.; Klocke, F. Dependencies of the die-roll height during fine blanking of case hardening steel 16MnCr5 V-ring using a nesting strategy. *Int. J. Adv. Manuf. Technol. 2018, 95, 3083-3091.*

51. Luo, C.; Chen, Z.; Zhou, K.; Yang, X.; Zhang, X. A novel method to significantly decrease the die roll during fine blanking process with verification by simulation and experiments. *J. Mater. Process. Tech. 2017, 250, 254-260.*

52. Phyo, W.M.; Hagihara, S.; Tanaka, T.; Taketomi, S.; Tadano, Y. Determination of the values of critical ductile fracture criteria to predict fracture initiation in punching processes. *J. Manuf. Mater. Process. 2017, 1, 12.*

53. Pacas, I.; Hernandez, R.; Casellas, D.; Valls, I. Strategies to increase the tool performance in punching operations of UHSS. *IDDRG. 2010, 325-334.*

54. Kwak, T.S.; Kim, Y.J.; Seo, M.K.; Bae, W.B. The effective of V-ring indenter on the sheared surface in the fine blanking process of pawl. *J. Mater. Process. Tech*. *2003, 143-144, 656-661.*